University of Alberta

Blast Damage Mechanisms at Ekati™ Mine

By

Jeffrey Andrew Peterson ©

A thesis submitted to the Faculty of Graduate Studies and Research in partial fulfillment of the requirements for the degree of Master of Science in Mining Engineering

Department of Civil and Environmental Engineering

Edmonton, Alberta

Fall 2001

National Library of Canada
Acquisitions and Bibliographic Services
395 Wellington Street
Ottawa ON K1A 0N4
Canada

Bibliothèque nationale du Canada
Acquisitions et services bibliographiques
395, rue Wellington
Ottawa ON K1A 0N4
Canada

Your file Votre référence

Our file Notre référence

The author has granted a non-exclusive licence allowing the National Library of Canada to reproduce, loan, distribute or sell copies of this thesis in microform, paper or electronic formats.

The author retains ownership of the copyright in this thesis. Neither the thesis nor substantial extracts from it may be printed or otherwise reproduced without the author's permission.

L'auteur a accordé une licence non exclusive permettant à la Bibliothèque nationale du Canada de reproduire, prêter, distribuer ou vendre des copies de cette thèse sous la forme de microfiche/film, de reproduction sur papier ou sur format électronique.

L'auteur conserve la propriété du droit d'auteur qui protège cette thèse. Ni la thèse ni des extraits substantiels de celle-ci ne doivent être imprimés ou autrement reproduits sans son autorisation.

0-612-69811-4

Canada

University of Alberta

Library Release Form

Name of Author: Jeffrey Andrew Peterson

Title of Thesis: Blast Damage Mechanisms at Ekati™ Mine

Degree: Master of Science in Mining Engineering

2002

Permission is hereby granted to the University of Alberta to reproduce single copies of this thesis and to lend or sell such copies for private, scholarly or scientific research purposes only.

The author reserves all other publication and other rights in association with the copyright in the thesis, and except as herein before provided, neither the thesis nor any substantial portion thereof may be printed or otherwise reproduced in any material form whatever without the author's prior written permission.

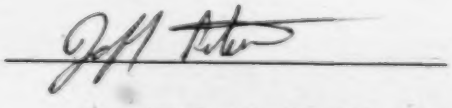

280 Douglasridge Close SE

Calgary, Alberta T2Z 2N2

Canada

October 25, 2001

University of Alberta

Faculty of Graduate Studies and Research

The undersigned certify that they have read, and recommend to the Faculty of Graduate Studies and Research for acceptance, a thesis entitled Blast Damage Mechanisms at Ekati™ Mine submitted by Jeffrey Andrew Peterson in partial fulfillment of the requirements for the degree of Master of Science in Mining Engineering.

Dwayne Tannant

Dr. Dwayne Tannant

Dr. Derek Martin

Philippe Erdmer

Dr. Philippe Erdmer

October 25, 2001

ABSTRACT

The ability to excavate stable pit slopes in large surface mines is critical to the safety and efficiency of the operation. The stability of the pit wall is greatly influenced by the drilling and blasting techniques in use at the operation. All too often, wall control blasts are designed by simply reducing the kilograms per delay of explosives in the holes near the final wall. The designs are focused around reducing the vibration levels or gas penetration into the final wall, and do not consider the other impacts from blasting which extend well beyond the limits of gas-penetration and vibration.

In the spring of 2000, a joint research project between the BHP Diamonds Inc., the University of Alberta and Western Explosives Limited, was initiated to address the blast damage mechanisms at the Ekati™ Diamond Mine. The objective of the project was to gain an increased understanding of the blast damage mechanisms and the impacts to the final wall.

Gas-penetration was not detected behind the production and wall control blasts, however it was detected 5m behind a pre-shear blast.

ACKNOWLEDGEMENTS

I would like to acknowledge the efforts of those people who assisted in the successful completion of the current thesis. Firstly, I would like to thank academic supervisor Dr. Dwayne Tannant, whose friendship, support, patience and insight continue to be greatly appreciated. I found myself looking forward to our regular discussions about the project as it progressed, and I was able to grow as an engineer from the challenges put forth by Dr. Tannant. I would also like to extend my gratitude to the engineering and geology staff at the Ekati™ Diamond Mine for their significant assistance during the completion of the monitoring program.

The completion of the current thesis would not have been possible without the financial assistance provided by BHP Diamonds Inc. and Western Explosives Limited.

Finally I would like to thank my family, friends and colleagues for their love and support while I completed my program. The completion of my graduate studies program has been a positive experience, and I would like to thank all those who made it possible.

Table of Contents

1 INTRODUCTION 1

1.1 Background 1
1.2 The Ekati™ Joint Research Project 2
1.3 Scope of Work 2

2 LITERATURE REVIEW 5

2.1 Blasting Theory 5
2.1.1 Shock Energy Breakage 6
2.1.2 Gas or Heave Energy Breakage 7
2.2 Forms of Blast Damage 10
2.2.1 Overbreak 10
2.2.2 Excavation Stability 10
2.3 Blast Monitoring 11
2.3.1 Vibration Monitoring 11
2.3.2 Time Domain Reflectometry 16
2.3.3 Gas Pressure Monitoring 16
2.4 Wall Control Blasting 17
2.4.1 Modified Production Blasting 17
2.4.2 Trim Blasting 18
2.4.3 Pre-splitting 19

3 GEOLOGY 21

3.1 Regional Geology 21
3.2 Panda Pit Geology 22
3.2.1 Faults 23
3.2.2 Joints 24
3.2.3 Domain I 25
3.2.4 Domain II 27
3.2.5 Domain III 28
3.3 Geotechnical Properties 29
3.3.1 Rock Strength 29
3.3.2 Rock Modulus 29

3.3.3 Fault Gouge Shear Strength 30
3.3.4 Discontinuity Shear Strength 30
3.4 Summary 30

4 DRILLING AND BLASTING 31

4.1 Pre-strip Blasting 31
4.2 Production Blasting 31
4.3 Wall Control Blasting 35
4.3.1 435 Bench 36
4.3.2 420 Bench 37
4.3.3 405 Bench 39
4.3.4 390 Bench 40
4.3.5 375 Bench 41
4.3.6 360 Bench 43
4.4 Current Wall Control Blast Design 43

5 INSTRUMENTATION 46

5.1 Data Acquisition System 46
5.2 Geophones 47
5.3 Pressure Sensors 49
5.4 Time Domain Reflectometry 51

6 BLAST MONITORING 52

6.1 Production Blast (345-38) 52
6.1.1 Blast Layout and Monitoring Objectives 52
6.1.2 Blast Observations 55
6.1.3 Gas Pressure Data 57
6.1.4 Vibration Data 58
6.1.5 Time Domain Reflectometry Data 60
6.2 Wall Control Blast (345-40) 61
6.2.1 Blast Layout and Monitoring Objectives 61
6.2.2 Blast Observations 62
6.2.3 Vibration Data 64
6.2.4 Gas Pressure Data 66
6.2.5 Time Domain Reflectometry Data 66

6.3 Pre-shear and Wall Control Blast (330-45PS & 345-50) 68
6.3.1 Blast Layout and Monitoring Objectives 68
6.3.2 Blast Observations 69
6.3.3 Vibration Data 70
6.3.4 Gas Pressure Data 71
6.4 Conclusions Regarding Instrumentation for Blast Monitoring 73

7 INTERPRETATION OF RESULTS 76

7.1 PPV vs. Scaled Distance Relationships 76
7.2 PPV Predictions 80
7.3 Dynamic Properties of Rock Mass 86
7.4 Fracture Criteria 91
7.5 Gas Pressures and Observations of Rock Fractures 95
7.6 Discussion 103
7.7 Recommendations 108

8 SUMMARY 111

9 REFERENCES 114

LIST OF FIGURES

Figure 2-1: Section through face during detonation showing expanding strain wave front from a bottom primed cylindrical charge. (From: Explosives and Rock Blasting, 1987) 6
Figure 2-2: Vibration response from slope elements. 13
Figure 2-3: Piezoresistive accelerometer (Dowding, 1985) 14
Figure 2-4: Compression (left) and shear (right) piezoelectric accelerometers (Dowding 1985) 14
Figure 2-5: Cross section and isometric view of geophone. (Oyo Geospace Corporation, 2000) 15
Figure 2-6: Modified production blast showing reduction in explosive load and sub-drill of last two rows 18
Figure 2-7: Pre-split loading techniques in varying geology (Dyno Nobel, 1991) 20
Figure 2-8: Jointing affects pre-shear results (Dyno Nobel, 1991) 20

Figure 3-1: Idealized model of a Southern African kimberlite pipe (Mitchell, 1986).....22
Figure 3-2: Intersecting faults in Panda Pit west wall 24
Figure 3-3: Large scale structures and unique structural domains in Panda Pit (After Mathis 1997).....25
Figure 3-4: Northwest corner of Panda Pit showing domain I geology 26
Figure 3-5: Example of fabric of rock in domain II east wall of Panda pit.....27
Figure 3-6: Joint set 1 in the west wall of Panda pit in Structural Domain III.....28
Figure 3-7: Triaxial test data for quartz diorite (BHP 1997, 1998).....29
Figure 4-1: Shovel face showing poor fragmentation and tight digging in upper half of the bench.....32
Figure 4-2: Typical hole load for production blasting.....34
Figure 4-3: Plan view of V and Echelon detonation timing patterns.....35
Figure 4-4: Wall design at Ekati™.....36
Figure 4-5: Offset of bench toe as a result of drill cab overhang 37
Figure 4-6: Damage to bench crest behind pre-split caused by buffer row.....38
Figure 4-7: Mid bench lip from a double bench causing falling rock to bounce over catchment.....39
Figure 4-8: Loading of pre-shear holes with Dynosplit - C and Blastex toe load 42
Figure 4-9: Structurally controlled failure in pre-sheared wall in domain III 42
Figure 4-10: Final wall showing effective crack propagation between pre-shear holes....44
Figure 4-11: Section view of trim blast design for upper half of 30m bench.....44
Figure 4-12: Section view of trim-blast design for lower half of 30m bench.....45
Figure 5-1: Configuration of resistors on geophone.....48
Figure 5-2: Geophone mounting system.....49
Figure 5-3: Voltage output from pressure sensor 50
Figure 5-4: Pressure sensor setup 51
Figure 6-1: Plan view of Panda pit showing blast locations.....52
Figure 6-2: 345-38 Production blast pattern design showing monitoring locations, initiation sequence and free face.....54
Figure 6-3: 345-38 Production blast and instrument locations.....55
Figure 6-4: Cross section showing varying degrees of damage observed behind blast....56
Figure 6-5: 345-38 Production blast muck pile 56
Figure 6-6: Back break plus rock fractures created by the 345-38 blast (pressure sensor at array #1 was 5m off last row). 57

Figure 6-7: Gas pressure and vibration trace from 345-38 production blast 5m behind last row at instrument array # 1 58
Figure 6-8: Vibration trace from instrument array #1 for blast 345-38 59
Figure 6-9: Vibration trace from instrument location #2 for blast 345-38 59
Figure 6-10: Time domain reflectometry data from TDR cables at instrument array #1 60
Figure 6-11: Blast layout, tie in and instrument location for the 345-40 wall control blast 62
Figure 6-12: Damage and rock on catchment in the back corner of blast 63
Figure 6-13: Structurally controlled back-break on 345-40 blast, and damage to rock mass 63
Figure 6-14: Disturbed rock mass in southwest corner of blast 64
Figure 6-15: 345-40 vibration trace instrument array #1 65
Figure 6-16: 345-40 Vibration trace instrument array #2 65
Figure 6-17: Gas pressure data 345-40 location 2 66
Figure 6-18: Time domain reflectometry data location 1 67
Figure 6-19: Time domain reflectometry data from location 2 67
Figure 6-20: Plan view of 330-45PS pre-shear and 345-50 wall control blast 68
Figure 6-21: Photo of the 330 bench after drilling the 330-45PS 165mm blastholes and prior to loading the explosives 69
Figure 6-22: Photo of the 330-45PS blast after detonation 70
Figure 6-23: Vibration trace from 330-45PS Pre-shear blast 5m away from holes 71
Figure 6-24: Gas pressure trace location 1 72
Figure 6-25: Gas pressure trace location 2 72
Figure 7-1: Description of parameters for the Holmberg equation (after Holmberg and Persson, 1979) 78
Figure 7-2: Comparison of PPV vs. scaled distance for production and wall control blasting 81
Figure 7-3: Comparison of Holmberg equation for production and wall control blasting 82
Figure 7-4: PPV from pre-shear compared to production and wall control blasts. 84
Figure 7-5: PPV vs. Scaled distance for all vibration data 85
Figure 7-6: Difference in arrival time at two locations of a compressive strain pulse caused by one blasthole in the 345-40 wall control blast 87
Figure 7-7: Radial distances used to calculate P-wave velocities 87

Figure 7-8: Single production hole at 19m showing separate arrival of shear and compressive waves Δt = 2ms 88
Figure 7-9: Single production hole at 30m showing separate arrival of shear and compressive waves Δt = 4ms. 89
Figure 7-10: Zone of fresh fracturing and extension of existing fractures, for 270mm hole loaded with 1.15 g/cc 70% emulsion/30% ANFO blend, based on best fit vibration data. 94
Figure 7-11: Gas flow into dilated joints or new fractures causing reduction of pressure in monitoring hole 97
Figure 7-12: Pressure drop when second last row is detonating 98
Figure 7-13: Face in front of 345-38 monitoring location 1 after muck cleared 99
Figure 7-14: Pressure trace from 345-40 wall control blast 99
Figure 7-15: Pressure data plotted against values published by Brent & Smith (1999) and Ouchterlony (1996) 100
Figure 7-16: Increase in volume vs. scaled distance from data and literature (Brent and Smith, 1999) 101
Figure 7-17: Gas penetration after pre-shear detonation 102
Figure 7-18: Schematic showing heaving taking place beyond gas penetration distance as a result of vertical movement around blasthole forcing uplift .106
Figure 7-19: Structurally controlled heaving of blocks behind production blasts 106
Figure 7-20: Heaving damage to upper section of bench crest (note lack of fracturing in lower section of bench face) 107
Figure 7-21: Effects of initiation sequence on thrust into wall 110

List of Tables

Table 3-1: Joint sets for domain I 26
Table 3-2: Properties of joint sets in domain II 27
Table 3-3: Rock fabric data - Panda pit structural domain III 28
Table 7-1: Summary of site constants and correlation coefficients from vibration prediction equations. 86
Table 7-2 Theoretical PPV thresholds (mm/s) for incipient damage and rock fracturing 92
Table 7-3: Damage criteria for strong rock masses after Bauer and Calder 1978 93
Table 7-4: Damage radii for fresh fracturing and incipient damage around a production hole 93

1 INTRODUCTION

1.1 Background

The Ekati™ Diamond Mine is located approximately 300km northeast of Yellowknife, Northwest Territorries, Canada. The mine is a joint venture between BHP Diamonds Inc. (80%) and geologists Stewart Blusson and Chuck Fipke (10% each). The mine commenced production in October 1998 and has been producing between 2.5 and 2.6 million carats per year of diamonds since then.

Wall control blasting is critical at the Ekati™ Diamond Mine due to the potential for structurally controlled failures in the pit-wall. The quality of the final pit wall must be maintained for the following reasons:

- safety of mine personnel and equipment,
- maintain overall stability of final wall, and
- ensure pit wall is excavated to the design angles.

The safety of the workers in the mine is the most important issue as rock falls from the pit wall are a major cause of injuries and fatalities as well as damage to equipment in open pit mining. Poor quality walls have significantly more loose rock that may potentially fall as well as smaller catch bench widths to arrest falling rock. The overall stability of the wall is also an important issue. Production delays resulting from slope movements can be very costly and can also jeopardize the operation. The cost of remediation can also be very high. If the pit wall is not excavated to the designed angle the costs can be extremely high. In large open pit mining operations a reduction in pit slope angle of only a few degrees can cost several hundred million dollars.

1.2 The Ekati™ Joint Research Project

In the spring of 2000 a joint research project between Ekati™ Diamond Mine, the University of Alberta, and Western Explosives Limited was initiated to develop a further understanding of the blast damage mechanisms at Ekati™. The objectives of the project were threefold:

- Investigate the various techniques available for blast monitoring and develop a system for use at Ekati™.
- Monitor the rock mass response to production and wall control blasting.
- Develop and understanding of the blast damage mechanisms at Ekati™.

The research program included a detailed literature review on wall control blasting and blast monitoring techniques, preparation and installation of blast monitoring equipment, blast monitoring and interpretation of the data. The insights from these efforts have led to further understanding of the damage mechanisms at Ekati™. It is anticipated that this data may also prove useful at other large open-pit mining operations.

1.3 Scope of Work

This thesis, which is the result of one and a half years of research on blast damage mechanisms and blast monitoring in open pit mining, intends to cover the blast monitoring system developed for use in a large open pit environment and the blast damage mechanisms occurring at the Ekati™ mine. While an overview of current blasting theories is included, this thesis does not attempt to address in detail many of the more complex issues related to this topic.

This thesis has been organized with two main objectives:

- To present the design and layout of the blast monitoring system developed and tested at Ekati™.

- To interpret the data gathered and develop an understanding of the blast damage mechanisms at Ekati™.

Chapter 2 prevents a review of blasting theory, blast monitoring and wall control blasting as they exist today. First the mechanisms of rock breakage are outlined. Second, the various blast-monitoring techniques are introduced and discussed. Third the various wall control blasting techniques are presented.

Chapter 3 is a brief summary of the geology of the Panda Pit. First the regional geology is discussed followed by the Panda Pit geology. A brief discussion follows on the three geologic domains in the pit. To complete the chapter, the geotechnical properties of the rock mass are briefly presented.

Chapter 4 covers the evolution of the blasting program at Ekati™. It begins with the pre-stripping phase completed by contractors. It then covers in detail the production and wall control blast designs as they evolved over the next two years. The rationale behind the design modifications and the current designs are both covered. The chapter ends with a brief look at what future developments may be seen with the designs.

Chapter 5 describes the instrumentation used in the study. The data acquisition system, geophones, pressure sensors and time domain reflectometry are each covered in detail in this section. The characteristics of each sensor are covered as well as any modifications that were required.

Chapter 6 presents each blast that was monitored and the data that was gathered from each blast. The drill pattern, loading and initiation sequence for each blast are presented, as well as the data that were recorded from the various instruments. The objectives of each blast that was monitored are also covered.

The data which were gathered are subject to an in depth analysis in chapter 7. From the data it was possible to: develop scaled distance relationships, calculate the dynamic properties of the rock mass, develop PPV based damage criteria, assess the damage

potential of the blast gases and compare rock mass damage from production blasts with wall control blasts.

Finally conclusions and recommendations derived from the current research project are presented in chapter 8. This includes a discussion of the research work and outlines the current research project's most significant findings.

2 LITERATURE REVIEW

2.1 Blasting Theory

There are many models and theories that attempt to describe the breakage of rock by blasting. No single theory fully explains the mechanism of rock breakage in every situation. Blasting theory encompasses many sciences including chemistry, physics, thermodynamics, shockwave interactions and rock mechanics. Understanding the mechanisms by which rock is fractured by explosives is fundamental to the design of efficient blast patterns. They also relate to the damage that can be suffered by surrounding rock.

During a blast there are several different breakage mechanisms that have been identified (Hagan, 1967 & 1973 and Mercer, 1980):

- crushing,
- relative radial motion,
- release of load,
- spalling,
- gas pressure wedging open strain-wave generated or natural cracks,
- flexural rupture,
- shear fracturing along natural and strain-wave generated cracks, and
- in-flight collisions.

Each mechanism contributes varying amounts of breakage depending on the explosive properties, rock mass properties and blast geometry. These can be split into two categories, (1) damage caused by shock energy and (2) damage by gas energy (Brown, 1956).

2.1.1 Shock Energy Breakage

The detonation of an explosive rapidly produces a high temperature gas. When confined in a blasthole, this very rapid reaction causes pressures that usually exceed 18,000 atmospheres to be exerted against the blasthole wall. This energy is transmitted into the surrounding rock in a compressive strain wave traveling at a velocity of 3000 – 6000m/s. The dispersion of this wave depends on several factors, such as the location of the initiation point (or points), velocity of detonation (VOD) of the explosive, and the compressive strain wave (p-wave) velocity of the rock mass. Propagation of this shock wave in the near field is non-linear and it is extremely difficult to correctly measure or model mathematically. However, in a typical bottom primed, cylindrical charge encountered in bench open pit blasting, the strain wave propagation resembles Figure 2-1.

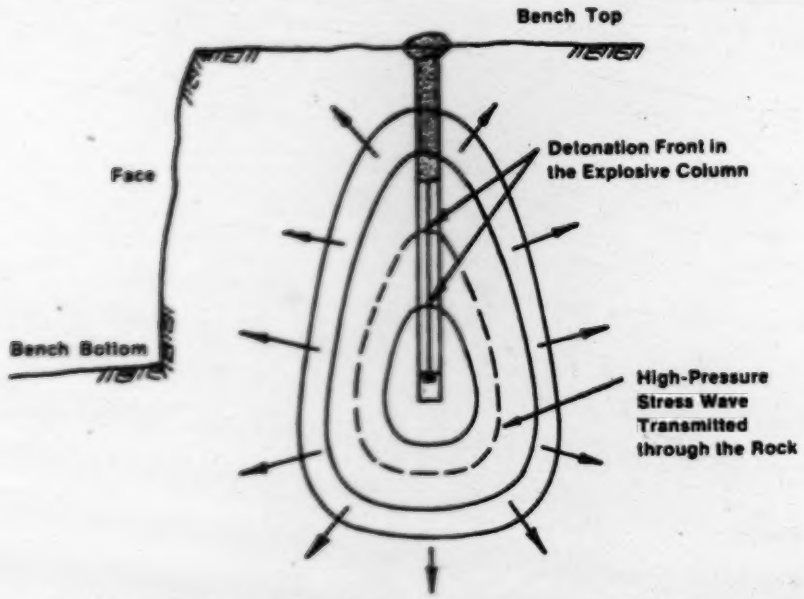

Figure 2-1: Section through face during detonation showing expanding strain wave front from a bottom primed cylindrical charge. (From: Explosives and Rock Blasting, 1987)

In granite it has been found that the compressive strain wave accounts for 10-18% of the total explosive energy, while in salt this value is only 2-4% (Clark, 1987). The shock

component of energy causes breakage by crushing, relative radial motion, release of load and spalling. Crushing occurs in the blasthole walls when the stress exceeds the dynamic compressive strength of the rock. When the dynamic stress in the pulse drops below the strength of the rock, crushing ceases to occur (Hagan, 1973). This crushed zone ends very close to the borehole wall. From this point on, the wave propagates away from the blasthole as a purely elastic compressive wave.

According to Mercer (1980) the rock outside the crushed zone is subject to very sudden compression due to the dispersing strain pulse. This compression (also referred to as relative radial motion) results in tensile stresses tangent to the blasthole wall that can cause the development of radial cracks from the borehole.

According to Clay et al. (1965) fracturing by release of load occurs immediately after the strain or compression wave passes in a local zone of decreased density and tensile strength. These fractures are aligned perpendicular to the direction the strain pulse travels.

If a compressive strain wave encounters a free face or discontinuity that is sufficiently close it will be reflected back as a tensile wave. If the tensile stresses are sufficiently strong then spalling will occur at the free face. According to Langefors and Kihlstrom (1973), in granite with relatively high tensile strength the spalling mechanism is important when the powder factor exceeds 1 kg/m^3.

2.1.2 Gas or Heave Energy Breakage

The previously described breakage mechanisms are a result of the shock energy or strain waves propagating away from an explosive charge. After the detonation front has passed a volume of high temperature and pressure gases occupy the blasthole. These gases then begin to penetrate the blast induced fractures and pre-existing joints in the rock mass. The gas pressure causes the cracks to wedge open and to extend. This opening of fractures can cause shear fracturing as adjoining rock is displaced at different times or

rates. The confinement times of these gases can range from a few milliseconds to tens of milliseconds (Chiappetta et al., 1983).

After the gases have penetrated and extended the natural and blast-induced fractures they exert forces in all directions with material movement occurring in the direction of least resistance. While the particles are in motion there will also be some in flight collisions that will also cause some degree of fracturing.

The gas pressure is active in the blasthole cavity for a considerably longer time than the strain wave. For this reason the displacement caused by the gas pressure can be considered quasi-static and occurs after the strain wave. Radial fractures around the borehole already exist by the time the gas starts to expand, extending favorably oriented fractures (Williamson and Armstrong 1986).

As gas flows into a joint or fresh fracture a pressure is applied over the area of the fissure. If the pressure is high enough it can overcome the resistance required to displace a block of rock. This displacement can result in lower stability in the rock mass.

The factors that influence explosive gas penetration can be divided into:

- rock fractures,
- rock strength,
- strain absorption coefficient,
- heat transfer coefficient,
- explosive type and quantity, and
- confinement.

The fractures are what provide pathways for the gases to travel along. A highly fractured rock mass already has numerous flow pathways present before those created by the shockwave. The orientation, continuity and aperture of these fractures influence the

resistance to the flow of gases in any direction. The resistance to gas flow is proportional to the permeability of the rock mass.

The compressive and tensile strengths of the rock will also affect gas penetration. The compressive strength determines the extent of crushing in the immediate vicinity of the blasthole. Bligh (1974) indicated that crushing could result in the blockage of cracks intersecting the blasthole slowing the flow of gases into them.

The tensile strength influences the number and length of radial cracks extending from the blasthole. If the rock mass is highly structured then this is of lesser influence. This also applies to the strain absorption coefficient that determines in part the amount of radial cracking generated by the shock wave.

The heat transfer coefficient is a measure of the rate of heat energy that is lost into the surrounding rock as the gases flow through cracks. The resulting drop in temperature causes a fall in gas pressure, and as a result limits gas penetration. The explosive type will change the peak borehole pressure, and temperature. These can be calculated from laws of thermodynamics.

Over confinement of a blasthole can lead to an increase in damage from gas penetration. Hagan (1973) states that if the effective burden (i.e. burden distance at time of detonation) is too large, the gasses are contained for an excessive period of time. As the gasses try to escape they stream into, wedge open and extend both natural and strain induced fractures around the blasthole. In a blast with proper burden, the cracks towards the free face will be opened and extended preferentially, as opposed to an over-confined blast where excessive overbreak results. In discussion on the effects of confinement Page (1987) suggests that the amount of damage from a given amount and type of explosive can vary four fold depending on the pattern, timing and geometry of the blast.

The blast gasses can cause damage in two forms:

- physical dislodgement of in-situ blocks of rock, and

- the associated large displacements can reduce the strength of joints that leads to immediate failure due to gravity, stress or blast vibrations.

Both mechanisms are a result of gas penetrating into the rock fractures.

2.2 Forms of Blast Damage

There are two main forms of blast damage, overbreak and reduction of excavation stability.

2.2.1 Overbreak

Page (1987) states that overbreak is generally limited to the burden distance appropriate for a given rock mass and can be considered as a reduction in rock quality of 80%. In good quality rock it is unlikely that a properly designed blast will have high enough strain energy to cause significant damage beyond the distance of one burden. Observations in the field have shown the zone of damage can be much greater than one burden especially in lower quality rock masses. Hagan (1973) states that more extensive overbreak results where the explosion gasses are able to flow into, wedge open and extend natural fractures in a rock with a well developed joint system. More overbreak occurs in a rock mass with open joints or joints with no infilling.

2.2.2 Excavation Stability

The stability of the walls of an open pit can be greatly reduced by poor blasting. Typically pit wall slopes in mining are designed with a factor of safety between 1.1 and 1.2, making them more susceptible to blast damage than those designed with a high factor of safety. This instability is seen in the form of sloughing or wedge failures.

McKenzie et al. (1992) state that blast vibrations will dilate a jointed rock mass in both the near field and the far field. This movement along joints will result in a reduction of the joint shear strength. This will result in a lower factor of safety for the excavation. Whether or not failure occurs depends on the initial factor of safety and the joint properties and orientations. Page (1987) offers guidelines to maximum tolerable

vibration levels. These guidelines are for mining excavations that are inspected on a regular basis. They are based on limiting the damage so that an efficient operation can be maintained.

- Excavations in poor quality rock: threshold limits 200 – 600 mm/s.
- Excavations in good quality rock: threshold limits 600 to 2000 mm/s.
- Excavations with unfavorable jointing defining potentially unstable blocks in walls; threshold limits 100 – 600 mm/s.

The rock mass damage caused by blasting may not result in immediate failure of the excavation. The damage does however make the slope more susceptible to gravity driven failure or vibration effects from other blasts.

The relationship between vibration and gas penetration and the dilation of fractures is described by McKenzie (1992).

- A negative pressure is measured, indicating vertical swell as horizontal fractures dilate followed by,
- an increase in pressure above ambient levels as gases penetrate into the system of dilated fractures.

McKenzie (1992) stresses the importance of dilation occurring prior to gas penetration. This is based on extensometer measurements that confirm vertical swell at considerable distances beyond blastholes. This vertical swell has also been reported by Ouchterlony et al. (1996) and Holmberg & Maki (1982).

2.3 Blast Monitoring

2.3.1 Vibration Monitoring

Particle vibration velocity (PPV) is often related to a blasts' ability to fracture rock, through the relationships between PPV and strain. McKenzie (1992) has identified two mechanisms by which blast vibrations can cause damage:

- generation of fresh fractures in intact rock, and
- promoting slip along unfavorably oriented joint and fracture surfaces.

The first is a near field effect, and the second can occur up to hundreds of meters from the blast.

Since particle velocity and induced strain are related it is possible to analyze blast vibrations to determine the likelihood of damage to the rock mass at various distances. Useful information can also be obtained by examining the frequency spectra, and the attenuation characteristics of blast energy. Hagan (1994) proposed that for rapid attenuation in poor quality rocks, explosive energy is being wasted in crushing the rock around the blasthole and using an explosive with a lower peak borehole pressure could increase blasting efficiency.

The frequency of blast vibrations has an effect on the amount of displacement between rock blocks. A low frequency vibration such as an earthquake with a wavelength several times greater than the block size will result in all of the elements moving together. A high frequency disturbance will result in no response from the individual blocks. When the wavelength matches the block size there is potential for displacement or resonance. These elements are illustrated in Figure 2-2.

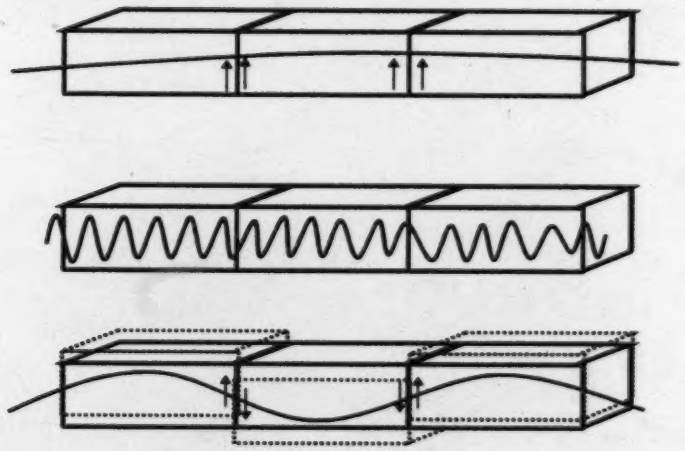

Figure 2-2: Vibration response from slope elements.

Vibration monitoring can also be used as a diagnostic tool. By comparing the vibration amplitudes of charges at various locations from a blasthole it is possible to determine if a burden is excessive and the accuracy of delays.

A typical vibration monitoring system includes the following components:

- transducers grouted into competent rock,
- cabling system to carry the signals from the transducers to the data acquisition system,
- a multi channel data acquisition system, and
- a PC-based analysis program.

Vibration monitoring can be done by using either accelerometers, which monitor acceleration, or geophones which monitor particle velocity. Accelerometers used in blast monitoring are typically piezoresistive (Figure 2-3) or piezoelectric (Figure 2-4) types. The piezoresistive accelerometers are passive accelerometers, which means they require and excitation voltage. They utilize piezoelectric strain gauges, which are basically a solid-state silicon resistor whose electrical resistance changes in proportion to the applied mechanical stress. These offer the advantage of a DC response and an upper frequency range of several thousand hertz.

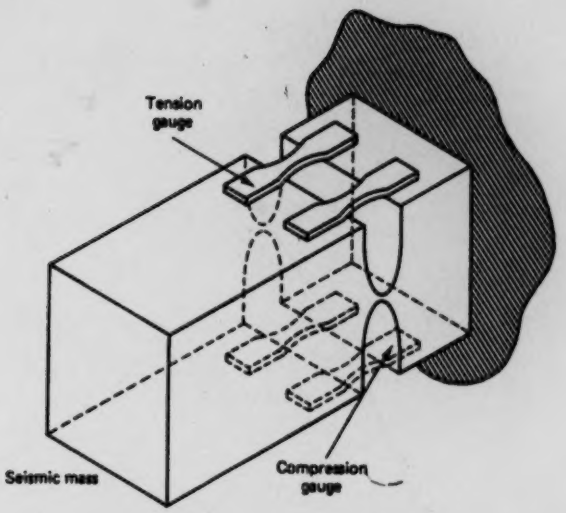

Figure 2-3: Piezoresistive accelerometer (Dowding, 1985)

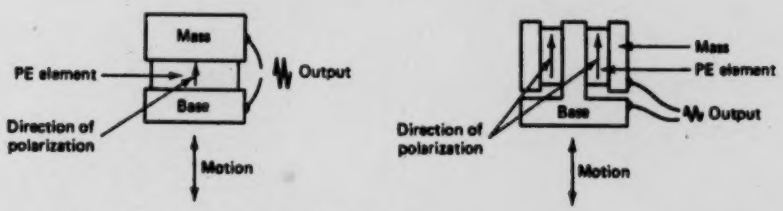

Figure 2-4: Compression (left) and shear (right) piezoelectric accelerometers (Dowding 1985)

Piezoelectric accelerometers utilize the property of certain crystals to produce a voltage difference between their faces when deformed. These accelerometers can be either shear or compressive (Figure 2-4) type depending on the orientation of the piezoelectric crystals.

There are relatively few velocity transducers on the market compared with accelerometers and strain gauges. Typically velocity is found through the integration of acceleration time histories. Although velocity transducers are a minority they are the principal type of transducer employed in blast monitoring.

The most common type of velocity transducer is a geophone. Figure 2-5 shows both an isometric and cross-sectional view of a geophone, which uses the motion of a spring-supported coil in the field of a permanent magnet to generate an output voltage. The amplitude of the signal is proportional to the relative velocity of the magnet and coil.

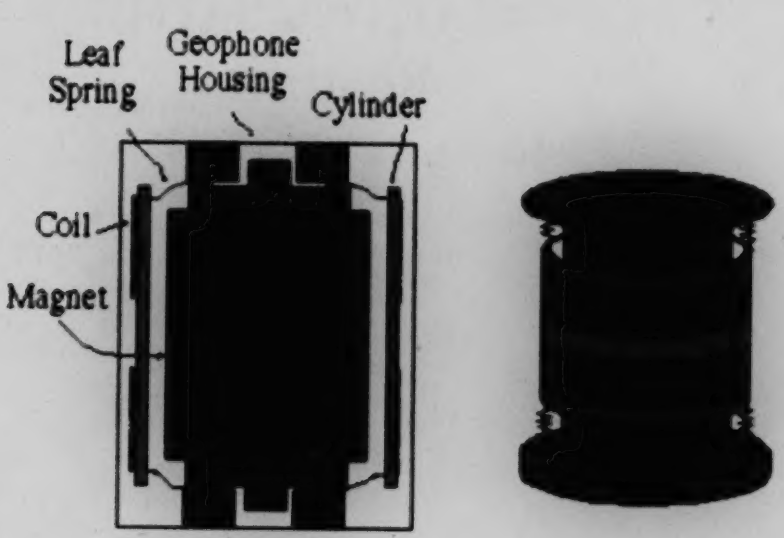

Figure 2-5: Cross section and isometric view of geophone. (Oyo Geospace Corporation, 2000)

When choosing between accelerometers and geophones several factors must be taken into consideration. These are:

- frequency of vibration,
- amplitude of vibration,
- properties of data acquisition system,
- availability of excitation voltage/current, and
- cost.

Each issue must be evaluated before selecting a sensor to use. Accelerometers can handle higher frequency and amplitude than geophones. This is because geophones are limited by the peak-to-peak travel distance of the spring. As a result, geophones can saturate when doing near-field monitoring and not give a true reading. The downfall of accelerometers is that they are more expensive than geophones and require an excitation current. Over the past ten years of blast monitoring, the consensus among the leading practitioners is that geophones are the best choice. Properly selected geophones which have a suitable dynamic range, are robust, cost effective and suitably grouted in place provide the best means of collecting vibration information (Forsyth, 1997).

2.3.2 Time Domain Reflectometry

The use of time domain reflectometry (TDR) involves the use of coaxial cables grouted into boreholes behind the blast to measure disturbance to the rock mass. An instrument sends an electrical pulse down a cable that has a known velocity of propagation. When the pulse reaches the end of the cable or a disturbed section of cable a pulse is reflected back towards the instrument. By measuring the arrival time of the reflected pulse it is possible to locate the end or damage along the cable. This technique has been used extensively in the monitoring of existing landslides and caving limits of underground excavations. Bulow and Chapman (1994) used this technique in conjunction with several others to measure blast damage behind open pit blasts. They found that the cables placed close to the blasts (8-8.5m) were sheared off close to the surface (2-3m) and the cables placed further away (13.5-14.5m) did not record any damage.

2.3.3 Gas Pressure Monitoring

Research on gas penetration monitoring has been published by Preston & Tienkamp (1984), Williamson & Armstrong (1986), Lilly (1987), LeJuge et al. (1994), Bulow & Chapman (1994), Forsyth et al. (1997), Ouchterlony et al. (1996), and Brent & Smith (1996, 1999). It is difficult to collect reliable and reproducible gas penetration data. The difficulties involve the instrumentation design and the location of the instrument and the local geology.

Typical monitoring systems involve pressure sensors sealed in boreholes at varying distances behind the blasts. The full waveforms from these sensors are recorded with high-speed data acquisition systems for analysis.

2.4 Wall Control Blasting

The objective of wall control blasting is to make the transition from a well-fragmented muck pile to an undamaged slope in as short a distance as possible. This is more likely to be achieved by improving the explosive distribution or designing the blast to direct the energy away from the wall, than by reducing the explosive charge. Most wall control methods will fall under one of the following three categories:

- modified production blasts,
- trim blasts, or
- pre or mid-splitting.

2.4.1 Modified Production Blasting

Modified production blasting is most successful in competent rock masses or on slopes designed with high factors of safety. The primary disadvantage of modified production blasting is that the wall is not protected from crack dilation, gas penetration and block heaving. In modified production blasting the energy level is decreased adjacent to the wall to prevent overbreak. This is sometimes achieved by simply reducing the charge weight by thirty to sixty percent in the row nearest the slope, and not making any changes to the pattern (Figure 2-6).

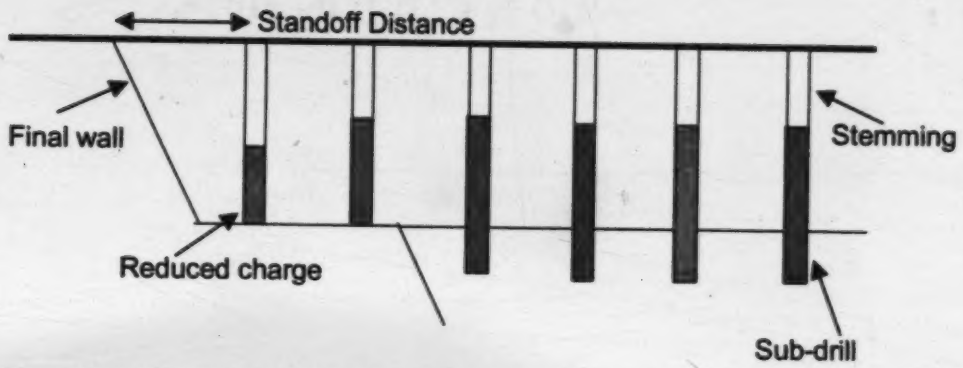

Figure 2-6: Modified production blast showing reduction in explosive load and sub-drill of last two rows

Most rock types require more design modifications to minimize blast damage. These modifications may include air decking, reducing of burden and spacing, reducing sub-drill, and / or increasing the delay between the last two rows.

When using modified production blasting it is intended that the excavator will dig beyond the final row of holes. It is critical that the standoff distance of the final row is accurate to ensure the final wall ends up being located where the design intends. The final wall stability and ease of excavating the toe of the slope depend on this standoff distance.

2.4.2 Trim Blasting

The second method of wall control blasting is trim blasting. Trim blasting is typically used when a rock mass is too weak for modified production blasting. A trim blast will contain three types of holes; trim, buffer and modified production holes. For trim blasting to perform properly an adequate free face must be established to permit forward movement of the muck away from the wall. Failure to do this will result in excessive damage to the final wall.

Trim blasting is similar to modified production blasting except that the burden and spacing of the pattern is also reduced. The blast normally involves four rows. Typically the loading and pattern of the last two or three rows next to the final wall are reduced. To achieve a smooth wall it is important that the spacing on the trim row is less than the

burden. For trim blasting to work it is imperative that free faces of the blast are cleaned up to ensure adequate horizontal movement of the blast. Trim blasting can greatly reduce wall damage as long as there is good relief, however pre-splitting will normally produce an even more stable wall. The trim blasting method does not protect the final wall from the adjacent rows as the trim row is fired last. The best combinations of pattern and loading should be decided through careful logging of wall conditions and pattern designs. Often an operation will have different designs for different sectors of the pit.

2.4.3 Pre-splitting

Pre-split blasting utilizes a row of closely spaced, lightly charged blastholes that are placed along the final limits. The holes are detonated prior to the drilling and loading of the adjacent pattern. The key factors in pre-split design are:

- drilling accuracy,
- geologic structure,
- pre-split spacing,
- pre-split charge, and
- standoff distance of buffer row.

One of the key elements in pre-split blasting is the charging of the pre-split row. The charge is normally de-coupled to reduce the borehole pressure. This decoupling can be achieved by air-decking or by using a charge diameter smaller than the blasthole diameter. As the geology becomes increasingly unfavorable better explosive distribution is required (Figure 2-7). The use of a continuous charge is the most expensive option, however it provides the best performance and the most consistent results in adverse conditions. Unless air-blast is a concern pre-split holes should be left unstemmed, to reduce borehole pressures further, and reduce damage to the crest. Although the most labor intensive and costly, in most situations the best results are achieved by pre-splitting.

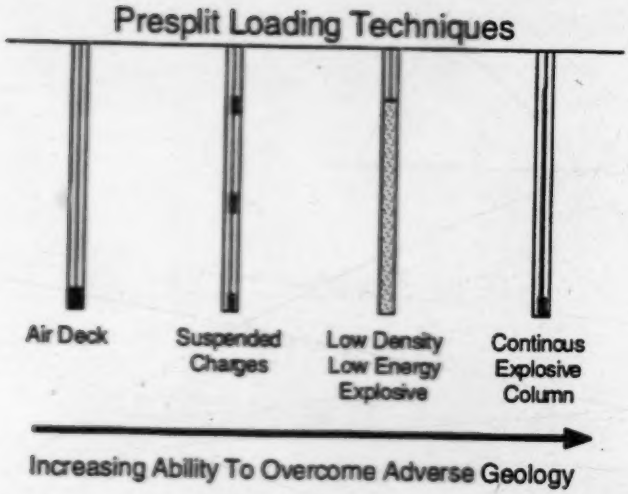

Figure 2-7: Pre-split loading techniques in varying geology (Dyno Nobel, 1991)

If the rock mass has joints that strike within 15-20° of the planned face it is likely that these joints will effect the final wall. The structure will interfere with the hole-to-hole interaction and result in a poor face (Figure 2-8).

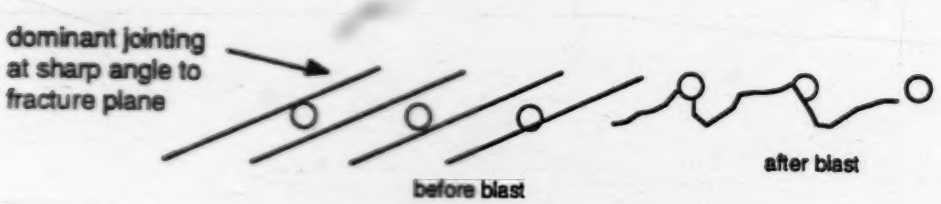

Figure 2-8: Jointing affects pre-shear results (Dyno Nobel, 1991)

3 GEOLOGY

3.1 Regional Geology

The area being investigated is located north of Lac de Gras in the east-central region of the Slave Structural Province, which is an Archean craton approximately 750km x 400km in size. The craton is a segment of the North American Craton that is composed of granites, gneisses, and supracrustal rocks. This region has remained stable since the end of Archean time. Sialic basement remnants in the western part of the province, some of the oldest rocks in existence, have been dated at 3.96 Ga (Bowring and Housch, 1995).

There are at least five swarms of Proterozoic diabase dykes that cut through the older units in the central Slave Province in the Lac de Gras region. The most important are the northeast trending Malley dykes (2.23 Ga), the east trending MacKay dykes (2.21 Ga), the northerly trending Lac de Gras swarm (2.02 Ga), and the dominant north-northwest trending Mackenzie swarm (1.27 Ga). (Le-Cheminant and van Breemen, 1994). Other undated dyke swarms intrude the southwestern sector of the Slave Province.

The kimberlite pipes intrude granites, metasedimentary rocks, and in some cases diabase dykes in both the eastern and western parts of the Slave Province. Kimberlites in the Lac de Gras area generally resemble the classical southern African pipe model (Figure 3-1) in terms of overall carrot shape and wall rock slopes, however they do exhibit some significant differences in morphology and petrology. The pipes at Ekati are also eroded below the level in Figure 3-1. Most Lac de Gras kimberlite pipes are small generally ranging from less than 2 hectares to slightly more than 12 hectares in surface area. Mudstone fragments from 13 of the pipes north of Lac de Gras contain fossils that range in age from 56 to 97 million years old (Pell, 1997).

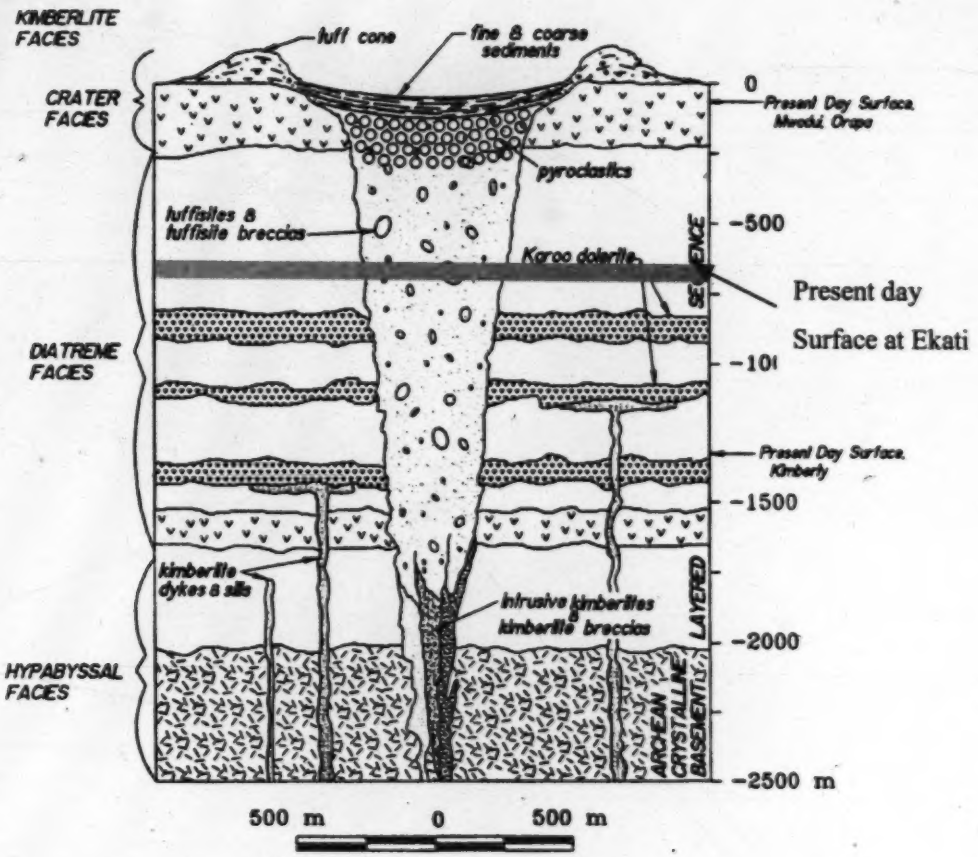

Figure 3-1: Idealized model of a Southern African kimberlite pipe (Mitchell, 1986).

3.2 Panda Pit Geology

Generally the Panda pipe is located in quartz diorite showing occasional gneissose texture. There are also pegmatite and aplite dikes crosscutting the area. The rock structure is strongly developed with joints being very planar and continuous. There are also several faults in the pit walls. As a result of the high strength of the quartz diorite, the pit design is based entirely upon structurally controlled failure modes.

To develop an understanding of the geologic setting of the Panda pit one must consider two distinct classes of rock structure:

Faults – large scale, continuous structures that affect the overall stability of the wall.

Joints – smaller scale discontinuities that have undergone little or no shear deformation.

The joints in the rock are divided into three structural domains and the faults are independent of these domains.

3.2.1 Faults

Information for the design of the Panda pit was gathered from several sources including: pit wall mapping, decline mapping, oriented core and aerial photographs (Mathis, 1997). Generally the major structures are related to faults or dikes emplaced along faults. The following characteristics apply to the major structures:

- continuous with relatively uniform strike directions over long distances,
- 3-20m wide altered zones with gouge 0.3m to 1m thick,
- NE striking fault set potentially dilational with pegamatitic dikes as infill, and in some cases kimberlite infill, and
- water bearing but frozen to a depth of approximately 280m.

A photo of several intersecting faults in the west wall of Panda Pit is shown in Figure 3-2.

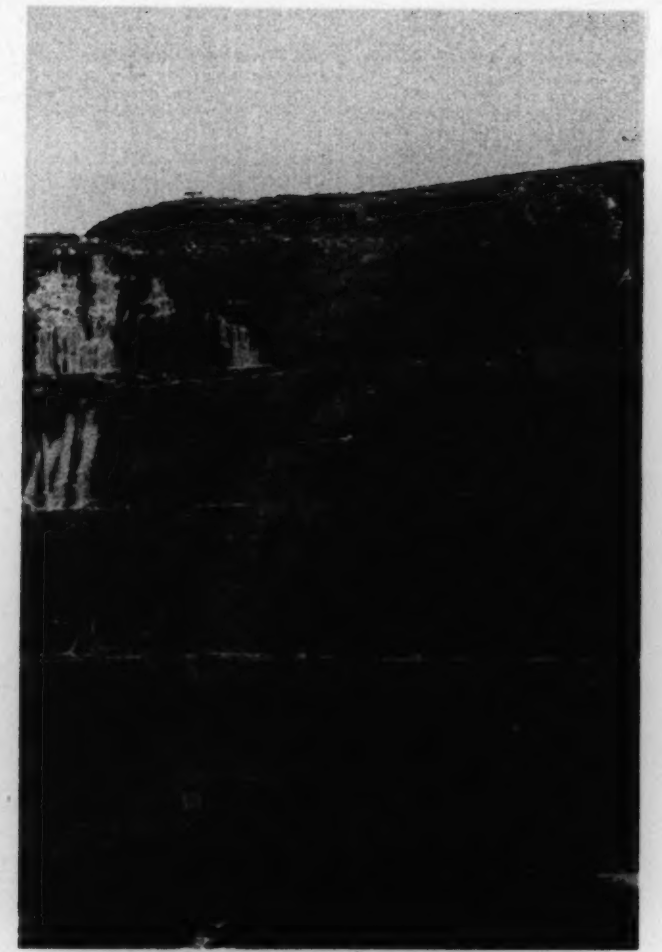

Figure 3-2: Intersecting faults in Panda Pit west wall

As mining progresses the major structures are mapped, recorded and analyzed for potential failures. At present no potential large-scale failures have been identified. A record of these structures is kept and plotted on a map pictured in Figure 3-3.

3.2.2 Joints

A database of rock joint data has been collected from three main sources in the Panda area. These are oriented core, decline mapping and in pit mapping. The oriented core data was collected using the clay imprint technique. The properties of the discontinuities

were also recorded. Mapping has revealed that there are three unique structural domains in the Panda pit (Mathis, 1997). These domains are shown in Figure 3-3.

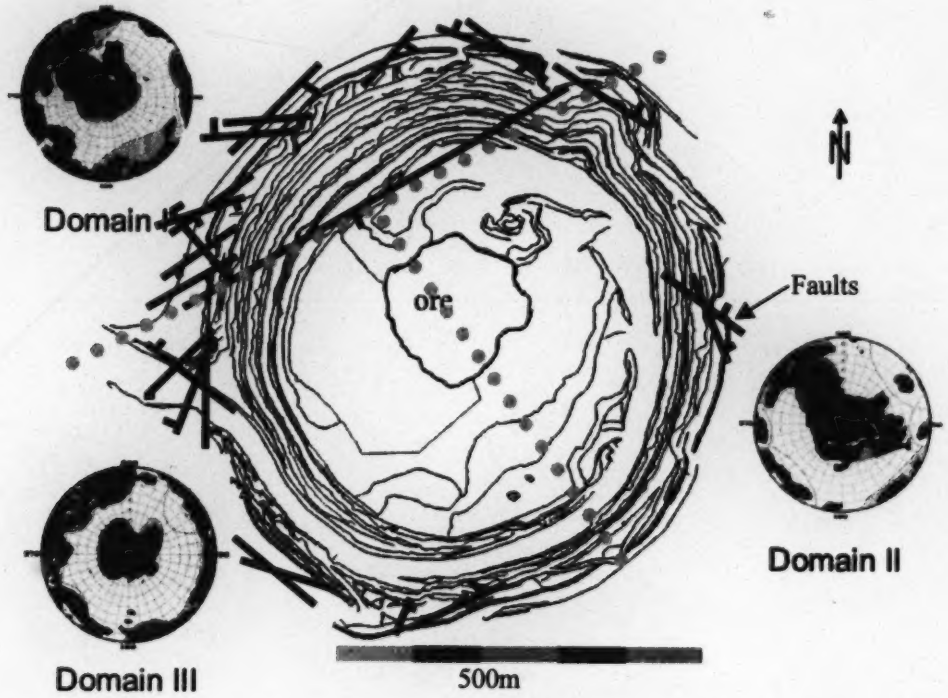

Figure 3-3: Large scale structures and unique structural domains in Panda Pit (After Mathis 1997)

3.2.3 Domain I

Domain I is located in the northwest corner of Panda pit (Figure 3-3). It is located north of the Dagger fault. There is a relatively high concentration of northeast striking faults in this specific area of the pit. The jointing in this domain is likely affected by the faulting. There is likely to be an increase in joint length, center density, relative motion along the structures and as well as the formation of accommodation structural sets (Mathis, 1997). A photograph of the pit-wall in domain I is shown in Figure 3-4. The joint sets in Domain I are summarized in Table 3-1.

Table 3-1: Joint sets for domain I

Joint set	Dip	Dip direction	Length (m)	Spacing (m)
1	86	153	4.7	3.7
2	86	98	3.1	7.5
3	86	72	3.8	6.1
4	39	138	3.6	8.5
5	43	307	6.3	6.0
6	3	32	8.0	2.2

Figure 3-4: Northwest corner of Panda Pit showing domain I geology

3.2.4 Domain II

Structural domain II encompasses the east and southeast areas of Panda pit (Figure 3-3). The joint sets are very steeply dipping or sub-horizontal. Joint set 4 is dipping at 42 degrees, however it is dipping into the wall. The only fault in the area is "Rock-it" which dips 30 degrees into the wall. The joint sets are summarized in Table 3-2. A photograph of the pit wall in Domain II is shown in Figure 3-5.

Table 3-2: Properties of joint sets in domain II

Joint set	Dip	Dip direction	Length (m)	Spacing (m)
1	85	136	7.0	1.8
2	88	267	6.5	1.9
3	88	228	3.3	4.7
4	42	145	10.4	2.7
5	8	137	5.8	3.5
6	16	306	7.3	2.4

Figure 3-5: Example of fabric of rock in domain II east wall of Panda pit

3.2.5 Domain III

The third structural domain is in the southwest corner of the pit (Figure 3-3). The jointing in this domain consists of 4 steeply dipping joint sets and 2 sub-horizontal joint sets. The properties of the joint sets are shown in Table 3-3. A photograph of the pit wall in Domain III showing joint set 1 dipping out of the face is shown in Figure 3-6.

Table 3-3: Rock fabric data - Panda pit structural domain III

Joint set	Dip	Dip direction	Joint length (m)	Joint spacing (m)
1	77	123	5.8	4.8
2	86	92	6.5	1.9
3	84	231	5.1	2.4
4	81	164	5.8	3.5
5	13	112	5.8	3.5
6	17	249	5.7	6.3

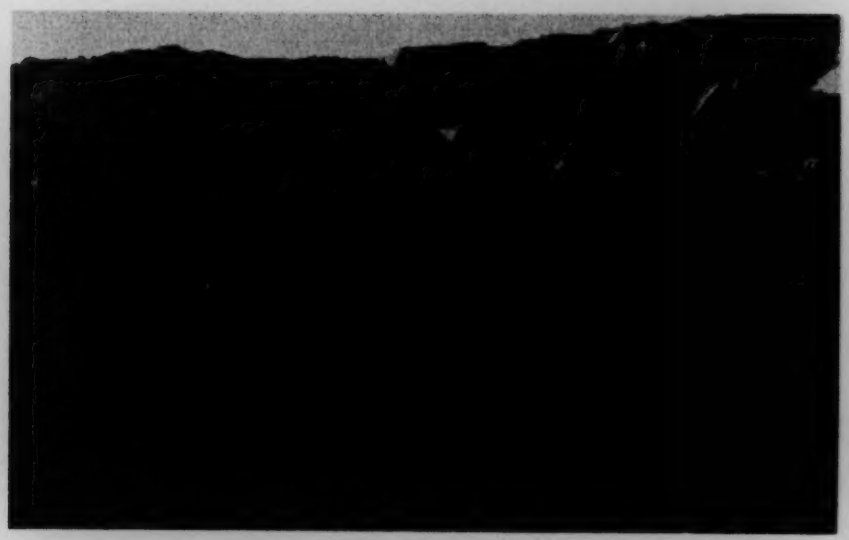

Figure 3-6: Joint set 1 in the west wall of Panda pit in Structural Domain III

3.3 Geotechnical Properties

3.3.1 Rock Strength

The quartz diorite from Panda pit has been tested in both unconfined and triaxial compression. The average unconfined compressive strength of the rock has been measured at 150 MPa and 160MPa in two separate sets of testing (BHP 1997, 1998). A series of triaxial tests have also been completed (BHP, 1998). The data from the UCS and triaxial tests are plotted in Figure 3-7. The Hoek-Brown failure criterion was then applied to these data. The data gave $m_i = 51$ and $\sigma'_{ci} = 152$MPa.

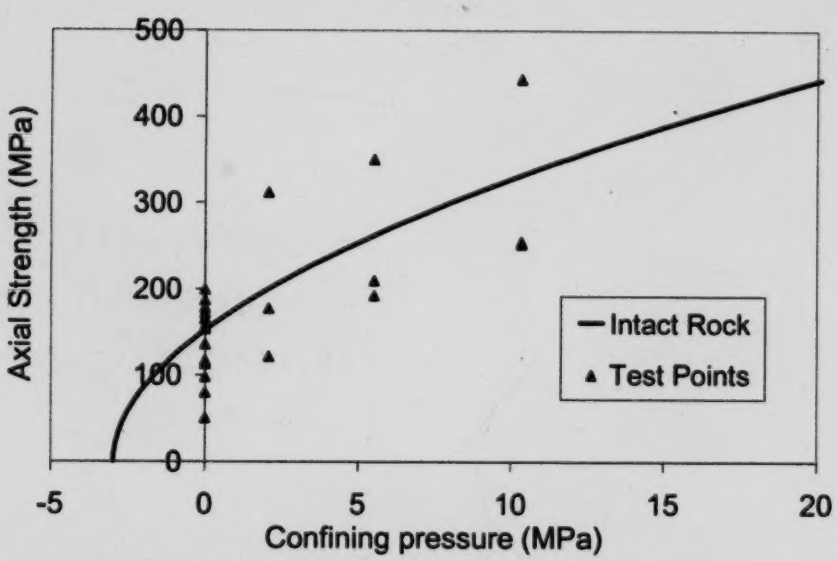

Figure 3-7: Triaxial test data for quartz diorite (BHP 1997, 1998)

For this study the UCS is the most important strength parameter. A value of 152MPa will be used throughout the study.

3.3.2 Rock Modulus

Testing done by BHP in 2000 gave an average Young's Modulus of 50GPa for the quartz diorite.

3.3.3 Fault Gouge Shear Strength

Direct shear tests were performed on remolded samples of fault gouge collected out of faults exposed in the pit walls. The samples were remolded because there was not enough sample recovered to perform the test on undisturbed samples. Of five samples tested two contained kimberlitic gouge. The strength did not appear to depend on the type of gouge. The results gave a friction angle of 24.5° and cohesion of 115 kPa (Mathis, 1997)

3.3.4 Discontinuity Shear Strength

The joints in the quartz diorite were also tested for shear strength. The values were obtained through direct shear tests on discontinuities found in core samples. The results from this testing were: $\Phi = 43°$ and c = 60kPa (peak) and $\Phi = 35°$ and 10kPa (residual). The residual strength was realized after 7mm of displacement (Mathis, 1997).

3.4 Summary

Overall the rock mass quality is the same throughout the structural domains. Due to the high strength of the rock, the design is based on structurally controlled failures.

4 DRILLING AND BLASTING

4.1 Pre-strip Blasting

During 1997 the Panda open pit was pre-stripped to prepare for mining. The pit was initially stripped in 10m high benches. Drilling was carried out with two pieces of equipment. These were an Ingersoll-Rand DM-45 that drilled 165mm holes and an Ingersoll-Rand DM-M2 that drilled 270mm holes. The smaller unit was used for pioneering work due to the rough terrain encountered. The larger rig was used once level benches had been excavated. The blast patterns used were a 4m by 6m staggered pattern for 165mm holes and a 6m by 7m staggered pattern for the 270mm holes.

In the early stages of pre-stripping it was found that the majority of the holes drilled contained water. This resulted in all of the holes being loaded with DYNOFLO Lite, a 70% emulsion / 30% Ammonium Nitrate and Fuel Oil (ANFO) chemically gassed bulk explosive. The cup density of the product was 1.2 g/cc. The product was manufactured at a temporary plant during the pre-stripping phase.

All of the blasts were tied in using detonating cord and millisecond connectors. This system was chosen because of the reliability of a dual path tie-in. The blast patterns were designed to have hole-by-hole initiation to ensure the optimum fragmentation and displacement in the muck pile. Typically the inter-hole delays were from 25 to 50 milliseconds with the inter-row delays 100 to 135 milliseconds.

4.2 Production Blasting

In the summer of 1998 BHP commissioned two D90KS drill rigs equipped for drilling 311mm holes. At the same time as the drills were commissioned the mine plan increased to 15m bench heights. Between the summer of 1998 and spring of 1999 several designs were tested before arriving at the current blast design.

The first design with 311mm holes was a 7.5m by 7.5m square pattern. The holes were loaded with 750 kg per hole of 70% emulsion / 30% ANFO blend at a density of 1.2g/cc. The sub-drill on the pattern was 1.5m giving a 16.5m total depth. This design resulted in 8m of stemming in the hole. Because of this there was very little explosive in the upper half of the bench. The resulting muck piles were poorly fragmented in the upper half of the bench and the shovel faces were standing close to vertical, resulting in lower productivity and increased wear on the shovel. A photo of one such shovel face is shown in Figure 4-1.

Figure 4-1: Shovel face showing poor fragmentation and tight digging in upper half of the bench

Several methods were tried to improve the blast performance. These included:

- dividing the explosive load into two decks to improve distribution,
- loading the holes with lower density explosives to improve distribution,
- increasing the total load per hole, and

- switching to a 7m by 8m staggered pattern.

There were varying degrees of success in each method tried. The use of two decks noticeably improved the digging conditions, however the blast crew productivity and the accessory costs suffered as a result.

During the winter of 1998 several blasts were loaded with ANFO in the top portion of the holes over a toe load of 70/30 emulsion / ANFO blend. By loading ANFO at a density of 0.83 g/cc as opposed to the 70% emulsion blend, the kilograms of explosive per metre of borehole was lowered by approximately 45%. This improved explosive distribution gave excellent results, however, the water conditions and lower blast crew productivity did not allow for this practice to continue. The pattern was also switched from the 7.5m square pattern to a 7m by 8m staggered pattern, which gave a better distribution of explosive for the same amount of drilling and the practice continued.

Problems with drill productivity as well as the desire to improve fragmentation and diggability led the operation to try using 270mm holes in the production patterns. Several patterns were tried on a 6m by 7m staggered pattern. The good results and increased drilling productivity led the mine to using 270mm holes on all production shots. The pattern was later slightly expanded to a 6.5m by 7.5m equilateral pattern.

The production holes are presently loaded with 70% emulsion / 30% ANFO chemically gassed to a density of 1.15 g/cc. Each production hole is loaded with 775 kilograms of explosive and stemmed with 10-20mm crushed rock. The holes are toe primed with a 454-gram pentolite cast booster on a 17m long 500 millisecond non-electric detonator. A typical column load is shown in Figure 4-2.

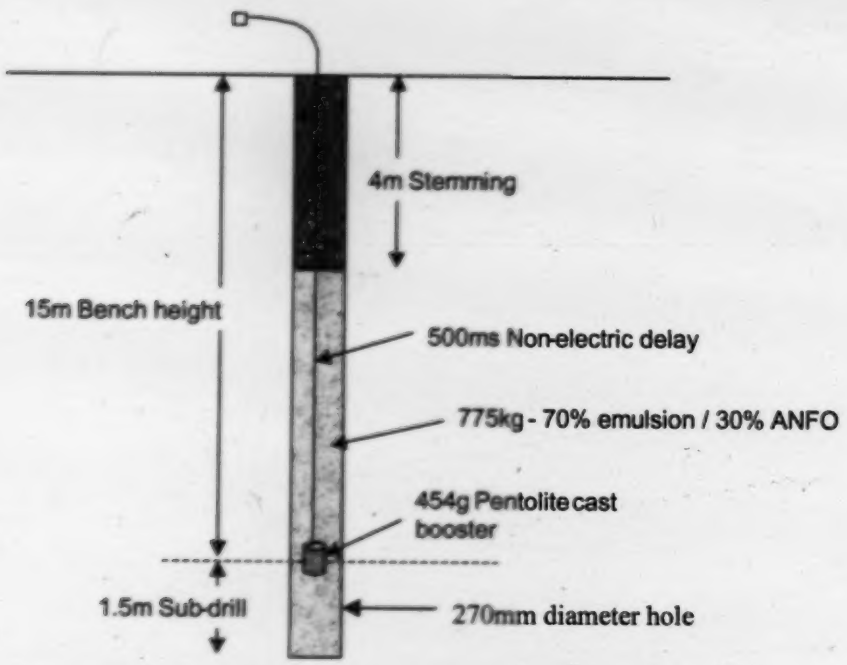

Figure 4-2: Typical hole load for production blasting

The blast initiation sequence and timing were also adjusted before the current design was adopted. Earlier blasts used 35 to 50 millisecond delays along the rows and 117 milliseconds between rows. The present design uses 65 millisecond delays between holes and 340 milliseconds between rows. It was found that the blast results improved when increasing the delay times. Depending on the shot geometry the blasts are shot either using an en-echelon or V pattern (Figure 4-3).

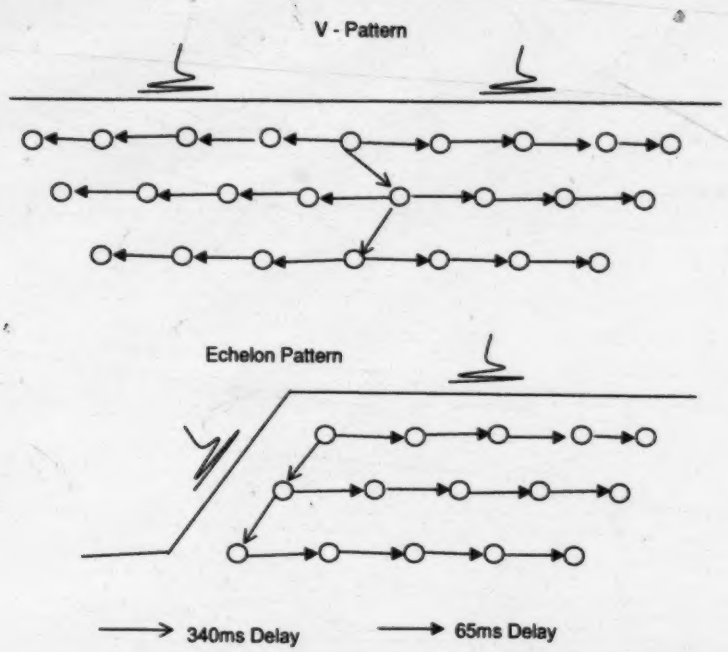

Figure 4-3: Plan view of V and Echelon detonation timing patterns

4.3 Wall Control Blasting

The steep bench faces (70°-80°) that are planned at Ekati™ require the final wall to be left as undisturbed as possible. As a result the blast patterns must be significantly altered when blasting against the final wall. During the pre-stripping phase there was little attention paid to wall control blasting. As the depth increased and the bench size increased to 30m it was imperative that the wall control blasting practices improved.

The first attempts at wall control blasting involved the use of large diameter 311m holes. Several trim blasts were also tried prior to attempting a pre-split.

Open pit development commenced at the 465m elevation and will conclude at the 150m elevation. This gives a total pit depth of 315m. The excavation of the pit was carried out by contractors down to the 435m elevation. The initial pit design consisted of 30 metre

high double benches drilled in 15m increments. Desired bench angles range from 75-85°. The approved pit design required a minimum catch bench width of 11 m (Figure 4-4).

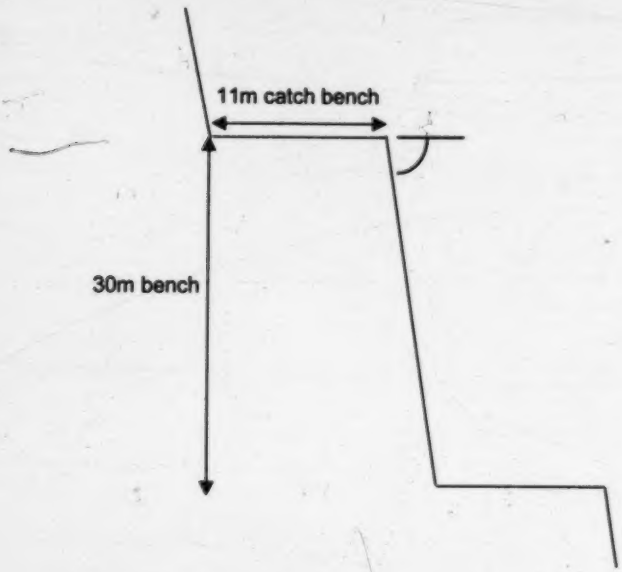

Figure 4-4: Wall design at Ekati™

A summary of the wall control blasting in the Panda pit is included in the following sections. Each bench covers the entire pit and is named based on the elevation that it will be excavated from.

4.3.1 435 Bench

For the 435 bench the following applied to the wall control blasts:

- 311mm hole diameter was used throughout;
- trim blast design;
- 70-85 kg 30/70 emulsion toe load in final row;
- final row burden 5.5 m; spacing 4.0 m; sub-drill 0-1.5 m.

This design resulted in the final crest being 6-13m with no predictable toe. The bench angle was too shallow ranging from 65-70°. These results are to be expected in a highly

fractured rockmass if improper wall techniques are implemented. The trim blast does little to protect the stability of the final wall since it is shot after the final production row.

The geometry of the Drilltech D90KS drills caused difficulty with the final wall design. The 3.5 m cab overhang prevents drilling on the design toe for a 15 m bench. As a result all trim holes offset the design toe line. This was not taken into account when the feasibility study was prepared (Figure 4-5).

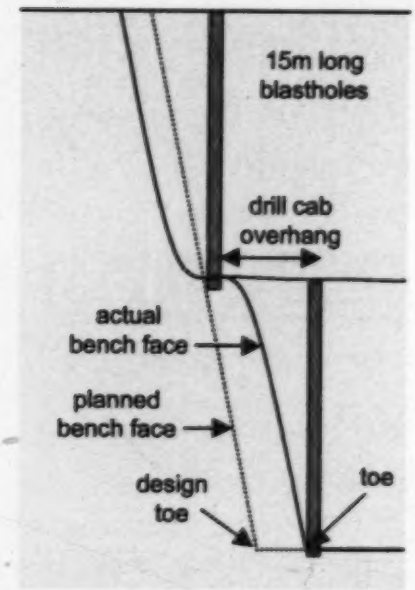

Figure 4-5: Offset of bench toe as a result of drill cab overhang

4.3.2 420 Bench

For the 420 bench the design was typically the following:

- 311mm hole diameter was used throughout;
- pre-shear design used;
- 50-70 kg 30/70 emulsion toe load;
- burden 5.5 m; spacing 4.0 m; subdrill 0-0.5 m.

As the trim shot did not provide satisfactory results for the 435 bench, a pre-split technique was implemented. Crest back break was reduced although the crest location was off by 5m in some sections. Borehole remnants were visible on the lower half of the face, however, for the majority of the wall a pre-split crack was not produced. Numerous small wedges were daylighted, creating dangerous potential failures that often had to be drilled and blasted down. There was also evidence of damage to the crest from heaving or cratering from the buffer row (Figure 4-6).

Figure 4-6: Damage to bench crest behind pre-split caused by buffer row

Unsatisfactory results were thought to occur from too high a toe load in the pre-shear, this is the reason for the load variation at this level (50 kg - 70 kg). Reducing the charge weight lead to poor breakage at the toe of the bench and therefore secondary blasting was required.

Due to the limitation imposed by the size of the D90KS drills, the guardrails were removed from both units prior to drilling on the 420 bench. This enabled the units to commence drilling on the design toe. To preserve the 420 catchment, no subdrill was used in the trim, buffer or first production row.

Another problem was also encountered on the 420 level. Double benching produces a "lip" between bench levels. The problems associated with the lip are two-fold: Firstly, the overall pit design cannot be maintained. This can be expensive, as the ultimate open pit depth can no longer be reached. Secondly, the lip counteracts the purpose of the catch bench, by causing falling rocks to bounce over the catch bench (Figure 4-7).

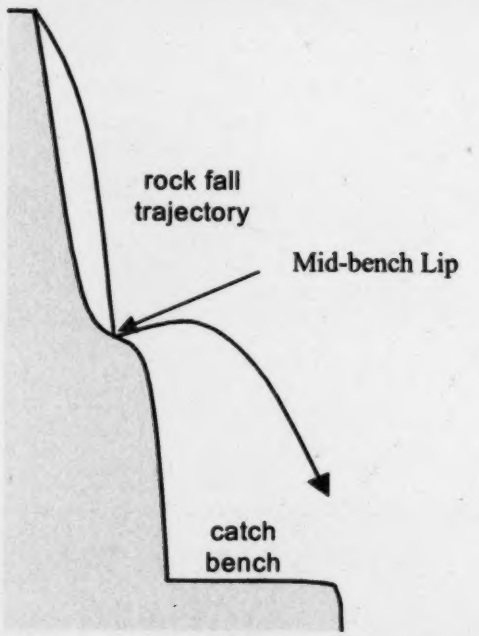

Figure 4-7: Mid bench lip from a double bench causing falling rock to bounce over catchment

4.3.3 405 Bench

For the 405 bench:

- 311mm hole diameter was used throughout;
- single pre-split row shot separately;
- 60-90kg 30/70 emulsion toe load for pre-split;
- spacing 2.5-3.0 m; sub-drill 0.5-1.0 m on pre-split.

The decision to implement a single pre-shear row fired prior to other shots in the pit sector was based on the damage seen on the final walls from the previous bench. The damage may not fully reflect the pre-shearing method employed. It is a combination of blasting damage caused by the production rounds in the pit. The 311mm blastholes contain a great deal of energy and there are indications that when production blasts are fired, gasses and vibrations were propagating considerable distances from the production rounds and causing the natural fractures and joints to dilate, disturbing the formation before the pre-split is fired. If the formation is already weakened, pre-splitting will not function properly because there will be paths for gasses to migrate from the pre-split holes into the final wall further damaging the wall rock to be left behind.

The spacing of the preshear row was reduced by 1.0-1.5 m compared to that used at the 420 m elevation. Air decking was used to achieve decoupling. However, so much damage was caused to the collar of the hole due to the subdrill on the previous bench, that the use of air decks caused severe cratering of the holes. The 60 kg holes had to re-loaded and re-blasted, as a pre-split crack did not form. A 75kg toe load produced a crack between the holes with minor cratering at the collar.

4.3.4 390 Bench

For the 390 Bench:

- 311mm and 270mm hole diameters were used;
- wall control design consisted of a single pre-shear row shot separately;
- 75 kg 30/70 emulsion toe load;
- spacing 3.0 m; sub-drill 1.0-1.5 m.

To reduce the amount of wall damage produced from production blasting, one D90KS drill was converted to drill a 270mm. Thus, wall shot hole diameters for this bench are both 270mm and 311mm.

The amount of overbreak decreased with this design. Fair to good walls resulted with remnant boreholes present over the extent of the wall. Some toes remained for secondary blasting.

4.3.5 375 Bench

For the 375 bench:

- hole diameter of 165mm used for pre-split;
- wall control design consisted of a single pre-split row shot separately;
- 311mm: 75 kg 30/70 emulsion toe load;
- 165mm: 44mm Dynosplit-C and Blastex toe load;
- spacing 2.0 m; subdrill 1.0-1.5 m on pre-split holes.

Although wall control results were improving, more dramatic results needed to be made in order to preserve the 390 catchment. A continuous explosive called Dynosplit C and a toe charge of Blastex chubs were introduced in the 165mm holes. Dynosplit C is a 44mm diameter packaged water-gel explosive and is a continuous, decoupled charge. Blastex is a 75mm diameter packaged emulsion explosive placed at the toe in order to reduce the prominent hard toe problems. The pre-split holes were initiated simultaneously with detonating cord on surface. The loading of pre-split holes is shown in Figure 4-8.

Results for the 375 bench were very encouraging. Borehole remnants are present over the extent of the wall and in most sections, the wall is nearly vertical. Wedge and plane failures have been greatly reduced as a result of the formation of a pre-split crack from hole-to-hole. However, in Domain I and III some small failures are still apparent (Figure 4-9).

Figure 4-8: Loading of pre-shear holes with Dynosplit - C and Blastex toe load

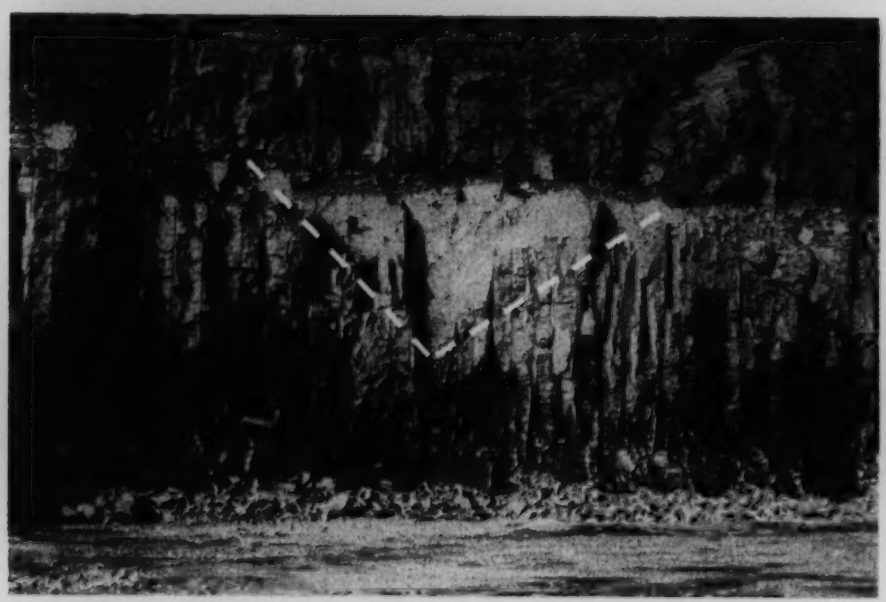

Figure 4-9: Structurally controlled failure in pre-sheared wall in domain III

4.3.6 360 Bench

For the 360 Bench:

- a hole diameter of 165mm was used;
- wall control design consisted of a single pre-shear row shot separately;
- Dynosplit C and Blastex;
- spacing 2.0 m, sub-drill 1.0 m;
- 30m double bench was pre-split.

The 30m pre-split resulted in an excellent wall however there are still some small structurally controlled failures at the crest of the bench.

4.4 Current Wall Control Blast Design

The current wall control blast design involves pre-shearing the entire 30m bench with smaller diameter (165mm) holes prior to drilling the trim blast. The trim blast is then drilled with the production drills (270mm).

The pre-shear holes are drilled 30m deep on 2m spacing. The holes are then loaded with a radially de-coupled charge. The product loaded is 44mm diameter Dynosplit – C. This product is a continuous watergel explosive containing a 25 grain detonating cord running the length of the product. The toe of the hole is loaded with two chubs of the packaged emulsion Blastex. The hole is loaded to a 3m collar and not stemmed to allow for further decoupling.

The use of this design has resulted in the effective pre-shearing of the rock. A photograph of the results is shown in Figure 4-10.

Figure 4-10: Final wall showing effective crack propagation between pre-shear holes.

The trim blast fired next to the pre-split consists of two rows that are loaded lighter and have less burden and spacing than the production rows. A general pattern layout is shown in Figure 4-11 and Figure 4-12.

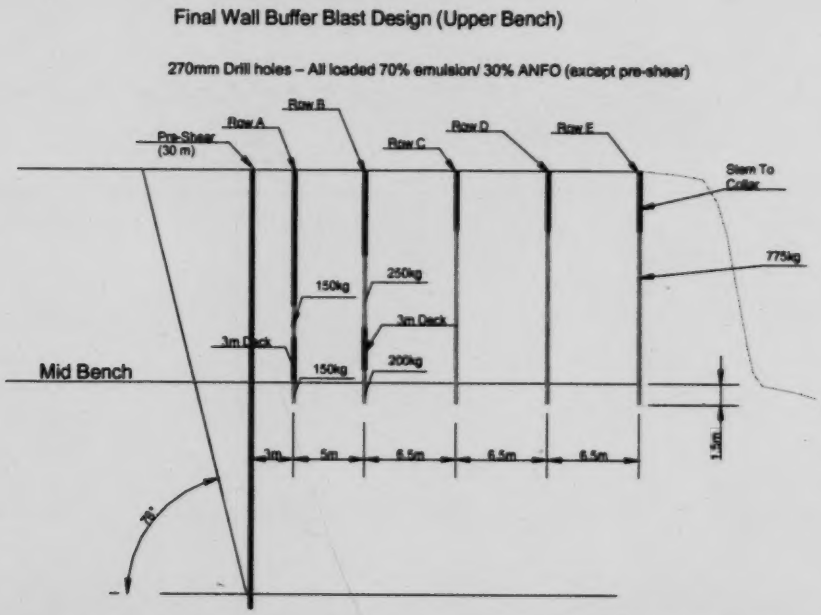

Figure 4-11: Section view of trim blast design for upper half of 30m bench

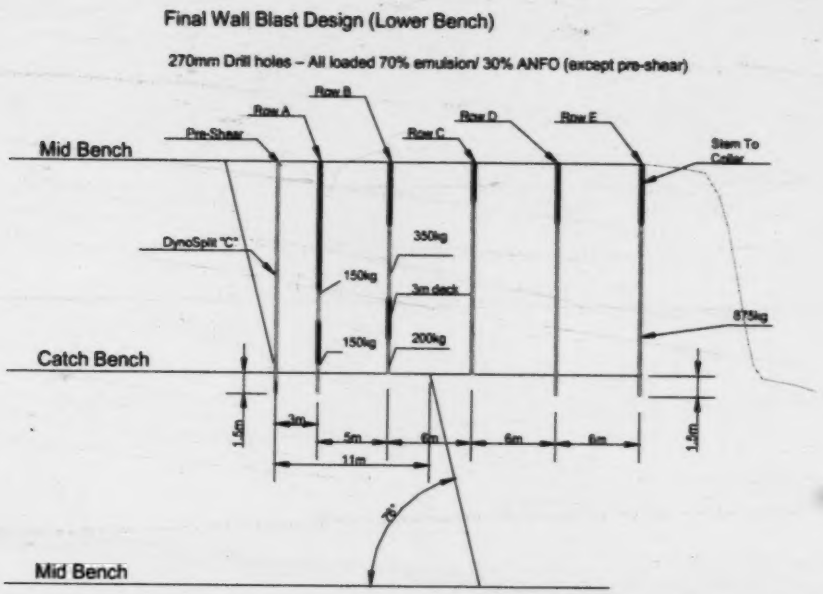

Figure 4-12: Section view of trim-blast design for lower half of 30m bench

5 INSTRUMENTATION

The blast monitoring system used at Ekati™ for this study consisted of several separate components. These individual components were: geophones for recording vibrations, pressure sensors to measure gas pressures in sealed boreholes, a data acquisition system to record the signals from the sensors, co-axial cables and a time domain reflectometry unit to record ground displacement, a notebook computer and software packages. Each of these components was an important tool in the acquisition or analysis of the experimental data.

5.1 Data Acquisition System

The voltage signals from the geophones and pressure sensors were recorded with an Instantel Mini-mate seismograph. The unit is a commercially available unit. The model used was configured for use with external sensors on eight channels. The sensors were wired directly to the unit through two four-channel universal break-out boxes which allowed for flexibility in the field with the lengths of monitoring cable. The Mini-mate samples at an overall rate of 64kHz. Depending on the number of channels selected the sampling rate per channel can be 8 or 16kHz.

The Mini-mate records the voltage signals produced by the sensors. It is capable of reading +/- 1.6V or 0 to 3.2V. The output from the sensors was adjusted with a voltage divider to ensure it would be within the range of the data acquisition system. The unit has a 1MB memory that can be downloaded into a PC via the serial port with the Instantel Blastware software package. The Advanced Module software package allows the user to configure the individual channels and perform detailed post blast analysis of the entire waveforms. It also allows the user the option of exporting the data in an ascii file for use in spreadsheets and other wave analysis software.

5.2 Geophones

The geophones used in this study were OYO Geospace 101LT 900Ω 14Hz horizontal or omni-directional models. This model was used based on discussions with people with extensive blast monitoring experience (Forsyth, 2000). The 101LT has a maximum peak to peak displacement of 4mm. This longer travel distance allows this model to be used for larger amplitude vibrations than other models.

The output voltage of the geophone is directly proportional to the strength of the magnetic field of the permanent magnet, the number of turns in the coil, the radius of the coil and the velocity of the coil relative to the magnet. Modern high sensitivity geophones have an output of 0.5 to 0.7 volts for a velocity of 1cm/s.

The geophone coil and springs constitute an oscillatory system with natural frequency in the range of 1 – 15hz. Since the coil continues to oscillate after the ground motion dies it is necessary to dampen the motion. This can be achieved by varying the shunt resistance since this changes the current through the geophone. If a geophone with a high resistance shunt is tapped lightly the coil will oscillate for some time. As the shunt resistance is decreased, the number of oscillations will decrease because of the increased damping until finally a point will be reached where a tap will just fail to produce an oscillation. At this point the geophone is critically damped.

The intrinsic sensitivity of the geophone is 0.042 V/mm/s. Due to the peak voltage limitations on the data acquisition system the output voltage had to be stepped down so it would not exceed ±1.6V. This was accomplished through the use of a voltage divider made with precision resistors. The resistance values for R1 and R2 are selected based on the maximum PPV expected and the resistors available. For this study a maximum PPV of 2500mm/s was chosen to ensure that the voltage limits of the data acquisition system would not be exceeded. The maximum voltage (V_{max}) output for a 101LT was calculated using the relationship.

Equation 5-1 $$V_{max} = PPV_{max} \times sensitivity$$

Where PPV max is the maximum expected PPV and sensitivity is the intrinsic sensitivity in volts/mm/s of the geophone.

The next step is to calculate the attenuation factor (A_f) required to reduce this maximum voltage to the maximum allowable. This is calculated with using the relationship:

Equation 5-2 $$Attenuation = \frac{V_{allowable}}{V_{max}}$$

The attenuation factor and the coil resistance (R_c) can then be used in Equation 5-3 to calculate the resistances R_1 and R_2. Due to the fact that resistors are only available in certain values there is some iteration required to get the desired attenuation.

Equation 5-3 $$Attenuation = \frac{R_2}{(R_2 + R_1 + R_c)}$$

The new sensitivity of the geophone (Ns) can then be calculated using Equation 5-4.

Equation 5-4 $$N_s = Attenuation \times Intrinsic\ Sensitivity$$

For this study $R_1 = 2200\Omega$ and $R_2 = 47\Omega$. A schematic of the circuit is shown in Figure 5-1.

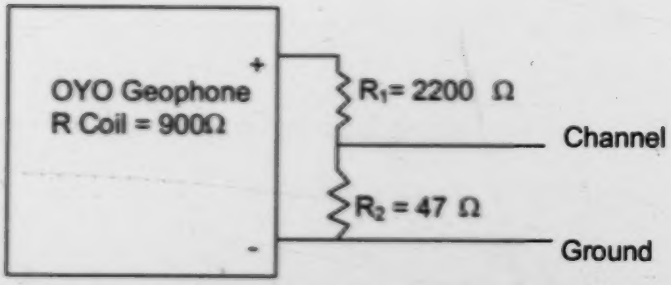

Figure 5-1: Configuration of resistors on geophone

The geophones and resistors were mounted as pictured in Figure 5-2. This unit was placed on the end of a placing rod that allowed for the geophone to be oriented towards the blast. The geophones were placed 7.5m deep in the holes and grouted into place with

Portland Cement grout which was mixed by hand in the field. Each geophone was grouted with one bag of grout.

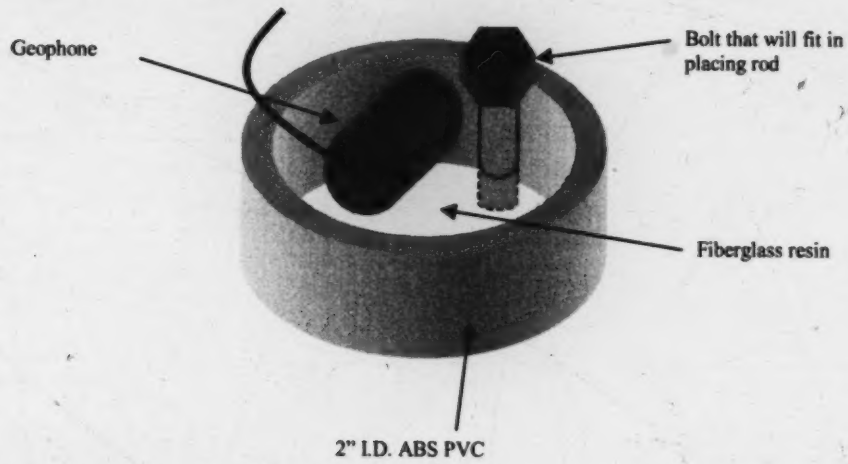

Figure 5-2: Geophone mounting system

5.3 Pressure Sensors

The sensor model utilized for this study was a Honeywell 186PC15DT differential pressure sensor. The pressure sensors contain sensing elements that consist of four piezoresistors buried in the face of a thin, chemically-etched silicon diaphragm. A pressure change causes the diaphragm to flex, inducing a stress or strain in the diaphragm and the buried resistors. The resistor values change in proportion to the stress applied and produce an electrical output. The sensor read bi-directionally through two ports (P1 and P2) up to +/- 137kpa gauge. Brent & Smith (1996) tested absolute and differential sensors in a side by side test and found that there were no differences in the resulting traces. For the sensor to operate an excitation voltage from 7-16V DC is required. For this experiment the excitation voltage was supplied via a 9V battery mounted with each sensor. The output from the pressure sensors had to be modified in order for the peak voltage to not exceed the 3.3V limit of the data acquisition system. As with the geophones, the output voltage was reduced through the use of resistors. To set the zero reading to 1.6V, R_1 was 5700Ω and R_2 was 4000Ω. A plot of the resulting voltage vs.

differential pressure output is shown in Figure 5-3. Due to the voltage output at zero pressure the sensor was connected to the Mini-mate to read from 0 to 3.2V.

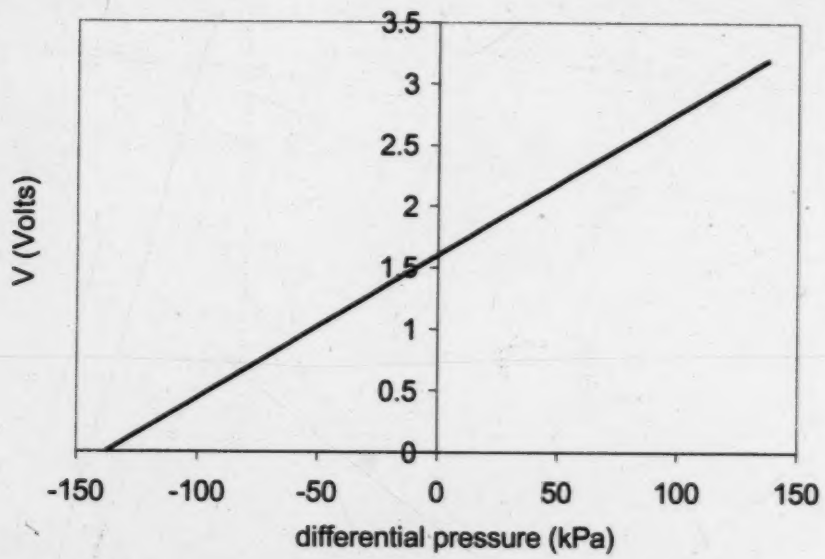

Figure 5-3: Voltage output from pressure sensor

The pressure sensor was installed with the P1 port venting to the atmosphere and the P2 port reading the pressure in the sealed borehole. The hole was sealed over the top 2m with expanding foam borehole plugs and drill cuttings. The configuration of the pressure monitoring hole is shown in Figure 5-4.

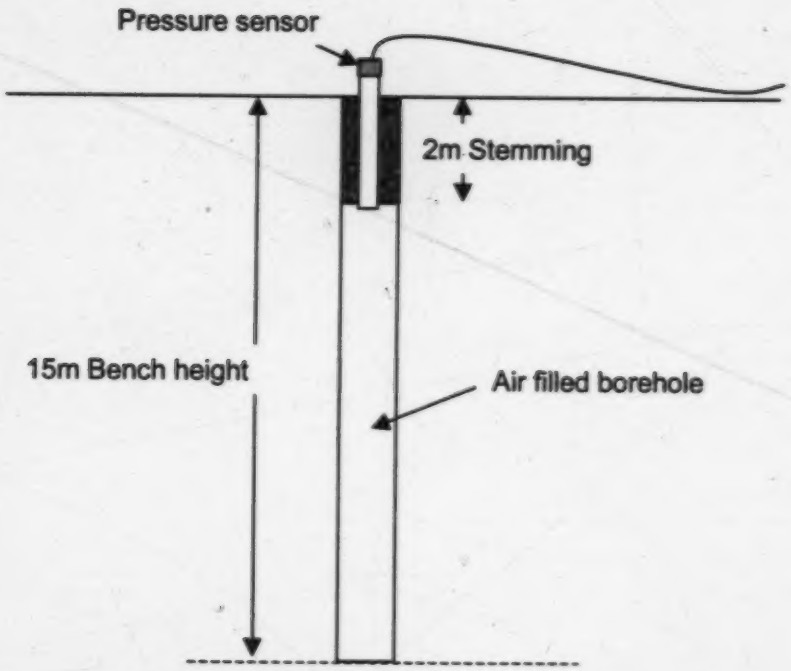

Figure 5-4: Pressure sensor setup

5.4 Time Domain Reflectometry

The time domain reflectometry system consisted of 2 coaxial cables per hole, a TDR measurement unit and a notebook computer and software. The instrument used to read the cables was a Tektronix 1502C metallic cable tester. Each waveform was downloaded into the notebook computer through the SP232.exe software supplied with the instrument. The data was then exported to an ascii file for analysis and plotting with a spreadsheet program.

The cable used was RG-57 coaxial cable. For this cable the propagation velocity was measured to be 2.4×10^8m/s. In each monitoring hole two cables were installed to ensure readings were accurate. The cables were grouted into place down the entire length of the hole. Cables were then read before and after the blasts.

6 BLAST MONITORING

Three blasts were monitored at the Ekati™ mine during August to October 2000. The blasts were the 345-38 production blast, 345-40 wall control blast and the 330-45PS pre-shear. The blast numbering system is as follows: the first number, in this case 345 denotes the bench elevation above sea level in metres that the shovels will load the blasted muck from. The second number is the number of the blast at that elevation. The 345-38 blast was the 38th blast on the 345 bench, and was drilled from the 360 bench. The 345-40 blast was also drilled from the 360 bench and was the 40th blast on the bench. The pre-split blasts are drilled every second bench to accommodate the 30m double bench. A plan view of the pit showing the location of each blast is shown in Figure 6-1.

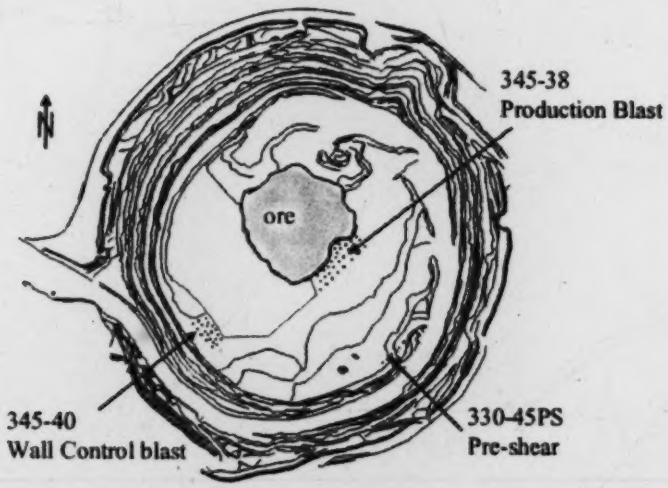

Figure 6-1: Plan view of Panda pit showing blast locations

6.1 Production Blast (345-38)

6.1.1 Blast Layout and Monitoring Objectives

On August 10, 2000 the 345-38 production blast was shot. The blast was monitored to gather data to: (1) develop PPV versus scaled distance for the site, (2) determine if explosive gases penetrate 5m beyond the last row of production holes, (3) determine if

rock dilation or new rock fracturing occurs beyond the penultimate row of holes, (4) assess whether TDR technology can be used to identify new fractures or dilation of pre-existing discontinuities, (5) document rock mass response from a production blast for later comparison with a wall control blast and (6) measure the p-wave velocity of the rock mass for use in calculating dynamic rock properties.

The blast pattern was drilled on the typical 6.5m by 7.5m staggered production pattern with 270mm holes and 1.5m of sub-drill (Figure 6-2). Each hole was loaded with 775kg of 70% emulsion / 30% ANFO explosive at a density of 1.15 g/cc. The pattern was along the contact of the previously mined kimberlite pipe, as a result the face of the blast was non-uniform. The face of the blast was also not entirely clear of muck. The hole locations, free face, initiation sequence and monitoring locations are shown in Figure 6-2. A pre-blast photograph showing the blast perimeter and instrument arrays is Figure 6-3.

The blast was shot in a flat echelon pattern with a delay of 340ms between rows and 65ms between holes as pictured in Figure 6-2. Other than small adjustments in the front row this timing was used for the entire blast.

The blast is located in the geologic domain III. The jointing in the area consists of four sub-vertical sets and two sub-horizontal sets. The joint spacing for these sets ranges from 2 to 6m, and the joint length is from 5.1 to 6.5m.

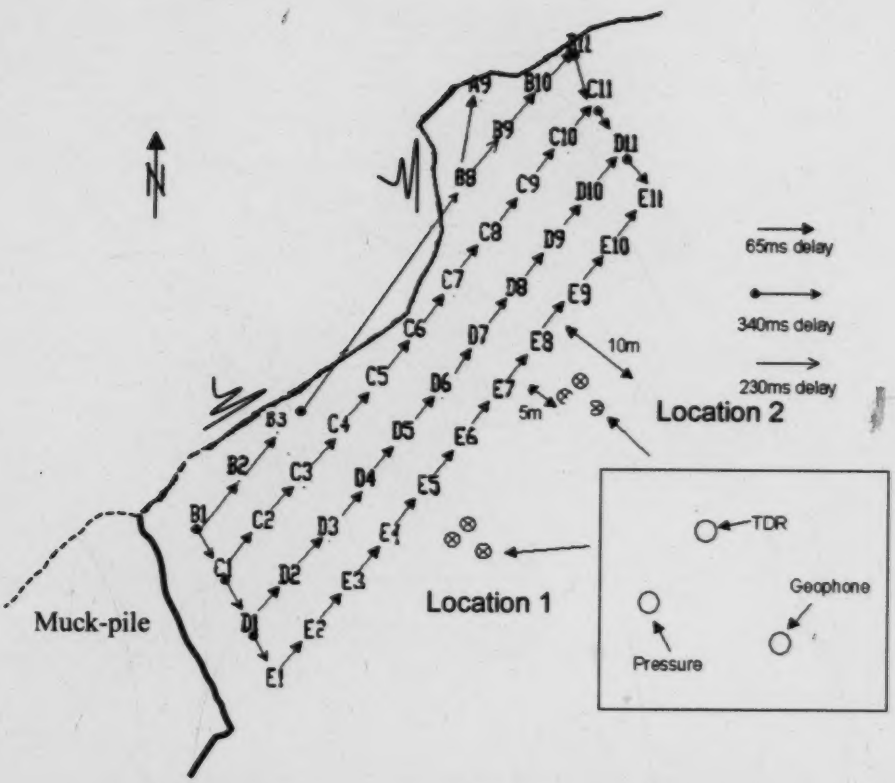

Figure 6-2: 345-38 Production blast pattern design showing monitoring locations, initiation sequence and free face

Two arrays of instrumented boreholes were located near the blast. The instrumentation holes were 100mm in diameter, drilled with an air track drill. The pressure sensor holes (Figure 6-2) and the TDR holes were drilled 15m deep and the holes for geophones were drilled 7.5m deep. The monitoring holes at location 1 were easily drilled with little or no re-drilling required. The intact rock was within one metre of the bench surface. The holes at location 2 were not as easily drilled. There were several metres of broken rock to drill through before hitting intact rock. As a result, one of the monitoring holes was moved by five metres in order to eliminate drilling difficulties, and the TDR hole at location 2 was not drilled.

Figure 6-3: 345-38 Production blast and instrument locations

6.1.2 Blast Observations

The blast was initiated simultaneously with a kimberlite blast on the bench below. The much smaller vibrations recorded at the instrument arrays allowed for easy differentiation of the vibrations from the kimberlite and the 345-38 production blasts.

There were varying degrees of damage at different distances behind the blast (Figure 6-4). A post blast photograph is shown in Figure 6-5. Back break was approximately 5m along the back of the blast which is typically expected and accounted for in the blast designs. This was based on the proximity of the instruments to the crest after the blast (Figure 6-6). There were also fine cracks extending back as far as 25m along the bench surface behind the blast. These cracks were linear and appeared to be related to be from displacement along joints.

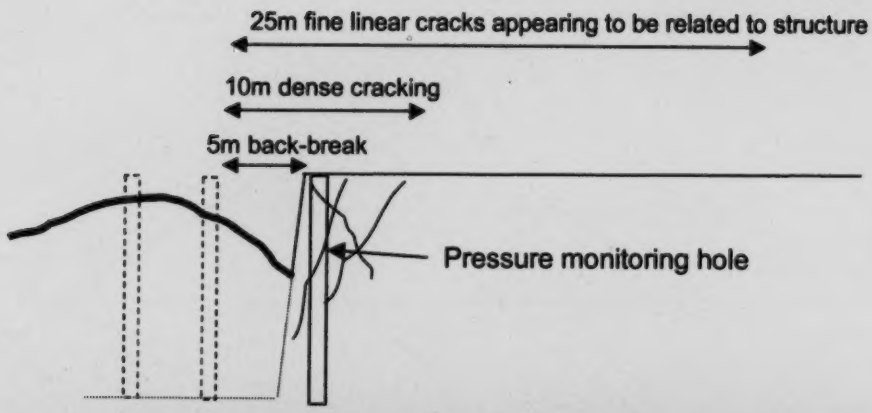

Figure 6-4: Cross section showing varying degrees of damage observed behind blast

Figure 6-5: 345-38 Production blast muck pile

Figure 6-6: Back break plus rock fractures created by the 345-38 blast (pressure sensor at array #1 was 5m off last row).

6.1.3 Gas Pressure Data

The pressure sensor at instrument array #1 functioned properly and recorded a maximum pressure drop or under-pressure of 67 kPa (gauge) at a time of 1.4s. This sensor did not record an overpressure. The pressure sensor at location 2 malfunctioned immediately and did not produce a reading. The pressure versus time record from pressure sensor 1 is shown in Figure 6-7. At a time of approximately 1.9 seconds, the pressure sensor began to malfunction. It appears that the high vibration levels encountered broke the contact with the power source. The design of the pressure sensors was slightly modified for subsequent blasts to prevent this from recurring. The small pressure spikes in the period 0 to 1.4s are thought to be electrical noise as there is no correlation to the vibration trace.

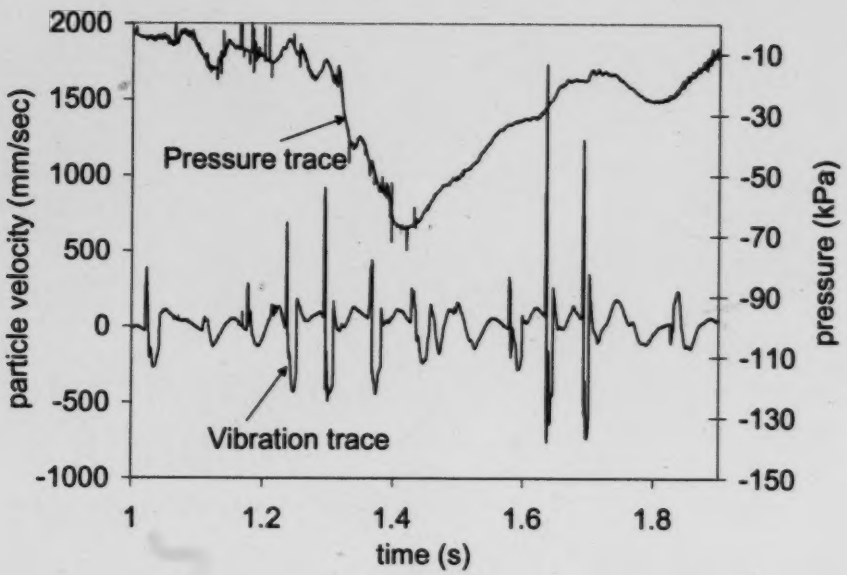

Figure 6-7: Gas pressure and vibration trace from 345-38 production blast 5m behind last row at instrument array # 1

6.1.4 Vibration Data

The geophone at each instrumentation array gave excellent readings. The blast vibration traces are shown in Figure 6-8 and Figure 6-9. The highest PPV reading on array 1 was 1730mm/sec. This reading was from a charge weight of 775kg at a horizontal distance of 11m. The highest reading on channel 2 was 1620mm/sec. This was from a charge weight of 775kg at a distance of 10m from the geophone. The individual spikes on the waveform correspond to the detonation of individual blastholes.

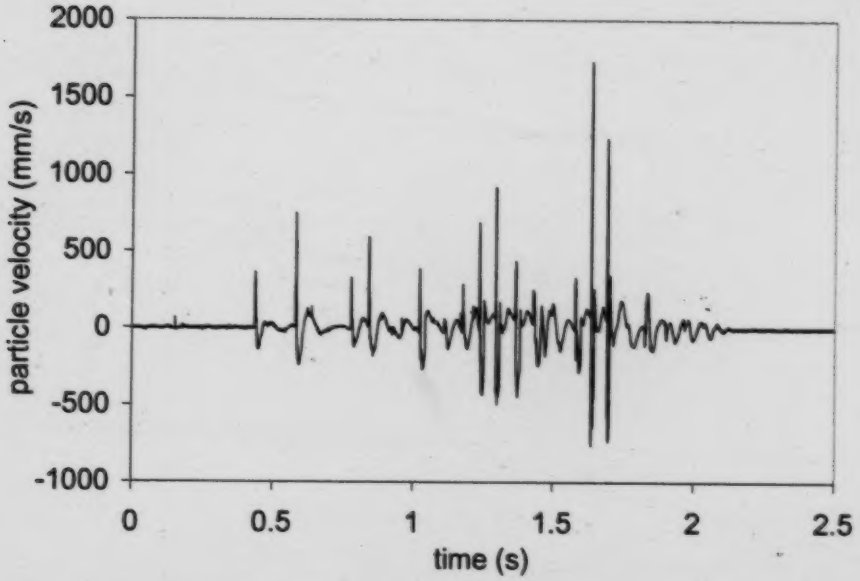

Figure 6-8: Vibration trace from instrument array #1 for blast 345-38

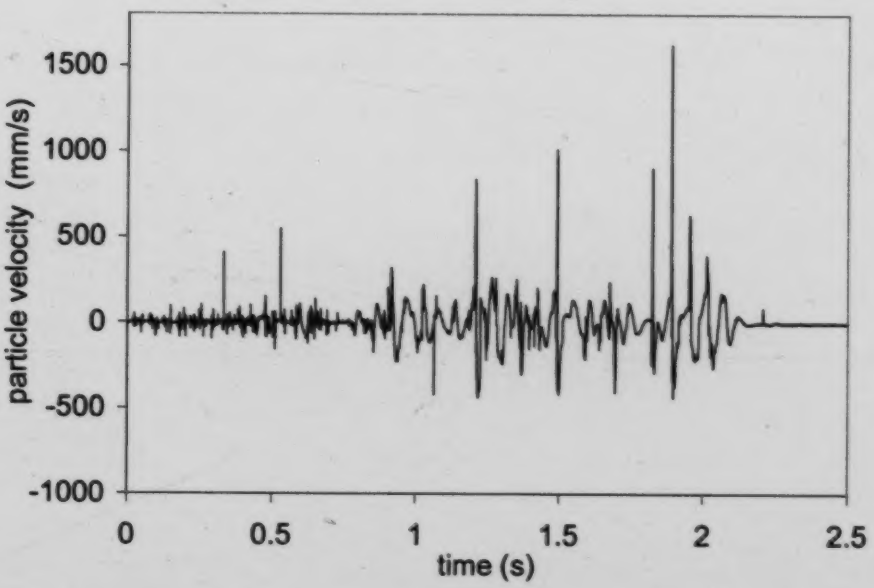

Figure 6-9: Vibration trace from instrument location #2 for blast 345-38

6.1.5 Time Domain Reflectometry Data

The TDR cables installed behind the blast were read before and after the blast. A comparison of the traces is shown in Figure 6-10. The plot compares the reflection coefficient in millirho to the distance along the cable. Changes in the reflection coefficient indicate that there has been a change in the cable. Based on the readings it appears both cables in the hole were disturbed at a depth of 2.5m. It is not known why the reading in one cable increases and the other cable decreases. There are several other fluctuations in the readings at depths greater than 2.5m, however, the reliability of these readings is questioned because the degree of damage to the cable at 2.5m is unknown. Attempts to lower borehole camera down the pressure sensor hole found the hole closed at a depth of approximately 2.5 m.

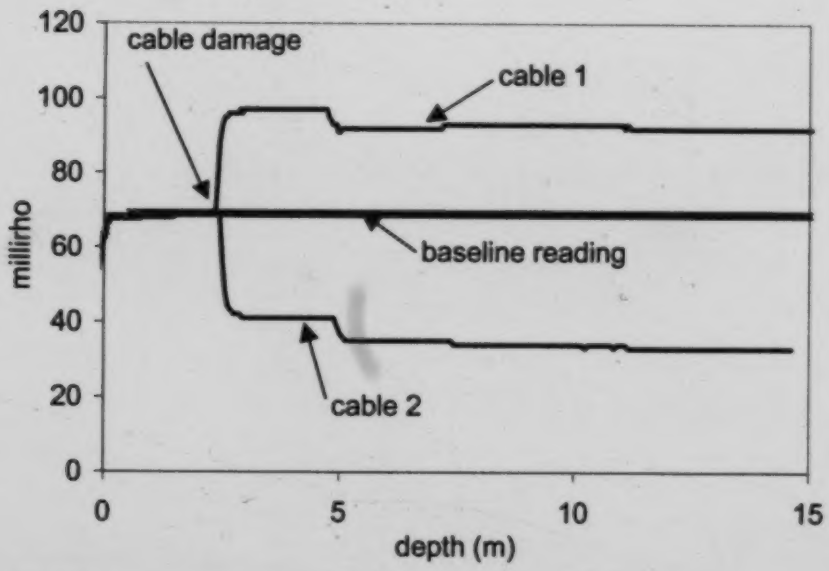

Figure 6-10: Time domain reflectometry data from TDR cables at instrument array #1.

6.2 Wall Control Blast (345-40)

6.2.1 Blast Layout and Monitoring Objectives

The 345-40 wall control blast was shot on August 15th, 2000. The pre-split blast had been shot prior to the installation of the instrumentation and was not monitored. A plan view of the blast, the initiation sequence and the instrument locations are shown in Figure 6-11. The blast was loaded with the same design as discussed in section (4.3.7) with two more production rows added on the front. It should be noted that the blast was choked on the north free face by muck from a previous blast that had not been entirely excavated (Figure 6-11). This blast was monitored to (1) develop PPV vs. scaled distance for wall control blasts, (2) determine if explosive gases penetrate beyond the pre-shear fracture, (3) determine if rock dilation or new rock fracturing occurs beyond the pre-shear, (4) assess whether TDR technology can be used to identify new fractures or dilation of pre-existing discontinuities, (5) compare rock mass response to that of production blasts and (6) continue to measure the p-wave velocity of the rock mass for use in calculating dynamic rock properties.

The blast was loaded with 70% emulsion / 30% ANFO bulk explosive. The first four rows (C-F) were loaded with 775kg per hole. The B row was loaded with 500kg per hole. The A row (or buffer row) was loaded with a 200kg deck in the toe, 5m of crushed gravel and a 150kg deck and then stemmed to the collar with crushed rock. The blast was initiated in a flat echelon pattern. The first four rows were initiated in the same manner as the production blasts with 340ms between rows and 65ms between holes. The second last row or "B row" had a decreased inter-hole delay of 50ms, and the last row or "A row" had an inter-hole delay of 35ms.

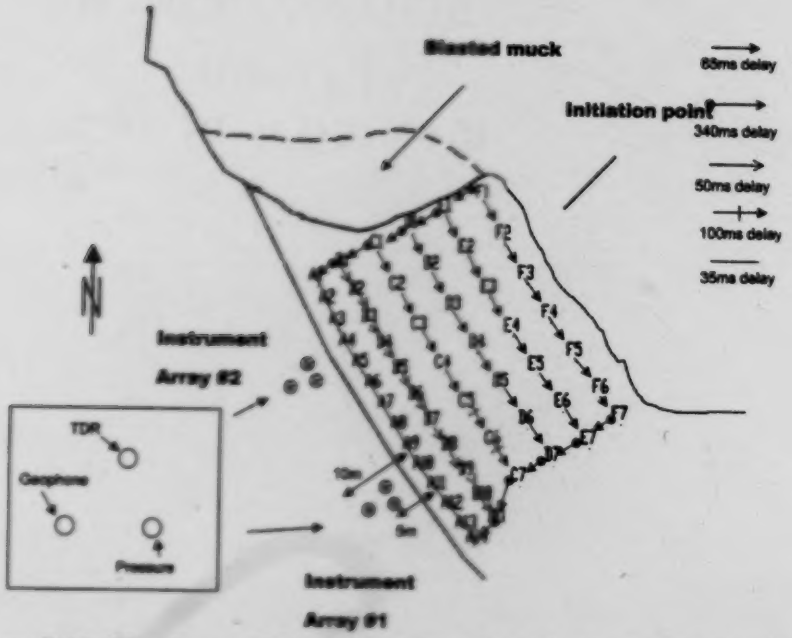

Figure 6-11: Blast layout, tie in and instrument location for the 345-40 wall control blast

The blast was located in a very wet region of the pit. The main reason for the water was drainage from an abandoned exploration decline that had been mined through several benches above. The blast had been loaded and then left eight days before being blasted. It is likely that the explosives would have suffered some degradation in that time. A large amount of water was draining across the bench into the pre-split fracture and not emerging on the bench below. Over 70% of the holes were recorded as wet on the explosives loading sheets. Some of the instrumentation holes were also wet within a few hours of being drilled.

The blast pattern was located in the geologic domain III in the southwest corner of the pit. The jointing in the area consists of four sub-vertical sets and two sub-horizontal sets. The joint spacing for these sets ranges from 2 to 6m, and the joint length is 5.1 to 6.5m.

6.2.2 Blast Observations

The blast was affected by being choked on one of two free faces. There was a considerable amount of rock thrown back onto the bench from the back row of holes, and

some evidence of damage in the back corner of the blast (Figure 6-12). There were also small wedge failures along the crest (Figure 6-13). In the southwest corner of the blast the rock face exposed showed the rock mass was greatly disturbed (Figure 6-14).

Figure 6-12: Damage and rock on catchment in the back corner of blast

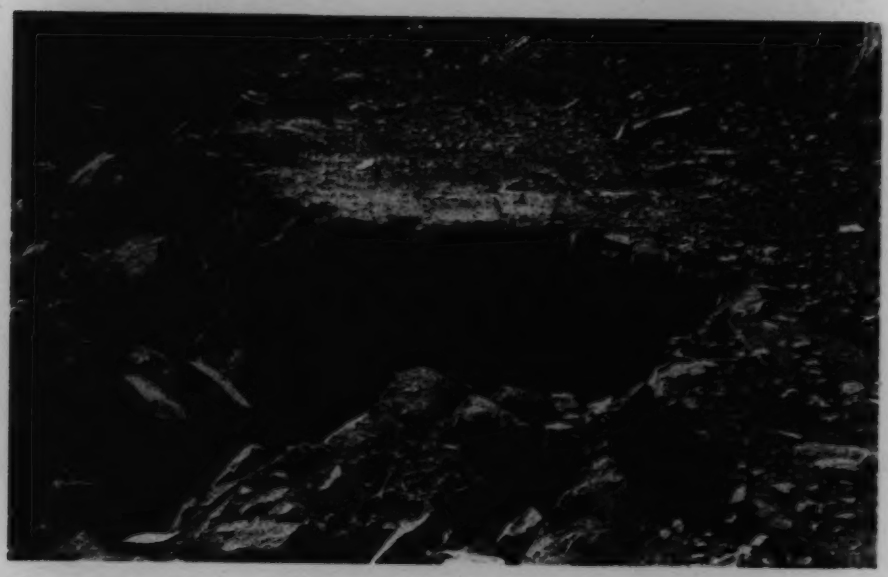

Figure 6-13: Structurally controlled back-break on 345-40 blast, and damage to rock mass

Figure 6-14: Disturbed rock mass in southwest corner of blast

6.2.3 Vibration Data

As in the previous blast, the geophones both provided excellent results. The full waveforms are shown in Figure 6-15 and Figure 6-16. The first hole was detonated at time zero seconds. The PPV values were generally significantly lower than the production blast. The exception to this is at instrument array #2 when the last row was firing. It appears that the confinement from the muck-pile on the north side of the blast and/or the water in the pre-shear fractures caused higher vibrations.

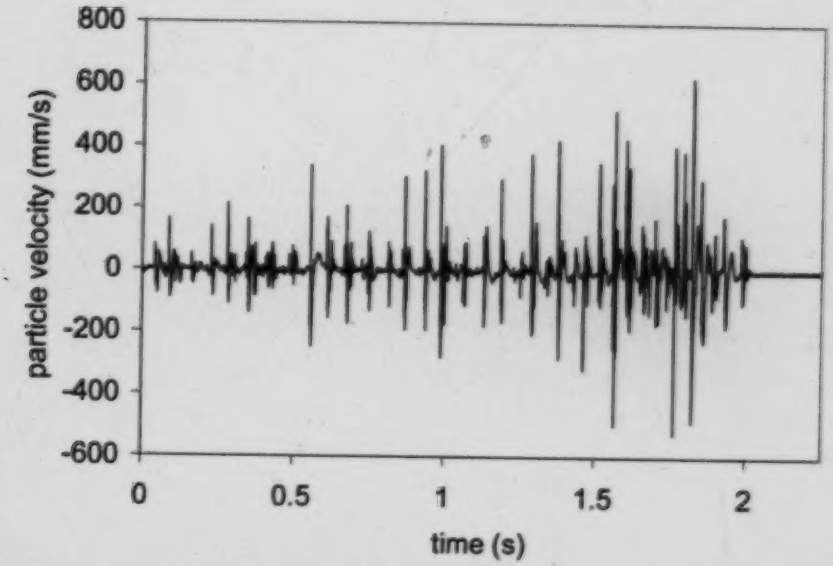

Figure 6-15: 345-40 vibration trace instrument array #1

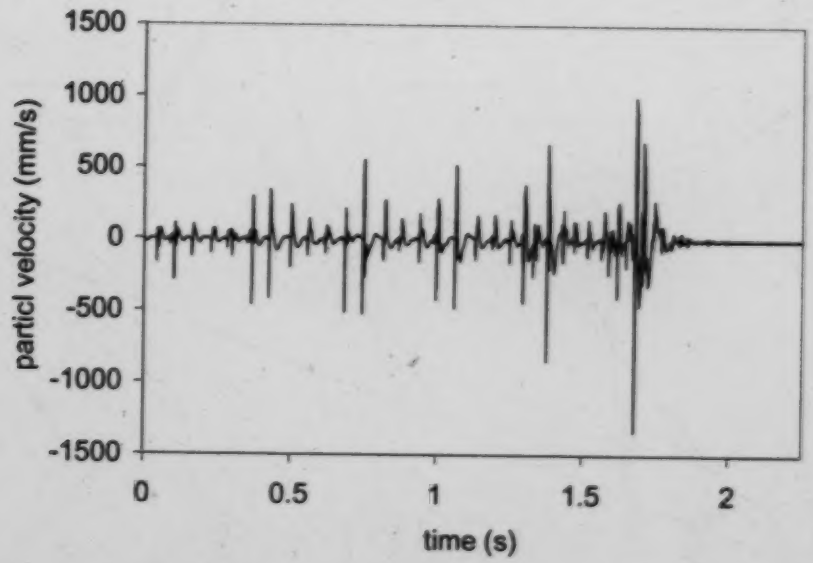

Figure 6-16: 345-40 Vibration trace instrument array #2

6.2.4 Gas Pressure Data

Immediately prior to the 345-40 blast the pressure sensor at location 1 ceased reading. Due to time constraints it was not possible to fix the sensor before the blast. The sensor at location 2 provided an excellent reading. As in the 345-38 production blast, under-pressures were recorded. The largest pressure drop was 70kPa at a time of 1.8s.

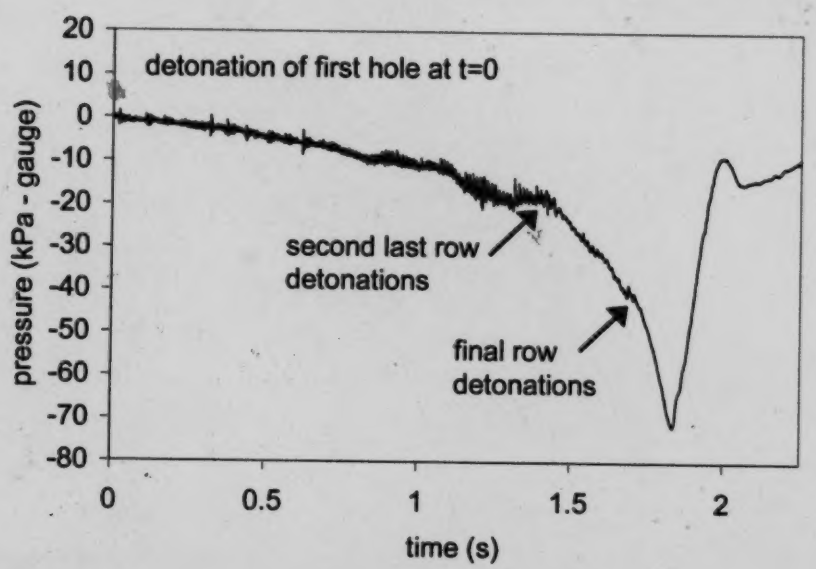

Figure 6-17: Gas pressure data 345-40 location 2

6.2.5 Time Domain Reflectometry Data

The TDR cables installed behind the blast were read before and after the blast. A comparison of the traces for each location is shown in Figure 6-18 and Figure 6-19. Based on the readings it appears that at both locations the cables in the holes were disturbed at a depth of 2-3m. It is not known why the reading at location 2 increases in one cable and decreases in the other cable. There are several other fluctuations in the readings at depths greater than 2-3m, however, the reliability of these readings is questioned because the degree of damage to the cable at 2-3m is unknown.

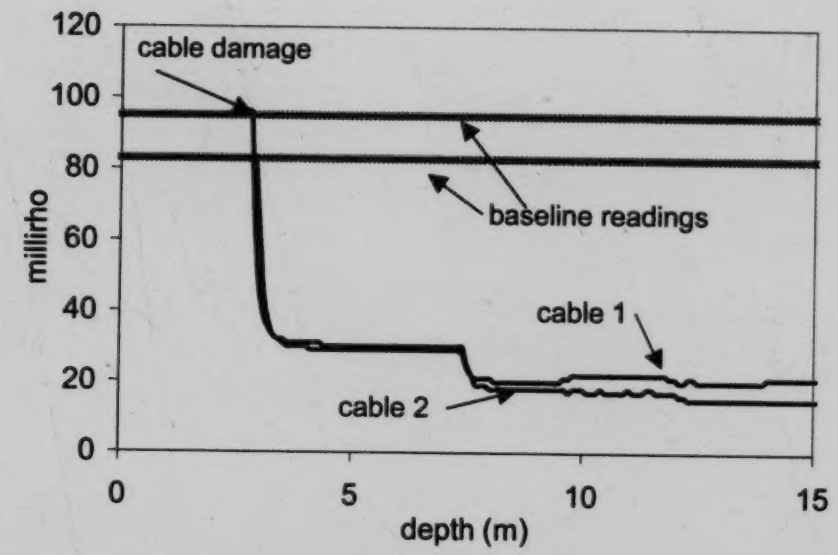

Figure 6-18: Time domain reflectometry data location 1

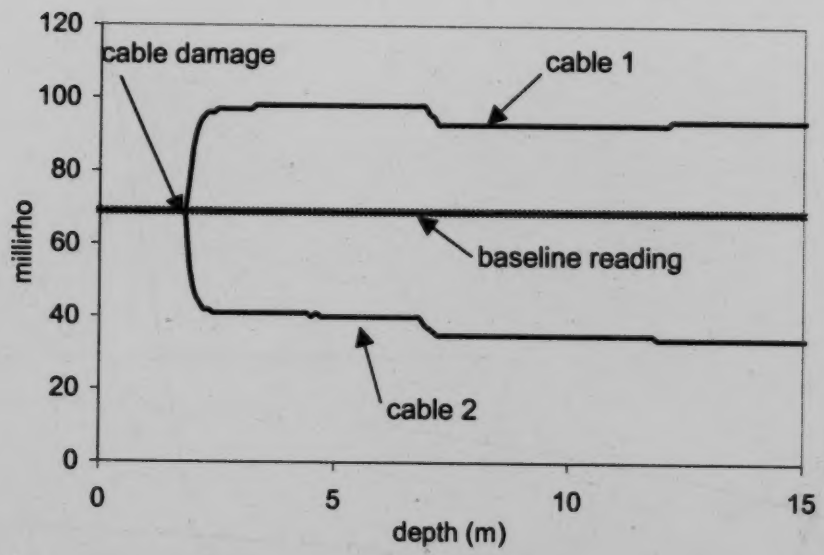

Figure 6-19: Time domain reflectometry data from location 2

6.3 Pre-shear and Wall Control Blast (330-45PS & 345-50)

6.3.1 Blast Layout and Monitoring Objectives

On October 12, 2000 the 330-45PS pre-shear was blasted. The blast was a 30m pre-shear for the double bench from the 360m elevation to the 330m elevation. The blast was monitored to: (1) measure the vibration level from the pre-shear blast, and (2) detect gas penetration 5m from pre-shear. Due to equipment limitations the holes drilled were 165mm in diameter instead of 100mm. This resulted in the amount of grout required for the installation of TDR cables to be excessive. Therefore the TDR cables were not installed for this blast. The blast was drilled with 100mm holes on 2m centers. Each blasthole was loaded to 4m below the surface with 44mm diameter Dynosplit-C. The blast was initiated with the 345-50 trim blast beside it. The pre-shear was detonated from the surface lines on the back row of the trim blast, which detonated 500ms before the in-hole delays. A plan view showing the two blasts and the instrumentation holes is shown in Figure 6-20. Photographs taken before and after the pre-shear blast are shown in Figure 6-21 and Figure 6-22.

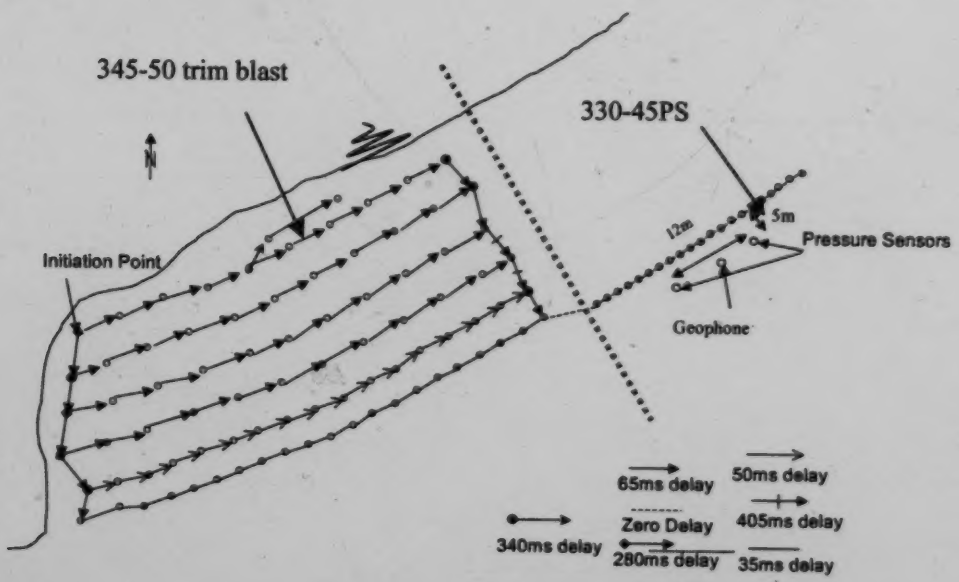

Figure 6-20: Plan view of 330-45PS pre-shear and 345-50 wall control blast

The blast is located in structural domain II. There are 3 sub-vertical joint sets, 2 sub-horizontal and one joint set dipping into the pit wall at 42 degrees. Generally the walls in this section of the pit experience less over-break than other sections of the pit.

6.3.2 Blast Observations

The pre-shear blast successfully generated a fracture between holes along the surface. Photographs taken before and after the blast are shown in Figure 6-21 and Figure 6-22. There was some cratering at the surface and slight displacement visible along joints crossing the pre-shear line. At location 2 there was significantly greater disturbance on the surface. After the blast, several large rocks were piled over the sensor location that likely destroyed the transducer and made it unrecoverable.

Figure 6-21: Photo of the 330 bench after drilling the 330-45PS 165mm blastholes and prior to loading the explosives

Figure 6-22: Photo of the 330-45PS blast after detonation

6.3.3 Vibration Data

The vibration levels from the adjacent wall control blast did not exceed 300mm/sec, and only on 2 occasions were the values over 200mm/sec. The pre-shear detonated at 1677ms and resulted in a PPV of 685mm/sec. The complete vibration trace is shown in Figure 6-23. The first hole of the adjacent trim blast was detonated at time zero.

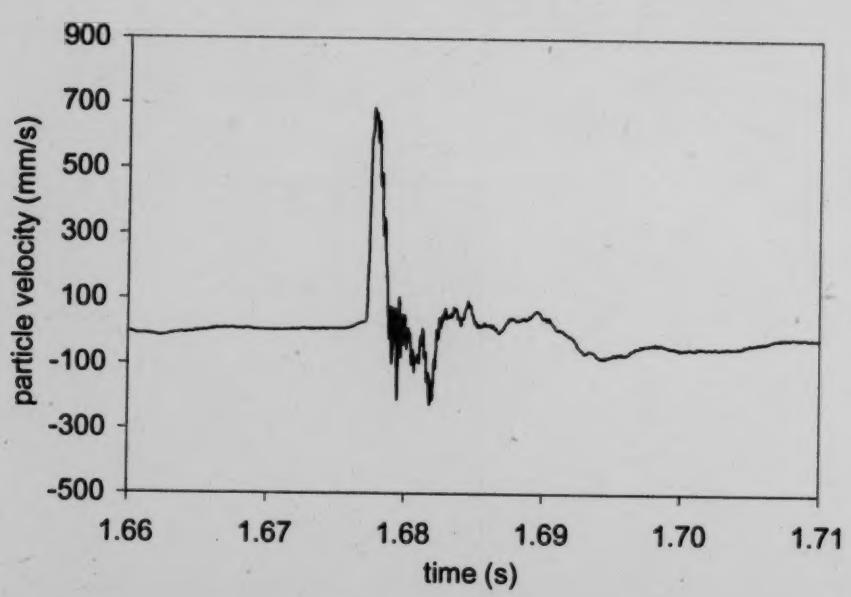

Figure 6-23: Vibration trace from 330-45PS Pre-shear blast 5m away from holes

6.3.4 Gas Pressure Data

The gas pressure sensors both gave readings from the pre-shear blast. The sensor at location 1 recorded an over-pressure of 67kPa. The sensor at location 2 did not pick up any gas penetration or record any significant under pressures. It appears as though the sensor may have been damaged at some point during the blast. After the blast the sensor at location 2 was buried under a pile of several large rocks. The sensor traces are shown in Figure 6-24 and Figure 6-25.

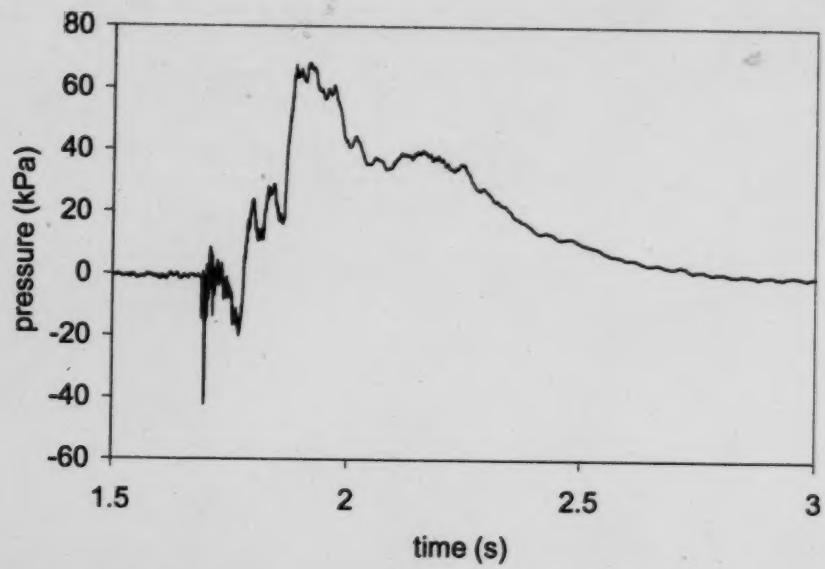

Figure 6-24: Gas pressure trace location 1

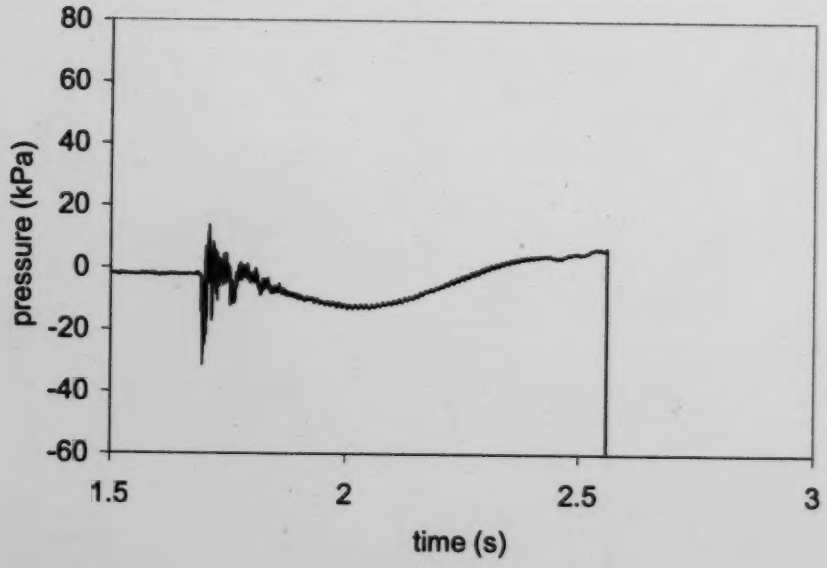

Figure 6-25: Gas pressure trace location 2

6.4 Conclusions Regarding Instrumentation for Blast Monitoring

The monitoring program carried out at the Ekati™ Mine provided several insights on blast monitoring in large open pits. Each technique used had varying degrees of success. There are several criteria that were considered in evaluating each system. (1) quality of data, (2) reliability, (3) cost, (4) durability, (5) ease of use and (6) applicability of data gathered.

The geophones proved to be an excellent tool for blast monitoring. All of the installations recorded consistent data throughout the blasts. As the closest fully loaded production blastholes (11m) were detonating there was some evidence suggesting that the dynamic range of the geophones was exceeded. While there may be some uncertainty in the readings at the higher vibration levels and frequencies, the increased cost of accelerometers prohibits their use. From the vibration traces, it is possible to identify each hole detonating and the respective PPV. This record proved invaluable in the analysis of the gas pressure data, the development of site specific scaled distance laws and the determination of dynamic properties of the rock mass.

The pressure sensors also proved to be a valuable tool for blast monitoring. The sensors that did not malfunction gave high quality readings that provided valuable information about the blast. When the sensors failed the cause appeared to be a loss of power from the battery leads. In the future the method of mounting the battery should be modified. It would be best to mount a battery holder on the outside of the cap. This would hold the battery rigidly in place, and allow for easy connection of the battery to the sensor shortly before the blast. This will eliminate having to thread the cap onto the pipe after connecting the battery, therefore, reducing the chance of breaking the contact.

For this study the borehole camera did not prove to be as useful as expected. There were several reasons for this:

- camera cannot be used in water-filled boreholes,
- in some cases observation holes were closed off after the blast,

- the equipment and generator were difficult to move to monitoring locations after blasting, due to lack of vehicle access or rough / wet terrain, and
- poor weather (freezing rain, snow).

While the borehole camera data would have helped in the study it was not easy to handle the camera in the field. One person could not handle the camera components and even with two people, it was difficult to carry the five separate components any distances over the broken rock on the bench. The site conditions need to be evaluated prior to using this type of equipment. A lighter unit with a self-contained power supply would likely be better in this environment.

The time domain reflectometry cables also provided readings for each blast. In both blasts monitored, the cable readings showed that they were severed or badly damaged within 3m of the bench surface. The time, materials and effort that were involved in installing the TDR were quite significant, and the resulting data did not provide much insight into the blast damage mechanisms. This technique would prove useful if one was investigating the effects of blasting at larger distances or the effects on a structure of known location such as a fault.

The Instantel Mini-mate data acquisition system performed well under these conditions. Temperatures below freezing were encountered with no significant effects on the instrument. In all three cases the blasts were monitored with four channels (two geophones and two pressure sensors). The sampling rate was 64kHz or 16kHz per channel. The sampling rate produced high quality data that was suitable for any subsequent analysis that was done. The data was easily downloaded to a laptop for storage and analysis.

Visual observations were also an important in this study. The extent and degree of damage could be easily observed after the blasts, however the damage mechanism (i.e. gas penetration or heaving etc.) is not necessarily discernable by looking at the damage. Often damage is assumed to be gas penetration when in fact it may be heaving.

Reference points were very important when looking at the back break from the blast. In any further work visual observations should be as detailed as possible.

The selection of blasts to be monitored was influenced mostly by the production schedule at the operation. In each case the monitoring systems were damaged enough that re-using them would not be feasible. There was also some difficulty encountered when drilling the monitoring holes in the region behind the pre-shear after it had been blasted.

In the future the possibility of measuring the effects of blasting on a fault or major structure should be considered. While there are not currently any critically oriented faults in the Panda Pit, it is possible that one may be encountered in the future or in subsequent pits. By installing instruments on a fault that transects a blast pattern it may be possible to record the effects on the fault. Such a system would involve drilling monitoring holes that intersected the fault at two or more distances from the blast. This could be accomplished through careful mapping, surveying and drilling. The use of geophones, TDR cables and the pressure sensors is recommended. Another aspect that could be considered for this scenario is the use of some type of extensometers, similar to that done by Holmberg and Maki (1982).

7 INTERPRETATION OF RESULTS

The blast monitoring data was analyzed to: (1) establish a scaled-distance relationship to predict vibration levels, (2) calculate the dynamic properties of the rock mass, (3) apply PPV-based damage criteria, (4) assess the damage potential of blast gases, and (5) compare rock mass damage from production blasts with wall-control blasts.

With a damage criteria established, the next phase was to compare this to the gas pressure data. The data were then correlated with field observations to confirm the damage criteria, and then to predict the break radius and damage radius around a borehole with various charge weights. These data were then used to analyze existing blast designs.

The vibration amplitude is a function of the charge weight per delay, rock type, scaled-distance and charge geometry. The data were then used to develop a scaled distance law that relates the PPV to the proximity of the charge.

As the monitoring was done from more than one distance, it was possible to measure the compressive and shear wave propagation velocities of the rock mass. From these velocities the dynamic properties of the rock mass were calculated using the theory of elasticity. These values, along with other properties of the rock were then used to calculate the PPV levels for fresh fracturing and incipient damage.

By using the PPV – distance relationships and the damage criteria it is possible to predict the break radius and the damage radius around a borehole. This is all based on the assumption that the same explosives, hole size and rock type are used in the calculation as were used in developing the relationships.

7.1 PPV vs. Scaled Distance Relationships

Typically blasting vibrations are back analyzed to establish empirical relationships between the PPV and a scaled distance term. The scaled distance combines the effects of

charge weight per delay on the vibration levels at different distances from the blast (Dowding, 1985). These relationships are in the form of Equation 7-1.

Equation 7-1 $$PPV = K\left(\frac{W^{\alpha}}{R^{\beta}}\right)$$

Where:

PPV = peak particle velocity (mm/sec)

W = charge weight of explosive per delay (kg)

R = distance between the charge and the point of interest (m)

K, α, β = site specific constants

Equation 7-1 is often expressed as (Dowding, 1985):

Equation 7-2 $$PPV = K\left(\frac{W^{n}}{R}\right)^{-\beta}$$

For square root scaling n =1/2 and for cube root scaling n=1/3. The term R/W^n is referred to as scaled distance. Square root scaling on the charge weight works best for long cylindrical charges and cube root scaling for spherical charges (Dowding, 1985). By plotting log(PPV) versus log(scaled distance) it is possible to calculate the constants K and β. Equation 7-2 was then used to predict the vibration level for a given scaled distance.

Most often Equation 7-2 is used for far field vibration prediction where the distance between the monitoring location and the blasthole is significantly greater than the charge dimensions. When estimation of vibration is required very close to the explosive source special near field equations are required that account for the explosive distribution in space. Holmberg and Persson (1979) developed Equation 7-3 to account for the spatial distribution of the charge:

Equation 7-3 $$PPV = Kl^{\alpha}\left[\int_0^H \frac{dx}{\left[R_o^2 + (R_o Tan\phi - x)^2\right]^{\beta/2\alpha}}\right]^{\alpha}$$

Where:

l = linear charge density (kg/m)

PPV = Peak particle velocity (mm/sec)

K, α, β = Site specific constants

R_o (m), ϕ (radians), x (m), H (m) = are defined in Figure 7-1

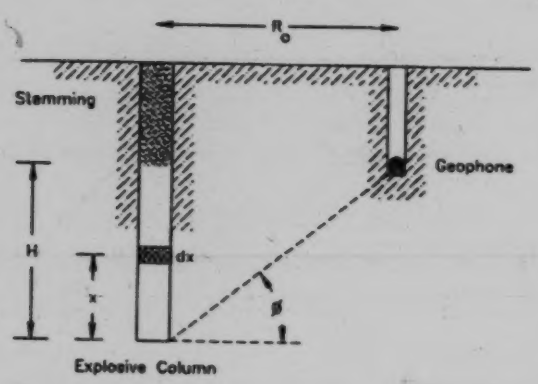

Figure 7-1: Description of parameters for the Holmberg equation (after Holmberg and Persson, 1979)

For the case of square root scaling (i.e. $\alpha = \beta/2$) the integrand in Equation 7-3 has an analytical solution that reduces the equation to:

Equation 7-4 $$PPV = K\left[\frac{l}{R_o}\right]^{\beta/2}\left[\phi - \arctan\left(\frac{R_o \tan\phi - H}{R_o}\right)\right]^{\beta/2}$$

From Equation 7-4 the Holmberg Term is defined as:

Equation 7-5 $$HolmbergTerm = \left[\frac{l}{R_o}\right]\left[\phi - \arctan\left(\frac{R_o \tan\phi - H}{R_o}\right)\right]$$

Equation 7-4 reduces the error associated with the assumption that the blasthole is a point source, however there are still potential sources of error with this method. Two limitations are:

- where blasthole layouts are geometrically complex (i.e. underground stope blasts) determination of R and ϕ can be very complex, and
- when a column is double primed it is difficult or impossible to determine which primer detonated first, therefore, H and ϕ are uncertain.

There are several other limitations for both methods. These are:

- effects of confinement (excess or insufficient burden or stemming) are not taken into account,
- shape and condition of the free face is not considered,
- influence of multi-point priming is not considered, and
- strength of explosive is not considered.

Based on the above limitations if Equation 7-2 or Equation 7-4 are going to be used as a predictive tool the following criteria should be met.

- The relationship should be based on the largest amount of field data possible.
- The blasting practices being evaluated (pattern, timing explosive type and hole size) should be the same as those used to develop the relationship.
- The rock type is the same as that used when developing the relationship.

Changing one or more of these factors may result in different site constants.

The value of β depends on the properties of the rock mass. As a seismic wave propagates through a rock mass its amplitude decreases in two ways: geometric spreading and

energy absorption. Geometric spreading does not result in a decrease in total energy it merely describes the dispersion of the expanding wave front. Energy absorption is caused by non-elasticity of the medium. A rock with a high modulus, and few discontinuities will behave closer to ideal elastic behavior, although all rock types will experience some degree of loss in vibration energy through frictional losses.

The factor β in Equation 7-2 and Equation 7-4 incorporates both geometric and frictional losses. When β is equal to 1 there are no frictional losses and vibration amplitude decreases as a result of geometric expansion only. For $\beta=1$, the vibration level is inversely proportional to scaled distance, and the vibration energy is related to the square of the distance. As the rock becomes less competent (less elastic) the value of β increases, typically it lies between 1 and 2 (Dowding, 1985). Like β the factor K also depends on the structural and elastic properties of the rock mass.

7.2 PPV Predictions

The blast reports were analyzed on a hole-by-hole basis to determine the scaled distance between the blasthole and the instrumentation array. The peak particle velocities were read off of the trace from each individual hole. A square root scaled distance was assumed because the expanding stress wave is best represented by a cylinder for the geometry encountered.

The vibration data from the 345-38 production blast and the 345-40 wall control blast were plotted in two forms: log (PPV) vs. log (Holmberg term) and log (PPV) vs. log (scaled distance). On each plot a linear regression lines were added. From each plot the site specific constants K and β were calculated. The plots for are shown in Figure 7-2 and Figure 7-3.

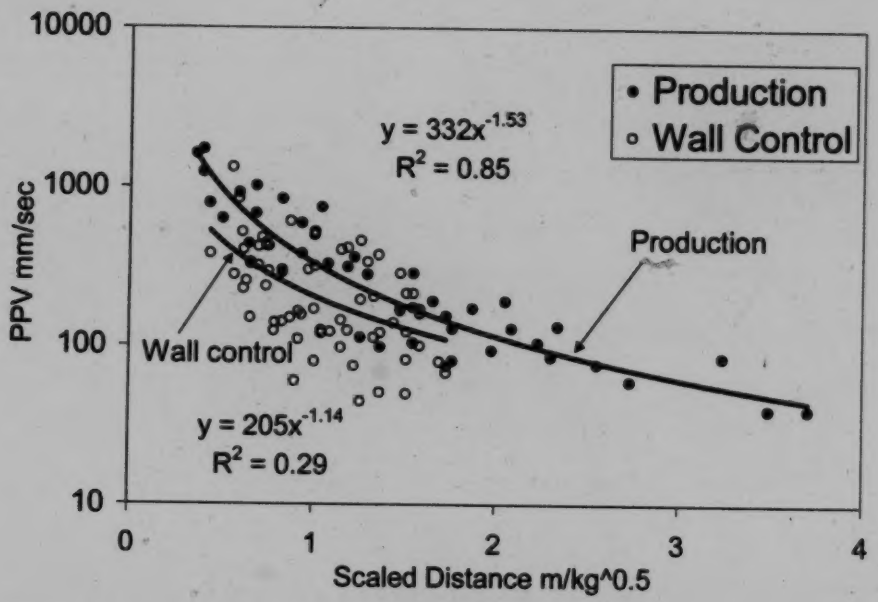

Figure 7-2: Comparison of PPV vs. scaled distance for production and wall control blasting

For the 345-38 production blast Equation 7-1 provides a best fit through the data with a coefficient of correlation of $R^2 = 0.85$:

Equation 7-6 $$PPV = 332\left(\frac{R}{\sqrt{W}}\right)^{-1.53}$$

For the wall control blast where the vibrations passed through a pre-shear Equation 7-7 applies with a coefficient of correlation of $R^2 = 0.29$.

Equation 7-7 $$PPV = 206\left(\frac{R}{\sqrt{W}}\right)^{-1.14}$$

Based on Equation 7-6 and Equation 7-7 it appears as though the vibration levels are the same whether the pre-shear exists or not when the distance from the final wall is greater than 60m (scaled distance ≥ 2.2 for a 775kg charge). This is likely a result of the pre-

shear selectively inhibiting only the higher frequency vibrations with wavelengths similar to the crack width from pre-splitting.

The second comparison was plotting log (PPV) against log(Holmberg term) (Equation 7-4). Again the production data fit better than the wall control data. A plot of log(PPV) vs. log(Holmberg term) is shown in Figure 7-3.

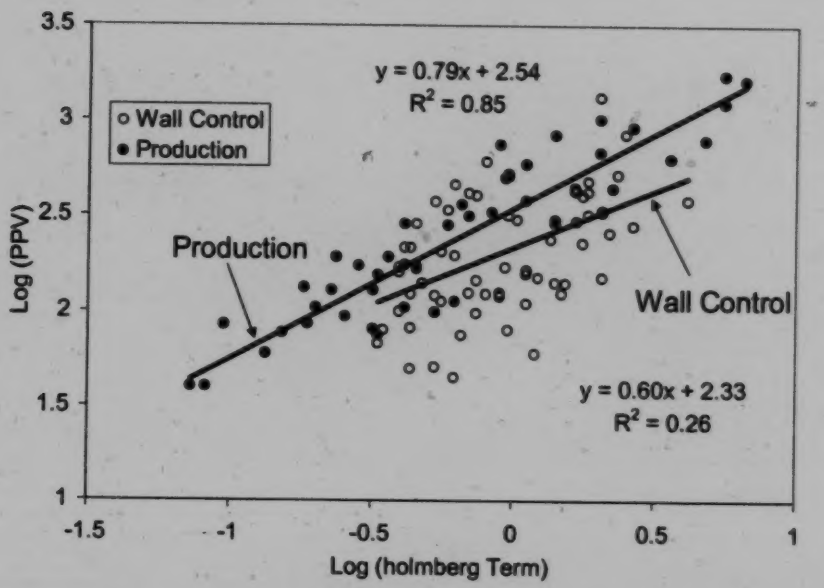

Figure 7-3: Comparison of Holmberg equation for production and wall control blasting

The use of the Holmberg equation resulted in a similar fit on the production data (R^2 = 0.85), but the wall control data fit decreased slightly (R^2 = 0.26). The regression resulted Equation 7-8 for production blasting.

Equation 7-8
$$PPV = 1686\left[\frac{l}{R_o}\right]^{0.79}\left[\phi - Arc\tan\left(\frac{R_o Tan\phi - H}{R_o}\right)\right]^{0.79}$$

The data from the wall control blast produced Equation 7-9.

Equation 7-9 $$PPV = 7644\left[\frac{1}{R_o}\right]^{0.60}\left[\phi - Arc\tan\left(\frac{R_o Tan\phi - H}{R_o}\right)\right]^{0.60}$$

The Holmberg relationship gave the constants K = 1650 and β = 1.58 for the production blast and K = 7644 and β = 1.20 for the wall control blast. A value of K = 1686 was used by Holmberg & Persson (1979) for a large open pit scenario. This agrees well with the K value of 1650 from the production blasting. The β value for the production shot monitored at Ekati™ was 1.58. The β value in the study by Holmberg and Persson (1979) was 1.78. Both values are within the range of 1 to 2 that is commonly encountered. Due to the effects of the pre-shear and choked face (Figure 6-12) it is difficult to compare the constants from the wall control blast to values from literature. The increased scatter in the data from the wall control blast may be attributed to one or a combination of the following factors:

- the blast was choked on one free-face,
- large amounts of water were draining into the pre-shear fracture,
- larger variation in the charge weight per delay than the production blast, and
- the geophones were located behind a previously blasted pre-shear.

For the conditions monitored at Ekati™ Mine both the square-root scaled-distance and Holmberg methods gave similar coefficients of correlation on the data. Based on this observation it is recommended that the square-root scaled distance relationship be used for simplicity. It is difficult to back calculate distances for the Holmberg equation, and no improvement in quality of PPV prediction is realized.

The vibration data from the pre-shear is a single PPV reading. As a result it is not possible to fit the data to any of the scaled distance equations. It would not be reliable to use the same relationships because they do not account for the decoupling that results from using Dynosplit C. The PPV from the pre-shear is shown in a PPV vs. distance plot in Figure 7-4. Based on general trend seen in the data, the PPV from the pre-shear is less

than that from the production and wall control blasts. This is expected and is a result of a lower weight of explosives and the effects of decoupling the charge.

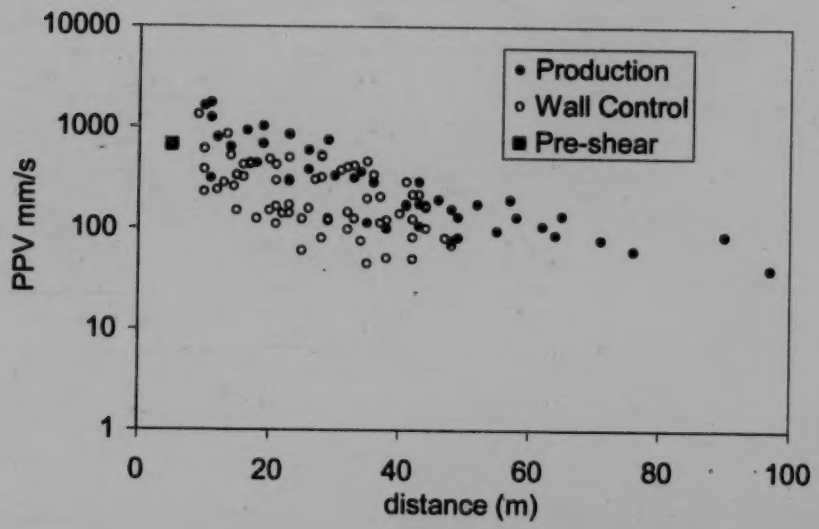

Figure 7-4: PPV from pre-shear compared to production and wall control blasts.

Since the middle of 1997, BHP has been gathering far field vibration data from the Panda pit and surrounding area. The data were gathered with a compliance monitoring type of system (White Seismology System). The monitoring was typically done with the geophone placed on the ground surface and secured in place with a weight or buried. The data from this monitoring were added to the data gathered in this study to establish an overall vibration prediction equation for the Ekati™ site. The entire database is plotted in Figure 7-5.

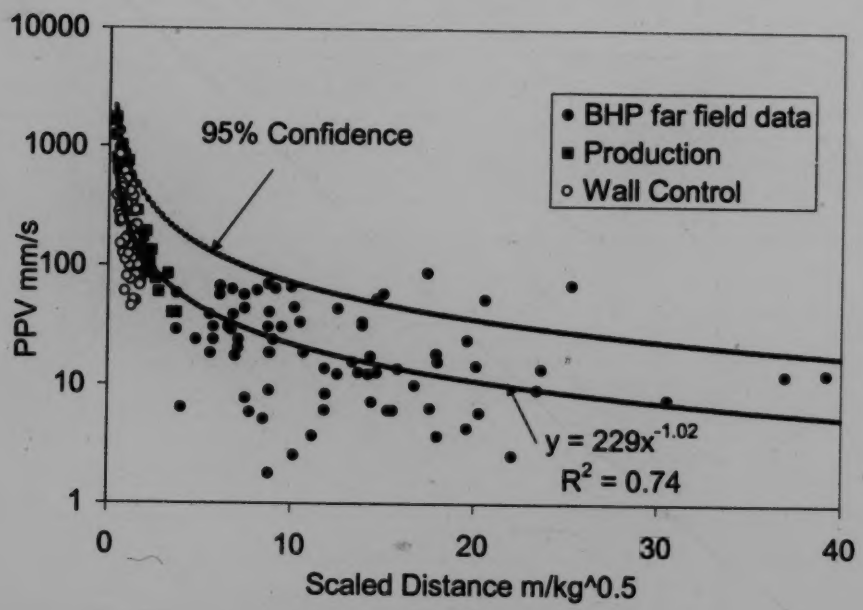

Figure 7-5: PPV vs. Scaled distance for all vibration data

It is evident that the far field monitoring data has a much larger amount of scatter. This is likely due to the various surfaces and materials that the geophone was placed on, and additional scatter may introduced by surface waves. The best-fit relationship to this data is:

$$PPV = 229\left(\frac{R}{W}\right)^{-1.02}$$

A summary of the site constants K and β is shown in Table 7-1. The 95% confidence levels for the upper limit of the K factor were also calculated and are also included in Table 7-1.

Table 7-1: Summary of site constants and correlation coefficients from vibration prediction equations.

	Holmberg Equation		Scaled Distance		
	Wall Control	Production	Wall Control	Production	Site wide
K	7644	1650	206	332	229
K-95%	62361	5669	790	742	758
β	1.20	1.58	1.14	1.53	1.02
R^2	0.26	0.85	0.29	0.85	0.74

The β values for the monitoring done in this study were similar in both equations. For the production blasting the values were 1.58 for the Holmberg equation and 1.53 for the scaled distance equation. Holmberg (1979) reported a β value of 1.78 in a similar experiment. For the wall control data the β values are also quite close, they were 1.14 for the scaled distance and 1.20 for the Holmberg equation.

While the Holmberg equation accounts for the charge geometry it does not give a better fit for the data. The equation is also very difficult to use without a computer spreadsheet. Due to these reasons it is recommended that the scaled distance equation (Equation 7-6) from the production blasts be used for vibration predictions within 100m and the site wide equation be used for larger distances.

7.3 Dynamic Properties of Rock Mass

As a result of having two geophones at different locations from the blastholes it was possible to calculate the p-wave velocity of the rock mass by measuring the difference in arrival times at the two geophones (Figure 7-6), and comparing this time to the difference in radial distance from the charge to each geophone (Figure 7-7). Equation 7-10 was used to calculate the p-wave velocity.

Equation 7-10 $C_p = \Delta D / \Delta t$

Arrival times from a total of 16 separate detonations (blastholes) from the 345-38 production blast and the 345-40 wall control blast were processed to obtain an average p-wave velocity of 4580m/s for the quartz diorite rock mass. The lowest value calculated was 4100m/s and the highest was 4967m/s. For comparison, Clark (1966) reported a p-wave velocity of quartz diorite of 4780m/s for intact rock.

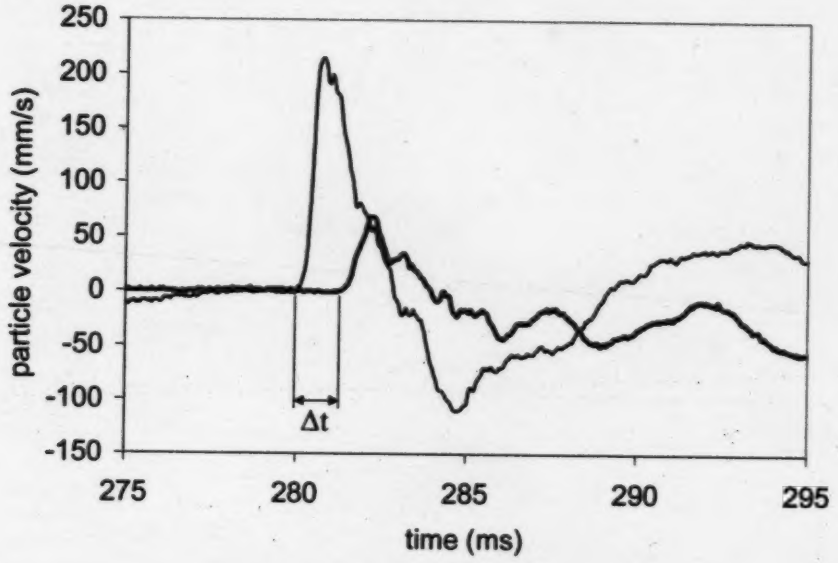

Figure 7-6: Difference in arrival time at two locations of a compressive strain pulse caused by one blasthole in the 345-40 wall control blast

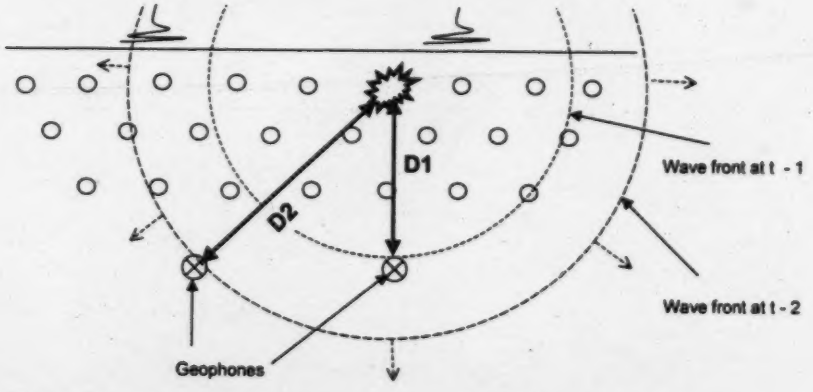

Figure 7-7: Radial distances used to calculate P-wave velocities

On some vibration traces it was possible to differentiate between the arrival of a compression wave and the slower shear wave. Two examples of this are shown in Figure 7-8 and Figure 7-9. The first plot (Figure 7-8) is a production hole detonating 19m from the geophone location. What appears to be the shear wave is seen on the downswing of the pulse at a time Δt after the peak in the compression wave. The second plot (Figure 7-9) is for a production hole that was 30m from the geophone. As expected, the second trace has a lower frequency and amplitude as well as a larger time Δt between the arrival of the p and s waves due to the geometric spreading and attenuation of the signal in the rock mass and the slower s-wave velocity.

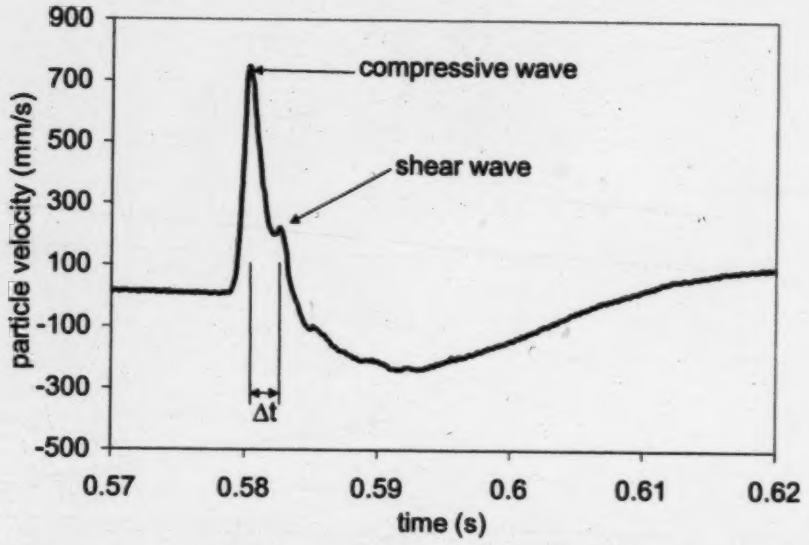

Figure 7-8: Single production hole at 19m showing separate arrival of shear and compressive waves Δt = 2ms

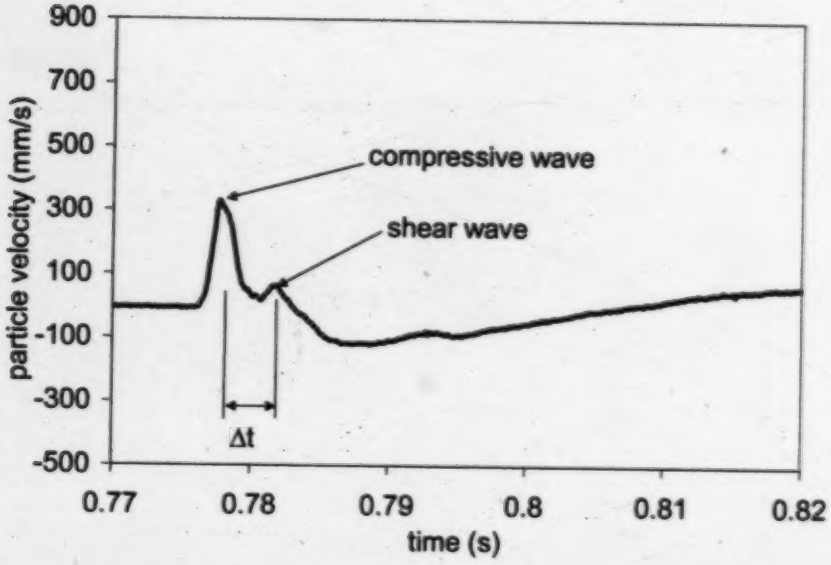

Figure 7-9: Single production hole at 30m showing separate arrival of shear and compressive waves $\Delta t = 4ms$.

By knowing the difference in arrival time, the distance from the source and the p-wave velocity (C_p) of the rock mass it was possible to calculate a value for the shear wave (C_s) velocity of the rock mass using Equation 7-11. The calculation gave a shear wave velocity of the rock mass of 2887m/sec. Clark (1966) reported the s-wave velocity for quartz diorite to be 3100m/s.

Equation 7-11 $$C_s = \frac{d}{\frac{C_p}{d} + \Delta t}$$

Where:

d = distance from borehole to geophone

The values P- and S-wave velocities can be used to calculate elastic properties of the rock mass. According to Dowding(1985) from the compressive wave velocity C_p of the rock

and the density (ρ) it is possible to calculate the constrained modulus M from the relationship:

Equation 7-12 $$C_p = \sqrt{\frac{M}{\rho}}$$

The constrained modulus, M can be approximated by Young's modulus E for most practical considerations (Timoshenko and Goodier, 1970). This gives the following relationship:

Equation 7-13 $$C_p = \sqrt{\frac{E}{\rho}}$$

Equation 7-13 and the velocity data from the 345-38 production blast and 345-40 wall control blast were used to calculate the dynamic modulus for the rock mass. The dynamic modulus value based on a compression wave velocity of 4580m/s is 56GPa.

By using the relationship between the shear modulus G and the shear wave velocity (Dowding, 1985),

Equation 7-14 $$C_s = \sqrt{\frac{G}{\rho}}$$

and the following relationship between E and G (Dowding, 1985):

Equation 7-15 $$G = \frac{E}{2(1+\nu)}$$

It is possible to back calculate the shear wave velocity C_s of the rock mass. Using an assumed Poisson's ratio of 0.25 which is typical for granitic rocks (Goodman, 1989), this calculation gives a shear wave velocity of 2896m/s. This is very close to the measured value of 2887m/s.

7.4 Fracture Criteria

Fracturing in rock can be induced by dynamic strains related to high vibration levels. The maximum induced strain (ε) is related to the peak particle velocity (PPV) from vibrations and the p-wave velocity C_p of the rock mass (Holmberg, 1979):

Equation 7-16 $$\varepsilon = \frac{PPV}{C_p}$$

The peak dynamic stress from a stress wave can be calculated from the following equation (Dowding, 1985):

Equation 7-17 $\sigma = \rho C_p (PPV)$

The PPV required to cause tensile failure can be calculated from Hooke's law and Equation 7-16 and Equation 7-17 which gives (Dowding, 1985):

Equation 7-18 $$PPV = \frac{\sigma_t C_p}{E}$$

Where: σ_t = Uniaxial tensile strength of rock (MPa)

E = Young's modulus of rock (MPa)

Equation 7-18 can be modified by use of the dynamic tensile strength and rock modulus to determine PPV instead of the static tensile strength. Mohanty (1987) measured the dynamic tensile strength to be 3.7 to 4.6 times the static tensile strength from Brazilian tests depending on the rock type. He also found the ratio between the Unconfined Compressive Strength (UCS) and the dynamic tensile strength is approximately 3.6.

The difference between static and dynamic modulii in many rocks may be attributed to departure from linear elastic deformation. Walsh and Brace (1966) reviewed theoretical studies of the elasticity of rock and reported that the presence of highly compliant pores or cracks strongly influences the deformation of rocks. Previous studies have shown that

at low confining pressure, the value of static modulus is generally less than the dynamic modulus because the presence of microcracks in the rocks affects the static deformation differently than the dynamic measurements, which are less affected by micro-cracks.

Field observations suggest that Equation 7-18 is useful for predicting extensive fracturing of rock as opposed to the initiation of fractures (Forsyth, 2000). A criterion proposed by the Mining Research Directorate (BLM Blastronics, 1995) suggests that the PPV associated with the furthest extent of incipient damage, which is the extension of existing fractures is observed to occur at about 1/4 the value predicted by Equation 7-18 using the static properties of Young's Modulus and tensile strength. CANMET (BLM Blastronics, 1995) also established a criterion for predicting the extent of incipient damage. The only difference between the CANMET criterion and the MRD criterion is that the CANMET uses dynamic tensile strength of the rock mass.

For the Ekati™ quartz diorite the assumed or measured rock properties are:

- Tensile strength σ_t = 8.3 MPa (BHP, 1997)
- Dynamic tensile strength = 43 MPa (UCS/3.6 after Mohanty, 1987)
- P-wave velocity C_p = 4580 m/sec (from monitoring)
- Young's modulus E = 50 GPa (BHP, 2000)
- Dynamic Young's modulus E = 56 GPa (from monitoring)

The critical PPV for fracture initiation calculated for the rock at Ekati™ are summarized in Table 7-2.

Table 7-2 Theoretical PPV thresholds (mm/s) for incipient damage and rock fracturing

Incipient Damage (mm/s)		Fracturing (mm/s)	
MRD	CANMET	MRD	CANMET
191	879	767	3517

The PPV thresholds are smaller for the MRD method because the dynamic tensile strength is significantly larger than the static tensile strength.

Holmberg and Persson (1979) used intact rock properties to estimate that PPV values of 700 to 1000mm/s are required to initiate fractures in hard igneous rocks. Bauer and Calder (1978) predicted damage criteria for strong rock masses based on the dynamic stresses produced by blasting, these are summarized in Table 7-3.

Table 7-3: Damage criteria for strong rock masses (Bauer and Calder, 1978)

Peak Particle Velocity (mm/s)	Effects on Rock Mass
Less than 250	No fracturing of the intact rock
250-650	Minor tensile slabbing will occur
650-2500	Strong tensile and some radical cracking
Greater than 2500	Complete breakup of rock mass

The predicted PPV values were used to back calculate the break radius and radius of damage around a 270mm production hole loaded with 775kg of 70% emulsion/ 30% ANFO blend (Table 7-4). For these calculations the PPV vs. distance relationships developed earlier were used (Equation 7-8 and Equation 7-8). These are based on the vibration data gathered at this site.

Table 7-4: Damage radii for fresh fracturing and incipient damage around a production hole

	Damage Radius (m) Fracturing		Damage Radius (m) Incipient Damage	
	MRD	CANMET	MRD	CANMET
Damage Threshold (mm/sec)	767	3517	191	879
Scaled Distance	13.5	5.8	33.7	14.5
95% Limit Scaled Distance	27	10	73	25

The average radius for fresh fracturing based on the CANMET criteria and PPV distance relationships is 5.4m, this correlates very well with data observed on the 345-38 production blast and other production blasts in the pit. According to Flemming (2000) this is in agreement with observed back-break on typical production blasts. The CANMET damage criteria provides a more realistic prediction of the PPV levels that cause damage to the rock mass, because it uses the dynamic strength and not the static strength.

By using the dynamic damage criteria (Table 7-2) and the PPV vs. scaled distance relationship from Equation 7-8, it is possible to predict the broken zone and the damage radius around a single borehole for various charge weights. These calculations are based on a 270mm hole loaded with 1.15 g/cc 70% emulsion/30% ANFO blend, in the rock mass at Ekati™. The values for fresh fracturing and extension of existing fractures are plotted in Figure 7-10. The break radius is the envelope where the PPV exceeds 3500mm/s, and the damage radius is the region where the PPV exceeds 880mm/s.

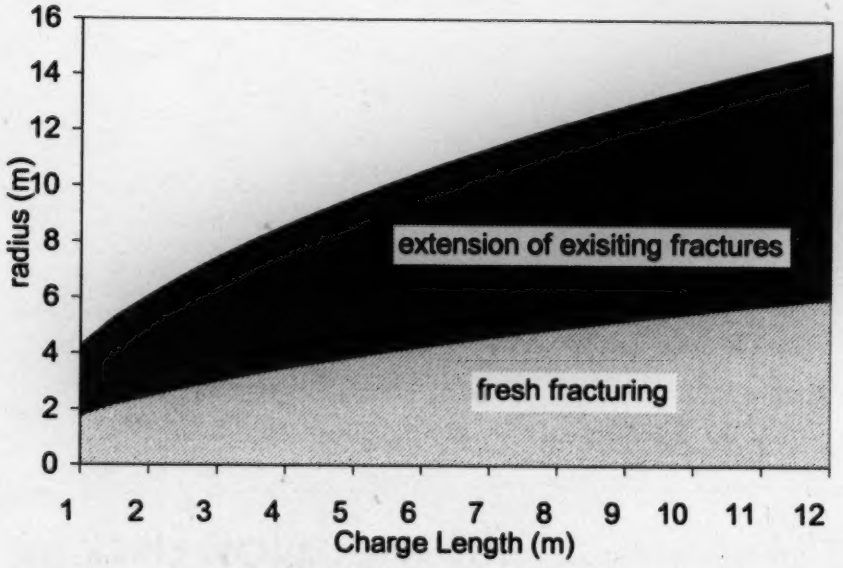

Figure 7-10: Zone of fresh fracturing and extension of existing fractures, for 270mm hole loaded with 1.15 g/cc 70% emulsion/30% ANFO blend, based on best fit vibration data.

The zones in Figure 7-10 were back calculated from Equation 7-6 and the PPV limits for incipient damage and fresh fracturing in Table 7-2. The plot for normal square root scaling plotted essentially identically to the Holmberg equation data. For the sake of simplicity it is sufficient to use Equation 7-6 for the prediction of vibration levels and damage envelopes. While these values are an approximation of the overbreak and damage radius for various charge sizes, the relationship is based on vibration and tensile strength, and does not account for factors such as:

- excess burden and poor breakout angles,
- damage mechanisms other than tensile strain,
- choked blasting, and
- under-cutting / day-lighting of structurally controlled failures.

These mechanisms are discussed in detail in chapter 2.

These calculations are all based on the assumption that the damage is exclusively a result of the tensile stresses from the strain wave traveling through the rock mass. This work may suggest that in some cases a reasonable estimate of overbreak can be made from PPV / scaled distance relationships when used in conjunction with the dynamic property based damage criterion. These methods are intended for unconfined rock. The effects of confinement will not be discussed here.

7.5 Gas Pressures and Observations of Rock Fractures

While monitoring of pressures in sealed boreholes behind blasts was originally applied to detect penetration of high-pressure gasses, it has been found that under-pressures or negative pressures with respect to atmospheric pressure often occur behind blasts. This phenomena is illustrated in Figure 7-11. Work done by Brent and Smith (1999) has supported that this phenomenon is a function of the new volume created due to crack formation and overall rock mass dilation. Their data are based on twelve free face blasts where there were no instances of high-pressure gas penetration along pre-existing

fractures. Pressures were monitored at distances less than one burden. This was also supported in work done by Ouchterlony (1996) where 10 of 13 blasts showed under-pressures, the three over-pressures coming from pre-split blasts.

The drop in pressure can be used to estimate the increase in volume. The thermodynamic relationship for the rapid expansion of the air without loss or gain of heat (adiabatic) in the monitoring holes is (Brent & Smith, 1996):

Equation 7-19 $$\frac{V_{new}}{V_{hole}} = \left(\frac{P_{atm}}{P}\right)^{1/\gamma} - 1$$

Where:

V_{new} = Incremental volume created within the hole (m^3)

V_{hole} = Original volume of hole (m^3)

P_{atm} = Atmospheric pressure (kPa)

P = Absolute pressure in monitoring hole at negative peak (kPa)

γ = Adiabatic expansion coefficient for air (1.4)

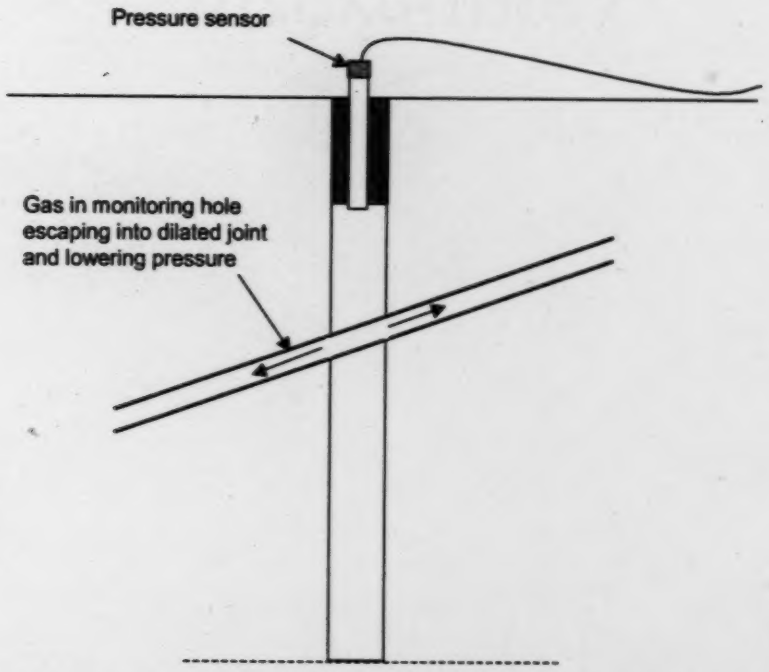

Figure 7-11: Gas flow into dilated joints or new fractures causing reduction of pressure in monitoring hole

It is proposed that this new volume created per unit of original volume of monitoring hole V_{new} / V_{hole} may be considered an indicator of the damage or disturbance to the rock at that location. Under-pressure data was compared to borehole camera observations made by Brent and Smith (1999).

Under-pressures were recorded during the 345-38 production blast. After a time of 1.3s the holes in the second last row of the blast are detonating, at a distance of approximately 12m from the pressure monitoring hole. Shortly after these detonations there is a significant pressure drop. The pressure monitoring location is 5m closer to the blast than the geophone; this corresponds to a predicted PPV of approximately 1200mm/sec. From Figure 7-12 it is evident that the dilation within the rock mass at the monitoring hole starts to occur as the second last row is detonating.

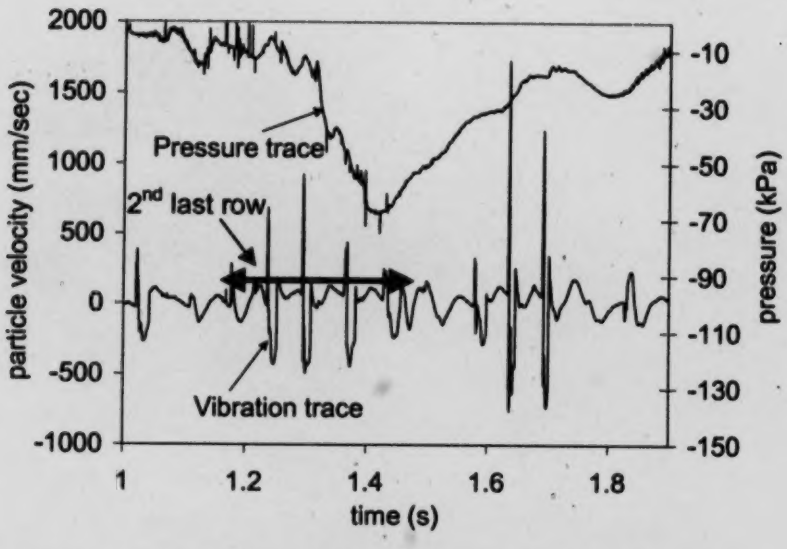

Figure 7-12: Pressure drop when second last row is detonating

To cause a pressure drop of 67kPa there must be a significant increase in volume. The volume increase calculated using Equation 7-19 is a 121%. The initial volume of the pressure-monitoring hole was $0.11m^3$ and the new volume created was $0.13m^3$, for a final volume of $0.24m^3$. This was at a scaled distance of 0.4 $m/(kg)^{0.5}$.

After the blast, attempts were made to survey the pressure sensor hole with a borehole camera. The hole was blocked completely at a depth of approximately 2.5m. The TDR cable in the adjacent hole also had a major disruption at the same depth. A photo of the face in front of monitoring location 1 is shown in Figure 7-13.

Figure 7-13: Face in front of 345-38 monitoring location 1 after muck cleared

The pressure trace from the 345-40 wall control blast is shown in Figure 7-14.

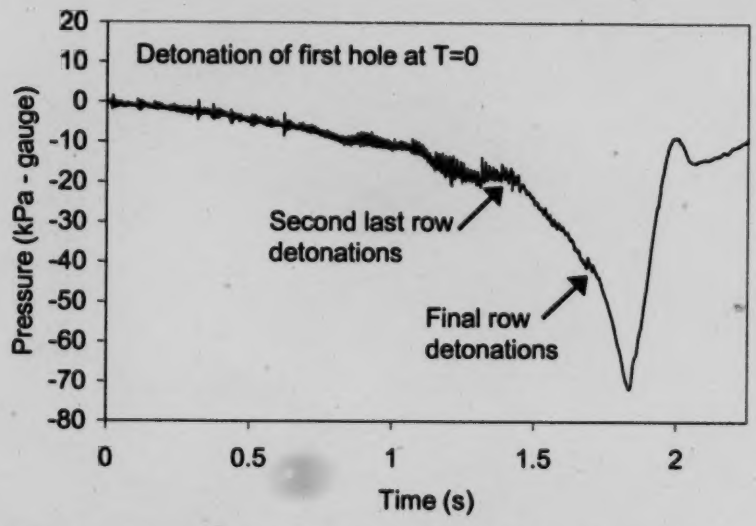

Figure 7-14: Pressure trace from 345-40 wall control blast

In the early stages of the blast (t<1.5s), there is a gradual drop in pressure. During this time the PPV readings are between 200-500mm/s. This gradual pressure drop is likely due to dilation of existing joints and possible fractures created by the pre-split. As the second last row of the blast detonates the PPV reaches 845mm/s. This is slightly over the incipient damage level calculated earlier. Immediately following the 845mm/s vibration the pressure begins to drop more rapidly, as a result of more dilation from disturbance of the rock mass. The pressure continues to drop until the last row detonates. The detonation of the last row results in a PPV of 1324mm/s, approximately double the PPV at location #1. When this occurs the pressure begins to drop even more rapidly until reaching a peak under-pressure of 70kPa below gauge. This is indicative of an increase in volume of the monitoring hole of 136%.

If the drop in pressure is accepted is an indication of the level of dilation of the rock mass, it is apparent that the dilation that occurred to the final wall at this location is approaching that is seen behind production blasts at a similar scaled distance.

The under-pressures recorded at Ekati™ are plotted in Figure 7-15 with the under-pressures that were recorded by Brent & Smith (1999) and Ouchterlony (1996).

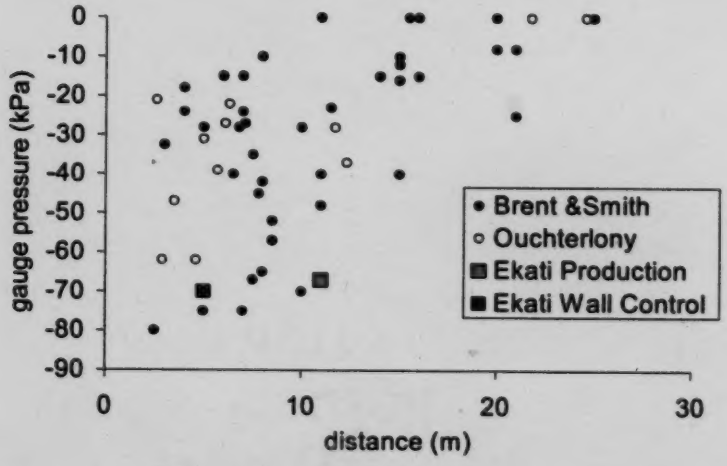

Figure 7-15: Pressure data plotted against values published by Brent & Smith (1999) and Ouchterlony (1996)

The data from the production and wall control blasts are plotted in Figure 7-16 as V_{new}/V_{hole} vs. scaled distance. The data from this study are plotted against data produced by Brent & Smith (1999).

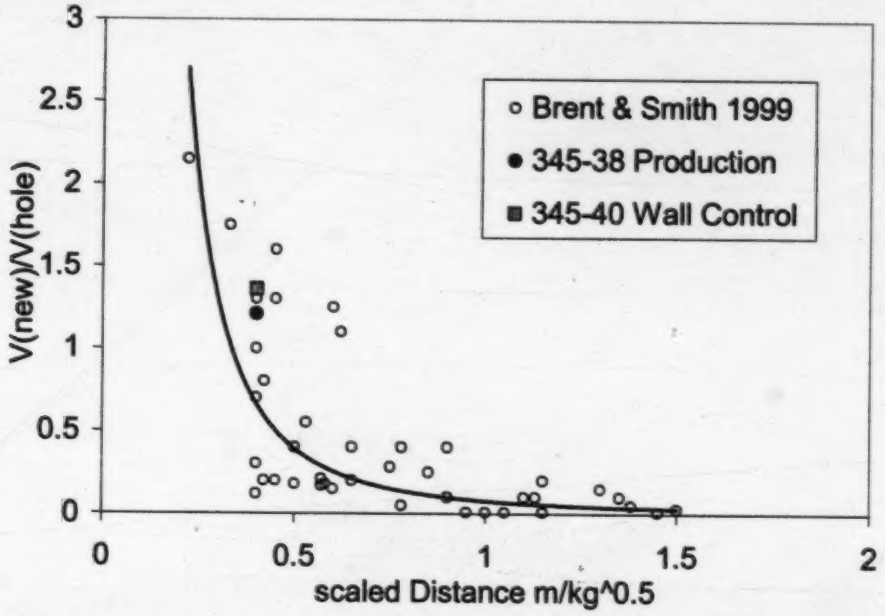

Figure 7-16: Increase in volume vs. scaled distance from data and literature (Brent and Smith, 1999)

The under-pressures recorded in this study support previous work. The data from both blasts shows that dilation is taking place from both the second row out and the closest row of the blasts. When comparing the volume increase to scaled distance it can be seen that the blasts at Ekati™ created similar volume increase from both blasts. Although the charge weights differ by 500kg the scaled distance is very similar.

The data from the 330-45PS pre-shear showed different damage mechanisms taking place. The vibration value recorded was lower than the incipient level damage predicted by the CANMET damage criteria. A detailed inspection of the pressure traces show that there is no under-pressure within 15ms of the pre-shear detonation (Figure 7-17). At a time of 15ms after the detonation there is what appears to be an under-pressure. This

under-pressure and the following high frequency noise, appear to be caused by the air-blast from the pre-shear affecting the differential pressure sensors. The air-blast from the pre-shear is likely to be large as there are 60kg of explosives per hole with no stemming, and the holes are detonated simultaneously. The arrival time of the air blast shows a velocity of the air-blast of 340m/s, which is consistent with the speed of sound in air.

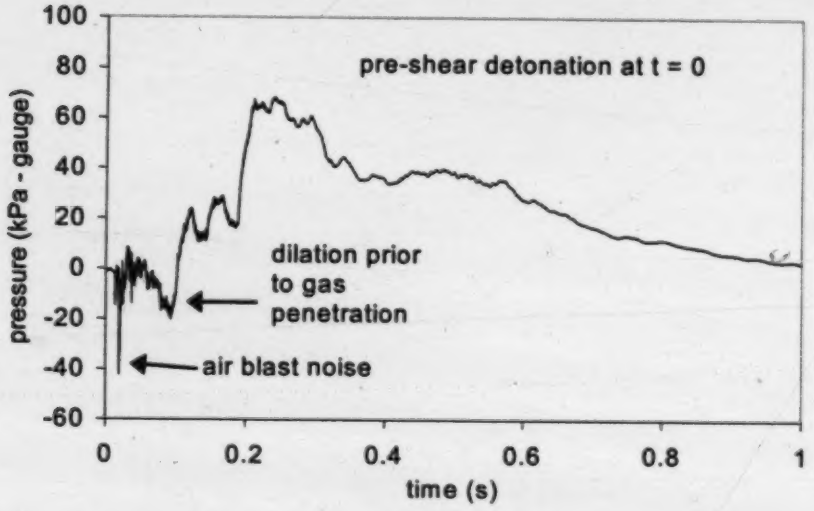

Figure 7-17: Gas penetration after pre-shear detonation

At a time of approximately 65ms after the pre shear detonation the pressure sensor #1 begins to read a drop in pressure (Figure 7-17). This pressure drop lasts 30ms and has a peak under-pressure of -18kPa (gauge). Immediately following this drop the pressure begins to increase in several steps over the next 120ms. McKenzie (1992) also reported the phenomena of rock dilation occurring prior to gas penetration, and noted extensometer readings that confirm this dilation. The pressure drop is likely due to the fractures being wedged open as the gas from the pre-shear begins to flow into the rock.

The increase in pressure lasts for approximately 1 second before returning to atmospheric pressure. The pressure increase in the monitoring hole suggest that gas is penetrating along joints, however the magnitude of the pressure increase is likely not indicative of the magnitude of the pressure along a joint. This is due to three reasons: the geologic

structure intersecting the hole is unknown, the volume of the hole may not be constant and the air in the hole is compressible.

The peak pressure in the monitoring hole is 67kPa. If this pressure were acting along a horizontal joint it would be able to lift 2.7m of rock. It is also quite likely that the pressure along the joint is much higher, and could therefore displace a greater height of rock.

7.6 Discussion

In reality blast damage is not only caused by strain waves. A significant amount of damage behind blasts results from the penetration of explosive gases along existing or new fractures and/or the upward displacement of rock blocks, or block heaving. This type damage is more difficult to quantify and predict and is highly dependent on the extent of rock structure and their orientation as well as the initiation sequence and delay timing of the blast.

The mechanisms of blast damage from gases are:

- physical dislodgement of in-situ blocks of rock, and
- significant reduction in the strength of the joints that increases the likelihood of failure due to gravity, stress or blast vibrations,

Both potential mechanisms result from gases penetrating into the rock fractures.

The paths that the gases follow are not well understood, however, it is widely accepted that gases will follow the path of least resistance. Gases will first penetrate existing fractures, joints and faults. Furthermore, longer fractures are preferentially extended over shorter fractures; this occurs because the stress concentration at the tip of the fracture increases with the length of fracture (Hagan, 1981). In highly fractured material the fracture spacing and orientation largely control the overbreak.

The gas pressure influences the depth that the gasses will penetrate into the rock. The pressure of the explosive gasses is dependent on two factors: the temperature of the gasses of detonation, and the confinement. The gas temperature is dependent on the explosive type and reaction rate, while the confinement depends on:

- amount and type of explosive,
- rock properties and structure,
- fracture network,
- amount and type of stemming, and
- burden.

Of particular interest in this study is unusually high pressures within the rock mass that can result from over confinement. Hagan (1979) states that where the effective burden is too large, the explosive gasses are contained within the blasthole for an excessive period of time. While trying to escape into the atmosphere these gasses stream into and wedge open both natural and strain induced fractures around the blasthole. When the burden distance is optimum the cracks will extend preferentially towards the free face. With excess burden this will not happen and excess overbreak is encouraged. According to Page (1987) the amount of damage from the same explosive load can vary 4 times depending on the pattern, timing and geometry of the blast.

LeJuge et. el (1994) observed that the blast damage can extend significantly farther than the gas flow does. This observation was based on gas pressure measurements made at three distances behind a pre-shear blast. The first hole recorded a trace similar to the pre-shear at Ekati™ (Figure 7-17) including the initial under-pressure prior to the increase in pressure. At the greater distances only under-pressures were recorded. They also reported extensometers placed 10, 20 and 30m behind a pre-shear and wall control blast. The pre-shear blast caused 15.7mm of permanent swell at the surface 10m behind the blast, and 2mm at 30m behind the blast. The subsequent trim blast resulted in 171mm of permanent swell 10m behind the blast and 34mm of permanent swell 30m behind the

blast. Ouchterlony (1996) reported vertical swelling without gas penetration extending 20 to 25m from the nearest blast holes, and assumed that this was due to an irreversible dilation of the fractures in the rock mass that it could be correlated to the under-pressures. Holmberg and Maki (1982) reported extensometer readings indicating 18mm of swell 16m behind a blast between the depths of 6 and 16m below the bench surface. At a distance of 8m behind the blast the swell over this same interval was 74mm.

Ouchterlony (1996) proposes the cause of the under-pressures is vertical movement in the rock that the shock fronts from the explosive charges initiate and which is amplified by the reflections from the top surface of the bench. This swelling opens up fractures connected to the measuring hole, increasing its effective volume. The pressure drops when the air in the hole is sucked into the fractures.

While there may be some dilation caused by the vibration, in this study the majority can be attributed to the heaving or mass movement as the broken and uplifted material around the blasthole moves upward and toward any free faces. It occurred well after the shock front had passed. This type of damage is heavily influenced by the structure of the rock mass. It also is likely that the gases entering longer joints act like a wedge and force the joints to open well beyond the extent of gas penetration. A general schematic of these processes is shown in Figure 7-18. This mechanism would result in under pressures being measured beyond the gas penetration limits.

Block heaving mechanism is thought to be the major source of damage to the walls of the Panda Pit. Visual observations and instrumentation data support this model. Figure 7-19 show some structurally controlled block heaving behind a blast in the vicinity of the 345-38 production blast. This type of damage has been observed up to 70m behind a blast in one extreme case, and typically 20 to 30m behind other blasts. Figure 7-20 shows some heaving damage to the crest. Often these can be correlated to choked face blasting, poor blast geometry, excessive stemming or sinking-cut blasts.

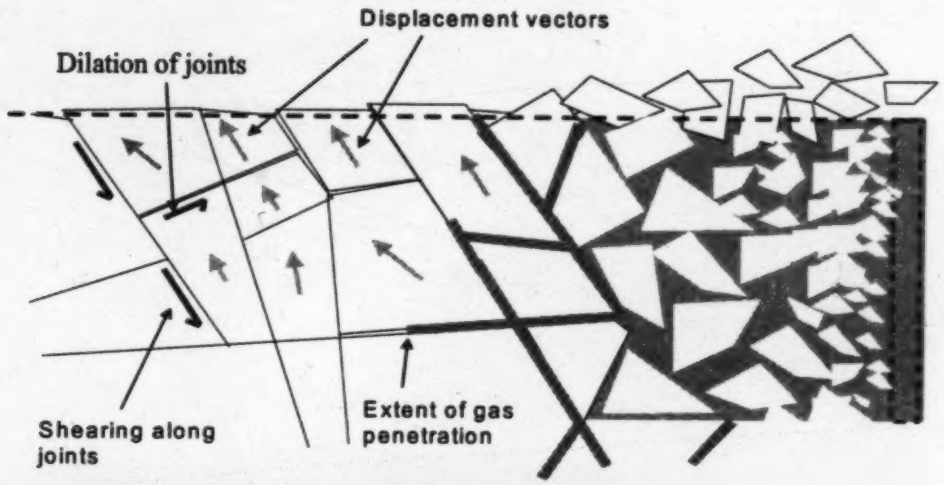

Figure 7-18: Schematic showing heaving taking place beyond gas penetration distance as a result of vertical movement around blasthole forcing uplift

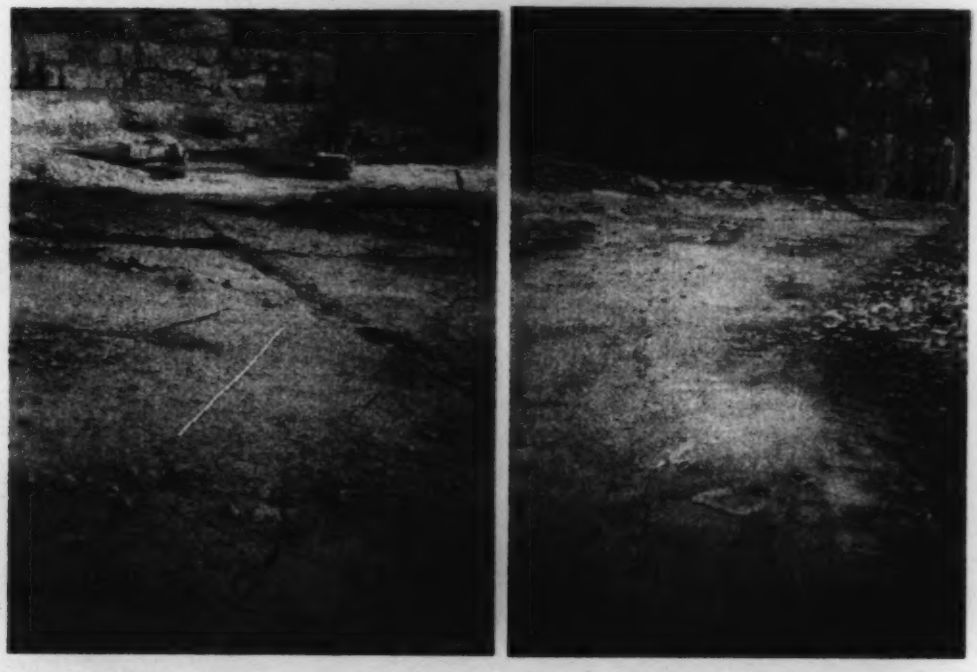

Figure 7-19: Structurally controlled heaving of blocks behind production blasts

Figure 7-20: Heaving damage to upper section of bench crest (note lack of fracturing in lower section of bench face)

There is little evidence to support that fresh fracturing from the strain waves is affecting the stability of the pit walls. Hagan & Bulow (2001) state that where ground vibration fails to produce new fractures or to extend existing fractures or blast-induced fractures significantly its contribution to instability is usually less than that of heaving. It can be argued that the recorded under-pressures are a result of fracturing of the rock mass, although the effects of the monitoring hole need to be considered. The stress conditions around the borehole are not truly representative of what is occurring in the rock mass. By drilling a hole in such close proximity to a blast it is likely that the hole will affect the dynamic stresses and hence the cracks generated in the vicinity of the borehole. The implications of this are that the new fracturing detected may be a result of the pressure-monitoring borehole itself, and may not be entirely representative of what is actually occurring. Brent and Smith (1996) show figures of and refer to vertical cracks occurring down opposing sides of boreholes, as well as randomly oriented cracks. It is quite likely that these vertical cracks are a function of stress magnification around the monitoring hole. These magnified stresses should be taken into consideration when analyzing

pressure data. Due to the stress magnification around the hole, fresh fracturing could begin to occur at a PPV levels below those predicted by the CANMET damage criterion. The data from the 345-38 production blast and the 345-40 wall control blast both show significant pressure drops when the PPV exceeds 1200mm/s.

7.7 Recommendations

Since the majority of the damage appears to be caused by block heaving and gas penetration, the blast design should reflect this. It is common practice for blast designers to reduce the powder factor at the periphery of an opening. The rationale behind this is that reduced charge weights will generate lower vibration levels and hence cause less damage. This concept may not be as effective as it seems. If a normally loaded production hole can successfully break and remove its burden, would it make sense to reduce this charge and expect the hole to move the same amount of burden? The result of this is excessive burden and increased confinement. This can lead to increase in the degree and extent of blast damage caused by trapped high pressure gas. Forsyth (1993) reports increasing the powder factor at the periphery of an excavation and seeing a reduction in the incidence of blast damage. Oriard (1970) explained the concept of charge configuration for reduced overbreak:

"To achieve control of the limits of a rock excavation, the concentration of the explosives must be commensurate with the desired smoothness and soundness of the final surfaces. For greater smoothness, there must be a greater dispersion of the charges. ***This does not mean lowering the powder factor.*** *There does not have to be a decrease in the total quantity of the explosives used, merely a change in the spatial distribution...The relationship would even apply if the powder factor were to be increased. Although this relationship seems obvious, it is unfortunate how often it is ignored in the field."*

Oriard (1970) also discusses confinement:

"Another important factor is confinement. The deeper the charge is buried, or the farther it is from the free face the greater the confinement. The more confinement to a

charge which is coupled in a normal fashion to the rock, that is the closer it becomes contained, the less able we are to control the line of rock breakage to some predetermined, neat surface, and the more extensive will be the fractures and mass movement away from the free face. The greatest damage usually is caused by the venting of explosive gasses. For a neat excavation, then, it is advisable to reduce the confinement."

This concept of reducing confinement and improving the explosive distribution as opposed to reducing the explosive energy is critical to developing an efficient wall control blast. There are several steps that can be taken to reduce the confinement and/or improve the explosive distribution. These steps are:

- use smaller diameter holes, closer hole spacing and reduced stemming,
- reduce stemming keeping the load the same in final rows,
- eliminate stemming in final rows,
- ensure previous blasts are completely cleared prior to blasting,
- reduce spacing on first row of blast to ensure toe breaks out to allow relief for subsequent rows.

One or a combination of these concepts may achieve the optimum results. The initiation sequence also has a significant impact on the stability of the final wall. According to Cunningham (2001) as the blast is initiated a substantial inertial thrust is developed behind the blast. Arranging the initiation sequence such that the thrust is more parallel to the pre-shear face can minimize the impact of this thrust. To accomplish this the blast should be initiated using a shorter inter-row delay and a longer inter-hole delay (Figure 7-21). This will cause the resultant thrust to act more along the split rather than into it, therefore reducing the impact. An added benefit of this procedure is that rock sticking to the split may be sheared off by the trim blast, leaving a cleaner face.

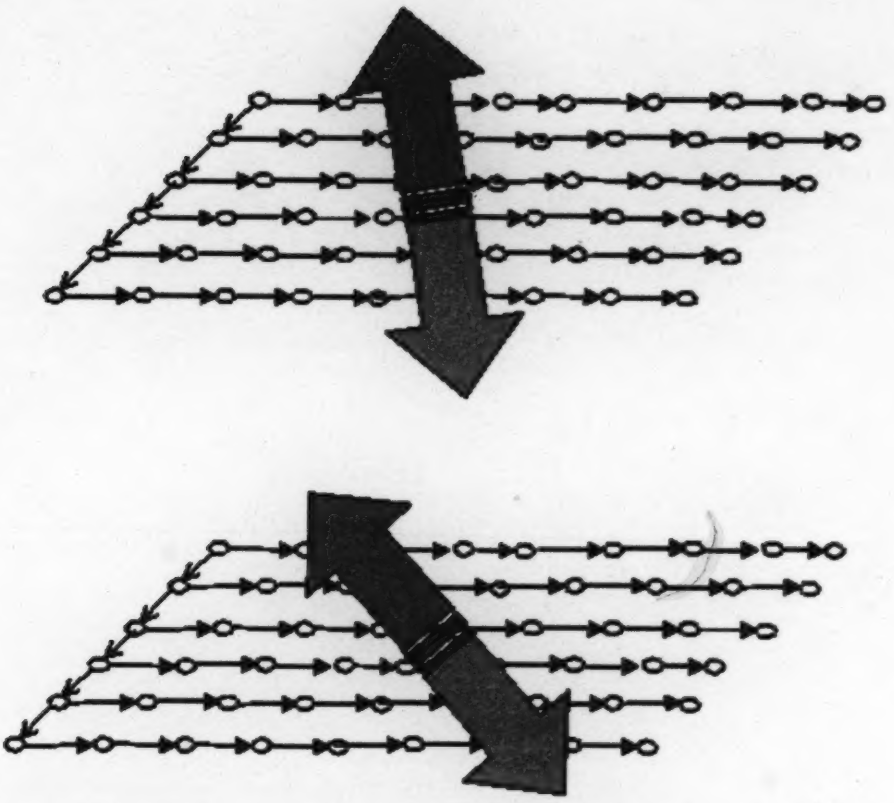

Figure 7-21: Effects of initiation sequence on thrust into wall

Reducing the damage to the final wall would best be accomplished by minimizing the confinement of the last two or three rows of the wall control blasts and changing the initiation sequence to reduce the thrust into the wall. LeJuge et al. (1994) saw improved results after eliminating decking and stemming of buffer holes in wall control blasts and Cunningham (2001) suggests adjusting the timing of the wall control blasts to deflect the thrust along the pre-shear which will reduce the disturbance. These two techniques can be attempted easily with the existing equipment and products currently used at Ekati™.

8 SUMMARY

As stated in Chapter 1 the objectives of the current thesis were threefold:

- To investigate the various techniques available for blast monitoring and develop a system for use at Ekati™.
- To monitor the rock mass response to production and wall control blasting.
- To develop and understanding of the blast damage mechanisms at Ekati™.

As described in the preceding chapters these primary objectives were successfully achieved. In chapter 5 the monitoring system that was used is described in enough detail to allow others to carry out a similar monitoring program. The piezo-electric pressure sensors proved to be an important tool in blast monitoring and performed well with the Instantel Mini-mate data acquisition system. The recommended modifications to the battery location will increase the reliability of the sensors. As expected the geophones also provided high quality data and were very reliable. The time domain reflectometry system also performed well, however, the data did not prove as useful in the interpretation.

The vibration data was used to develop scaled distance relationships, which were used to predict vibration levels for varying charge weights and distances. It was found that the use of square root scaling and assuming the charge is a point source provides similar accuracy as does accounting for the charge geometry. These relationships between scaled distance and particle velocity were essential in helping understand the blast damage mechanisms.

As a result of having two monitoring locations it was possible to measure the p-wave velocities of the rock mass based on the difference in arrival time of the compressive strain wave at the two locations. Using this p-wave velocity, it was then possible to calculate the dynamic modulus of the rock mass. A PPV based damage criteria was established based on the dynamic properties of the rock mass. The extents of fresh

fracturing and incipient damage (extension of existing fractures) were calculated based on the scaled distance laws and the damage criteria showed good agreement with observations in the field.

The only instance of explosive gas penetration was recorded from the pre-shear blast. On the production and wall control blasts only under-pressures were recorded. Similar monitoring programs by others have shown that the rock mass dilates a distances well beyond the limits of gas penetration. This dilation is caused by the vertical uplift from the blast and the joints or fractures wedging open ahead of the gases. This heaving mechanism is the major damage mechanism at Ekati™. While there is some gas penetration occurring during the pre-shear it is likely the damage is small compared to the damage caused from heaving from production and wall control blasting. This type of damage could be mistaken as gas penetrating excessive distances from the blast.

The heaving resulting from the blasts can be minimized by reducing the confinement of the explosive or by adjusting the initiation sequence. A reduction in confinement may be achieved by eliminating or reducing the amount or changing the type of stemming material placed over the explosives in the final rows and ensuring that the face is clear of blasted muck prior to blasting. The initiation sequence can be adjusted to reduce the inertial thrust into the final wall. This is accomplished by using a longer delay between holes than between rows. This will direct the thrust from the blast in a direction more parallel to the pre-shear instead of directly into the wall. These techniques are discussed in detail in the end of Chapter 7.

In the future the possibility of measuring the effects of blasting on a fault or major structure should be considered. While there are not currently any critically oriented faults or major structures in the Panda Pit, it is possible that one may be encountered in the future or in subsequent pits. By installing instruments on a fault that transects a blast pattern it may be possible to record the effect of nearby blasting on the fault. Such a system would involve drilling monitoring holes that intersect the fault at two or more distances from the blast. This could be accomplished through careful mapping, surveying

and drilling. In a case such as this the geophones, TDR cables and the pressure sensors could provide valuable information. Another aspect that could be considered is the use of some type of extensometers to develop an understanding of the extent of swell behind various blast designs. Recommendations for this type of monitoring are covered at the end of Chapter 6.

Regardless of the type of instrumentation used, particular attention should be paid to the geologic structure in the area of the blast. This should be done by mapping the bench faces before and after the blasts and measuring the orientation of the cracking that appears on the bench behind the blast. This detailed data will lead to a better understanding of the effect of the geologic structure on the extents of blast damage.

9 REFERENCES

Bauer, A., Calder, P.N. 1978. Open Pit and Blast Seminar, Course#63-321. Kingston, Ontario, Canada: Queen's University Mining Engineering Department.

Bligh T.P. 1974. Principle of breaking rock using high pressure gases. *Proc. 3rd Int. Congress Rock Mech.*, Denver. 8p.

BLM Blastronics 1995. Estimating and controlling blast vibration induced damage around underground excavations. *Report to the Mining Research Directorate*. 37p.

Bowring S.A. & Housch T. 1995. The earth's early evolution. EGS 1995-11: NWT Geological Mapping Division, DIAND, 21p.

Brent G.F. & Smith G.E. 1996. Borehole pressure measurements behind blast limits as an aid to determining the extent of rock damage. *Fragblast 5, Proc. 5th Int. Symp. on Rock Fragmentation by Blasting*, Montreal, Balkema, 103-112.

Brent G.F. & Smith G.E. 1999. The detection of blast damage by borehole pressure measurement. *Fragblast 6, Proc. 6th Int. Symp. on Rock Fragmentation by Blasting*, Johannesburg, Balkema. 5p.

Brown F.W. 1956. Determination of basic performance properties of blasting explosives. *Proc. 1st Symposium on rock Mechanics,* Colorado School of Mines.

Bulow B.M. & Chapman J. 1994. Limit blast design at Argylle Mine. *Proc. Open Pit Blasting Workshop*, Curtin University, Perth, 104 – 109.

Chiappetta R.F., Bauer A., & Burchell S.L. 1983. The Use of High Speed Motion Picture Photography in Blast Evaluation and Design. *Proc. 9th Int. Conf. On Explosives and Rock Blasting Technique.* Dallas, 258-309.

Clark G.B. 1987. *Principles of Rock Fragmentation,* John Wiley & Sons, New York.

Clark S.P. 1966. *Handbook of Physical Constants*. Geol. Soc. Am. Mem.

Clay R.B., Cook M.A., Cook V.O., Keyes R.T. and Udy L.L. 1965. Behaviour of Rock During Blasting. *Proc. of the 7th Symp. On Rock Mechanics.* Vol. 2, 438-461.

Cunningham C. 2001. Use of blast timing to improve slope stability. *Proc. 4th Int. Conf. Slope Stability in Surface Mining,* Denver. 131-134.

Dowding C.H., 1985, *Blast Vibration Monitoring and Control*, Prentice Hall, Inc., Englewood Cliffs, New Jersey, 297p.

Dyno Nobel 1991. Perimeter Control With Explosives.

Forsyth, W.W., 2000 personal communication

Forsyth W.W., Connors C. & Clark L. 1997. Blast damage assessment at the Trout Lake Mine. *Proc. 99th CIM Annual General Meeting*, Vancouver, on CD, 9p.

Forsyth W.W. 1993. A discussion of blast-induced overbreak around underground excavations. *Proc. 4th International Symposium on Rock Fragmentation by Blasting.* Vienna. 161-166.

Goodman, R. 1989. *Introduction to Rock Mechanics* John Wiley & Sons, New York, 2nd. Edition 489p.

Hagan T.N., Bulow B. 2001. Blast designs to protect pit walls. *Proc. 4th Int. Conf. Slope Stability in Surface Mining,* Denver. 125-130.

Hagan T.N. 1967. Performance Characteristics of Ammonium Nitrate/Fuel Explosives, *PhD thesis*, University of Queensland..

Hagan T.N. 1973. Rock breakage by explosives, *National Symposium on Rock Fragmentation,* Australian Geomechanics Society.

Holmberg R. & Maki K. 1982. Case examples of blasting damage and its influence on slope stability. *Proc. 3rd Int. Symp. On Slope Stability in Surface Mining,* Vancouver, 773-793.

Holmberg R. & Persson P.A. 1979. Design of tunnel perimeter blasthole patterns to prevent rock damage. *Proc. IMM Tunnelling '79 Conference*, London, 280-283.

Langefors U. & Khilstrom B. 1973. *The Modern Technique of Rock Blasting*. John Wiley and Sons, New York, 2nd Edition 405p.

LeCheminant A.N. & VanBreeman O. 1994. U-Pb Ages of Proterozoic Dyke Swarms, Lac de Gras area, NWT: Evidence for Progressive Break-up of an Archean Supercontinent. Geological Association of Canada, Program with Abstracts, Vol 19 p. A62.

LeJuge G.E., Jubber L., Sandy D.A. & McKenzie C.K. 1994. Blast damage mechanisms in open cut mining. *Proc. Open Pit Blasting Workshop*, Curtin University, Perth, 96-103.

Lilly J.D. 1987. Achieving pit wall integrity with large diameter blast holes. *Proc. 2nd International Symposium on Rock Fragmentation By Blasting*, Keystone, Balkema, 634-645.

Mathis J.E., 1997. BHP Diamonds Inc. Panda Pit Slope Preliminary Design

McKenzie C.K., Holley K.G. & LeJuge G.E. 1992. Rock damage from blasting. *Proc. Asia Pacific Conf. – Quarrying the Rim*, Hong Kong. 7p.

Mercer J.K. 1980. Some Aspects of Blasting Physics, *Quarry Mine & Pit,* Vol. 19, No. 2.

Mitchell, R. H. 1986. *Kimberlites: Mineralogy, Geochemistry, and Petrology*. Plenum Publishers, 460p.

Mohanty B.B. 1987. Strength of Rock Under High Strain Rate Conditions Applicable to Blasting. *Proc. 2nd International Symposium on Rock Fragmentation By Blasting*, Keystone, Balkema.

Oriard L.L. 1970, Dynamic Effect on Rock Masses From Blasting Operations. Slope Stability Seminar, University of Nevada.

Ouchterlony F., Nie S., Nyberg U. & Deng J. 1996. Monitoring of large open cut rounds by VOD, PPV and gas pressure measurements. *Fragblast 5, Proc. 5th Int. Symp. on Rock Fragmentation by Blasting*, Montreal, Balkema, 167-176.

Oyo Geospace Corporation. 2000, www.oyogeospace.com

Page C.H. 1987. Controlled Blasting For Underground Mining. *Proc. 13th Annual Conference on Explosives and Blasting Technique*, Miami 33-48.

Pell J.A. 1997. Kimberlites in the Slave Craton, Northwest Territories Canada. *Geoscience Canada*, Vol. 24, No. 2, 77-89.

Peterson J. 1998. Fragmentation Analysis - BHP Diamonds Inc. Ekati™ Mine. Polar Explosives Ltd., Report to BHP Diamonds, 9p.

Preston C.J. & Teinkamp N.J. 1984. New techniques in blast monitoring and optimization, *CIM Bulletin*, 77(867), 43-48.

Timeshenko S.P. and Goodier J.N. 1970. *Theory of Elasticity*, McGraw Hill Book Co., New York, 3rd Edition 567p.

Walsh J.B., and W.F. Brace. 1966. Elasticity of rock: a review of some recent theoretical studies. *Rock Mechanics and Engineering Geology*, Vol. 4, pp. 283-297.